Supplement of Geosci. Model Dev., 11, 1343–1375, 2018
https://doi.org/10.5194/gmd-11-1343-2018-supplement

Geoscientific Model Development
Open Access
EGU

Supplement of

LPJmL4 – a dynamic global vegetation model with managed land – Part 1: Model description

Sibyll Schaphoff et al.

Correspondence to: Sibyll Schaphoff (sibyll.schaphoff@pik-potsdam.de)

S1 Supplementary informations to the evaluation of the LPJmL4 model

The here provided supplementary informations give more details to the evaluations given in Schaphoff et al. (under Revision). All sources and data used are described in detail there. Here we present additional figures for evaluating the LPJmL4 model on a plot scale for water and carbon fluxes Fig. S1 - S16. Here we use the standard input as described by Schaphoff et al. (under Revision, Section 2.1). Furthermore, we evaluate the model performance on eddy flux tower sites by using site specific meteorological input data provided by http://fluxnet.fluxdata.org/data/la-thuile-dataset/ (ORNL DAAC, 2011). Here the long time spin up of 5000 years was made with the input data described in Schaphoff et al. (under Revision), but an additional spin up of 30 years was conducted with the site specific input data followed by the transient run given by the observation period. Comparisons are shown for some illustrative stations for net ecosystem exchange (NEE) in Fig. S17 and for evapotranspiration Fig. S18. Only 2 stations show a slightly better performance of LPJmL4 to NEE measurements and for evapotranspiration only 1 station, the others show a similar correlation as the simulations conducted with global climate input.

We use gauging station to evaluate the river discharge as an integrated measure (Fig. S19 - S66). Fig. S68a compares the two evaluation data sets against each other. The comparison of the global data set from (Jung et al., 2011) to the local data (Luyssaert et al., 2007) shows that both data sets are in good agreement. The comparison of LPJmL4 against the global data set of Jung et al. (2011) on the local scale (Fig. S68b show a slightly worse match as the comparison against the local data (see Fig. 4, main text). Fig. S68c compares LPJmL4 against the global data set from (Jung et al., 2011), but excluding outliers with very high GPP. That increases the match to these data to a NMSE of 0.69 and a R^2 of 0.51. These comparisons show also that the comparisons on both scales are meaningful and can give a good indication how good the model can reproduce global as well as local biomass estimations by different methods. Fig. S67 and Fig. S69a give a comparison with the global estimation of Carvalhais et al. (2014) for soil organic carbon resp. biomass. Additionally we have compared aboveground biomass in Fig. S69b with estimates by Liu et al. (2015). A spatial comparison of ecosystem respiration is shown in Fig. S70. Evapotranspiration comparison against MTE data (Jung et al., 2011) is shown in Fig. S71 and Fig. S72 shows a comparison of simulated fractional burnt area against remote sensing observations (GFED4: http://www.globalfiredata.org/ and CCI Fire Version 4.1: http://cci.esa.int/data). Remote sensing data are also used for the evaluation of FAPAR (Fig. S73) and Albedo (Fig. S74).

Sowing dates have been proved to be important to simulate crop variability (Fig. S75 - S83), a comparison with MIRCA sowing dates we show in Fig. S84 - S93.

Table S1 gives an overview of estimates for regional field application efficiencies, showing that LPJmL4 are in a similar range as other estimates.

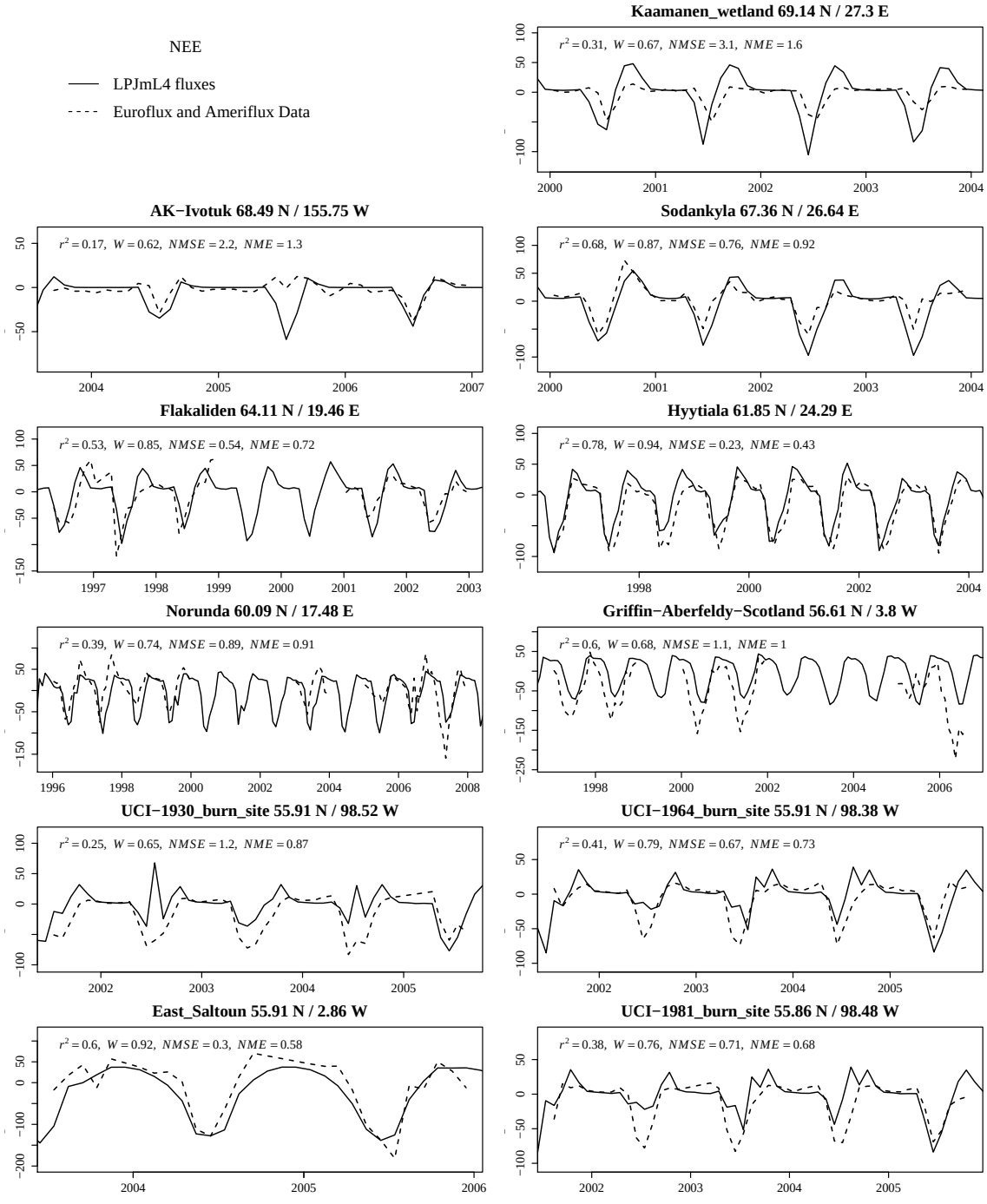

Figure S1. Comparison of NEE fluxes with EDDY-flux measurements.

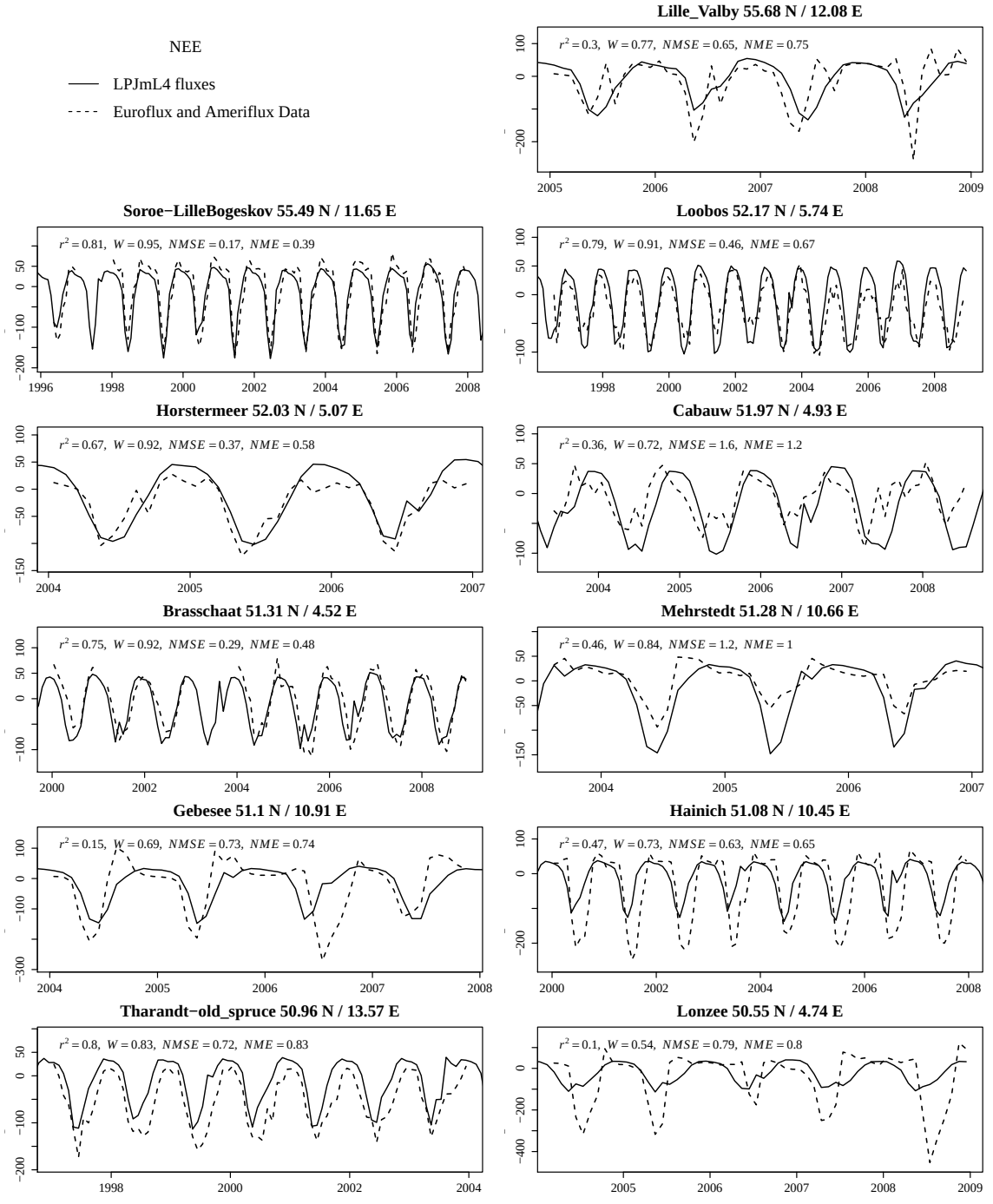

Figure S2. Comparison of NEE fluxes with EDDY-flux measurements.

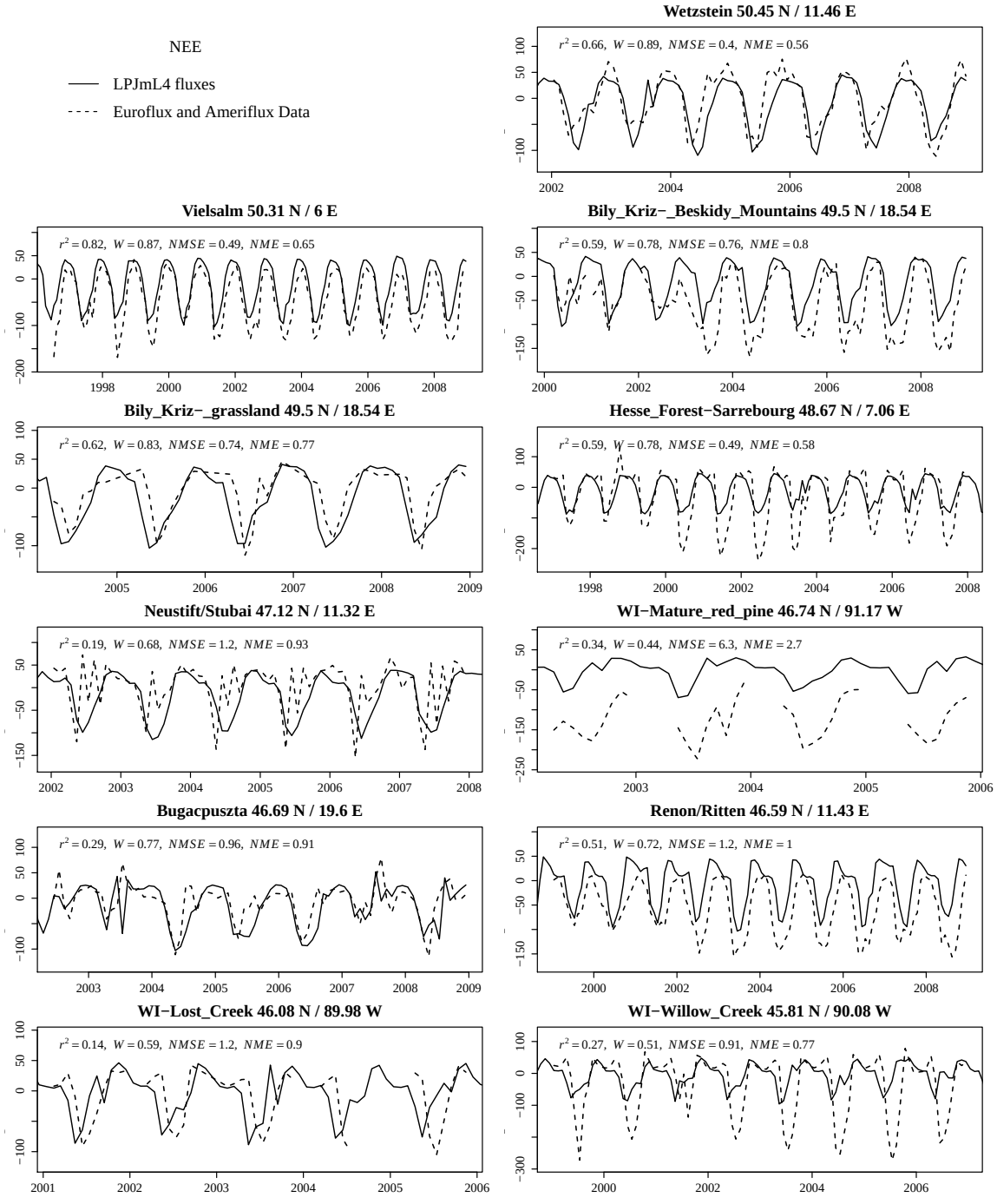

Figure S3. Comparison of NEE fluxes with EDDY-flux measurements.

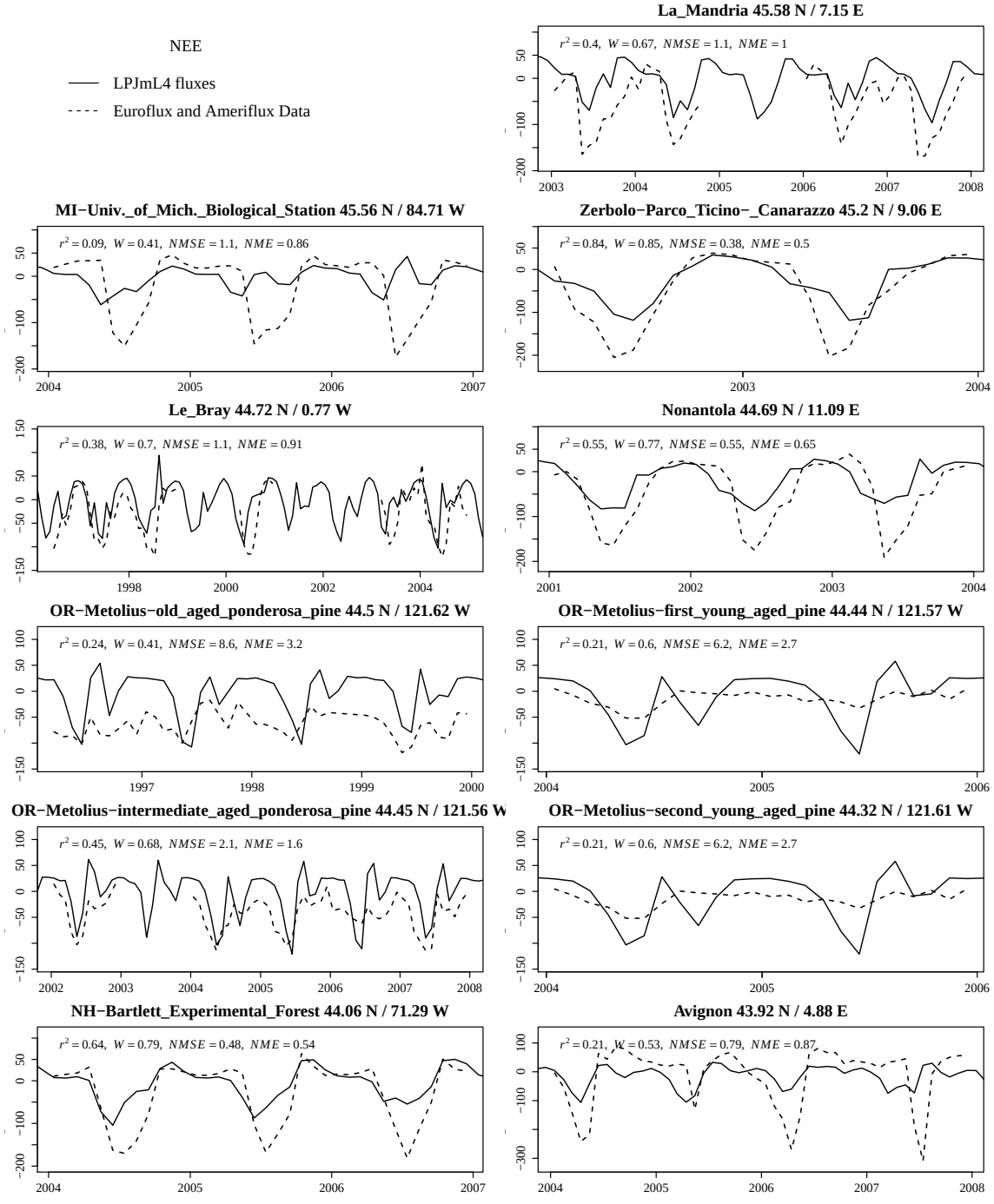

Figure S4. Comparison of NEE fluxes with EDDY-flux measurements.

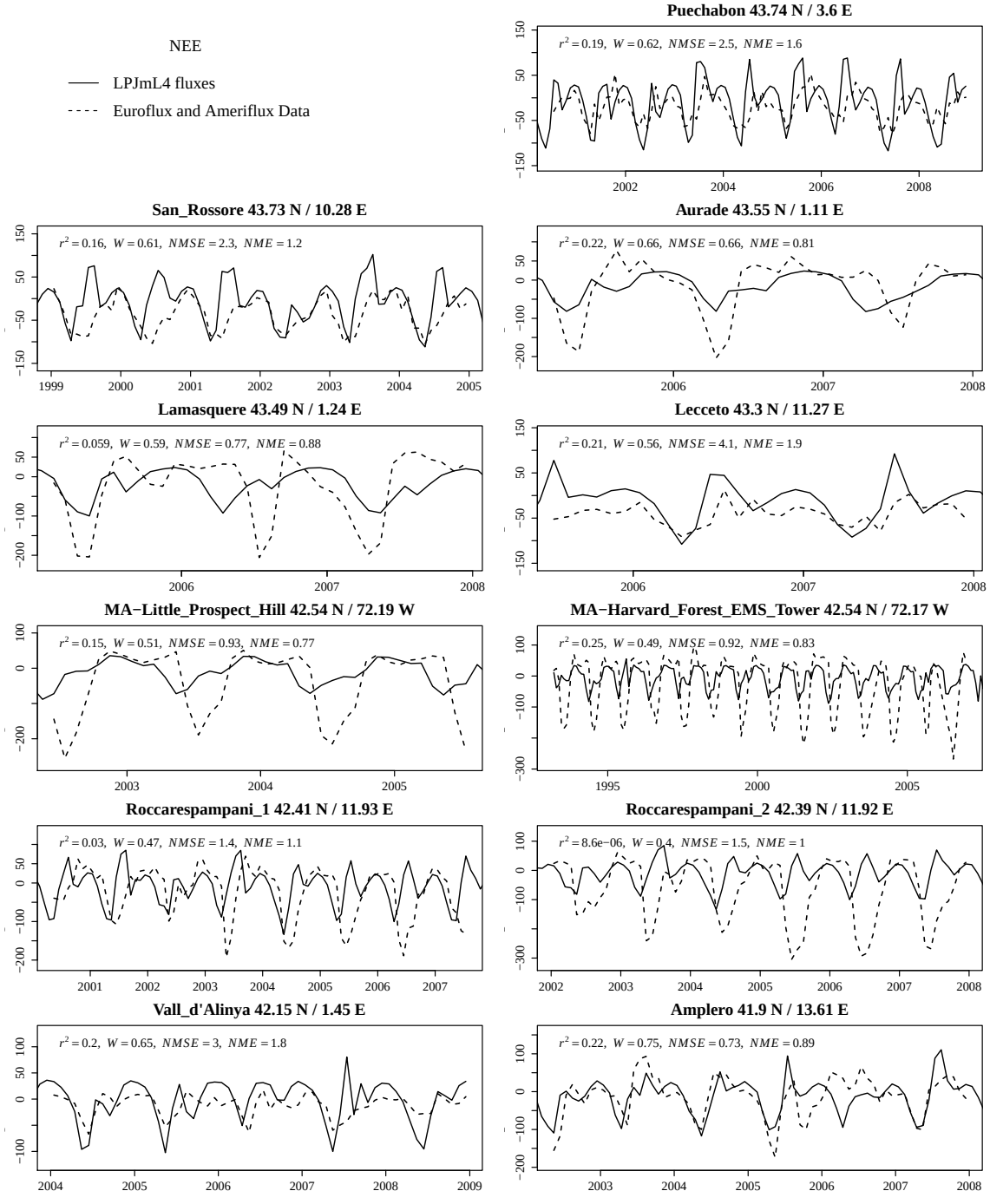

Figure S5. Comparison of NEE fluxes with EDDY-flux measurements.

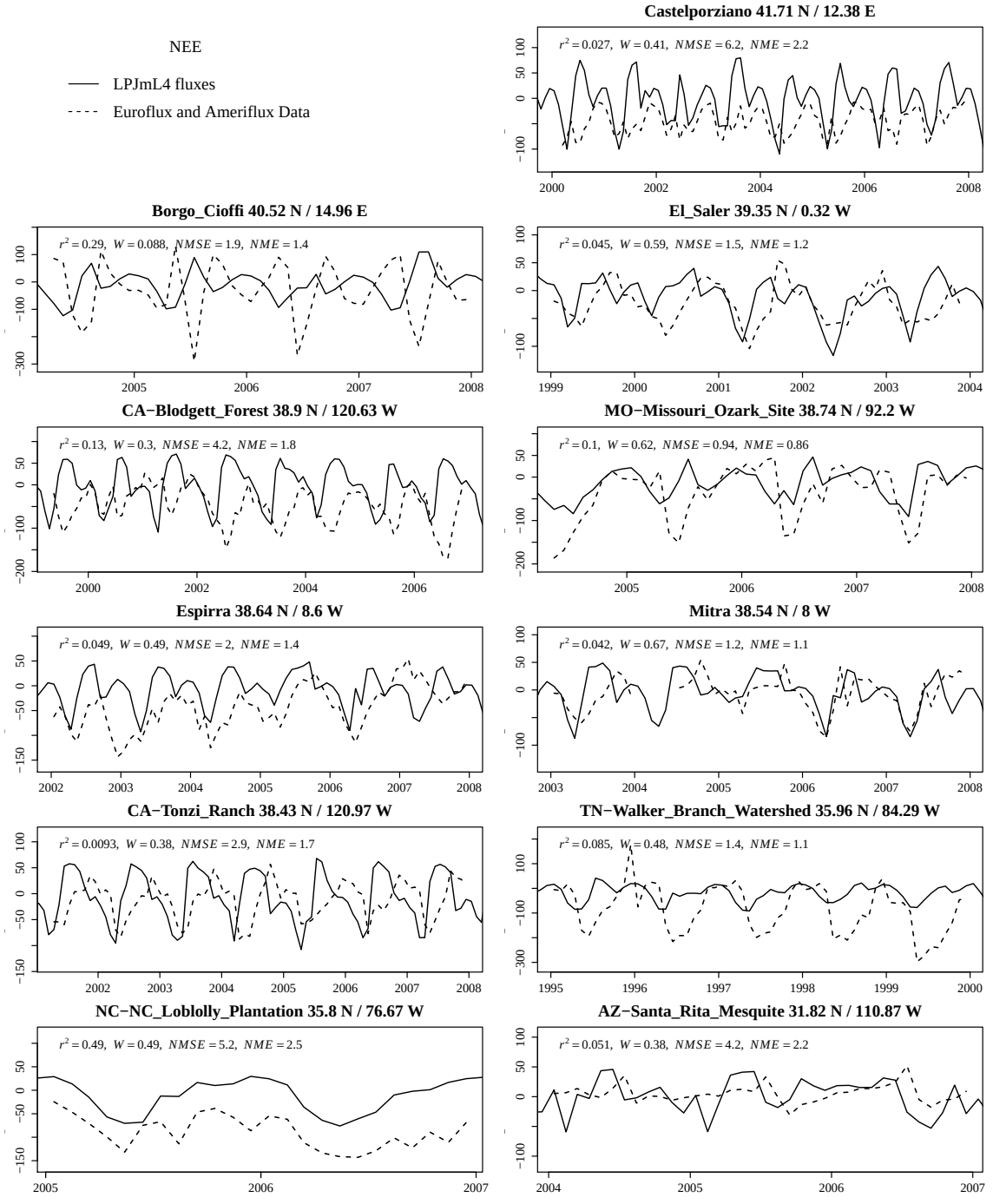

Figure S6. Comparison of NEE fluxes with EDDY-flux measurements.

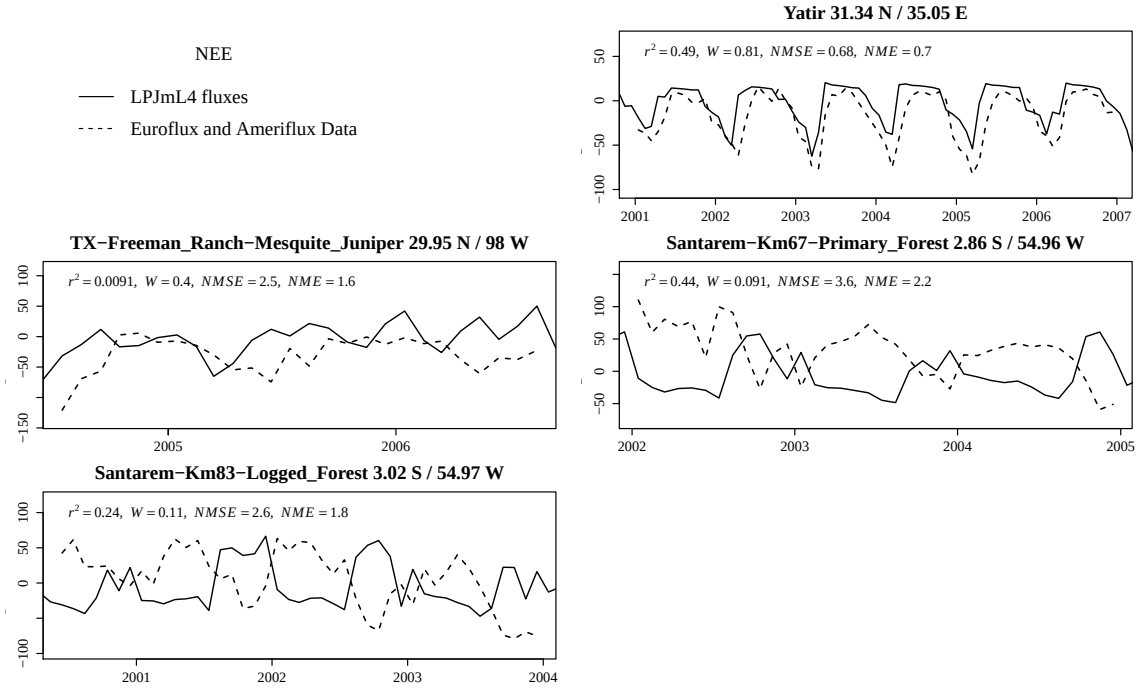

Figure S7. Comparison of NEE fluxes with EDDY-flux measurements.

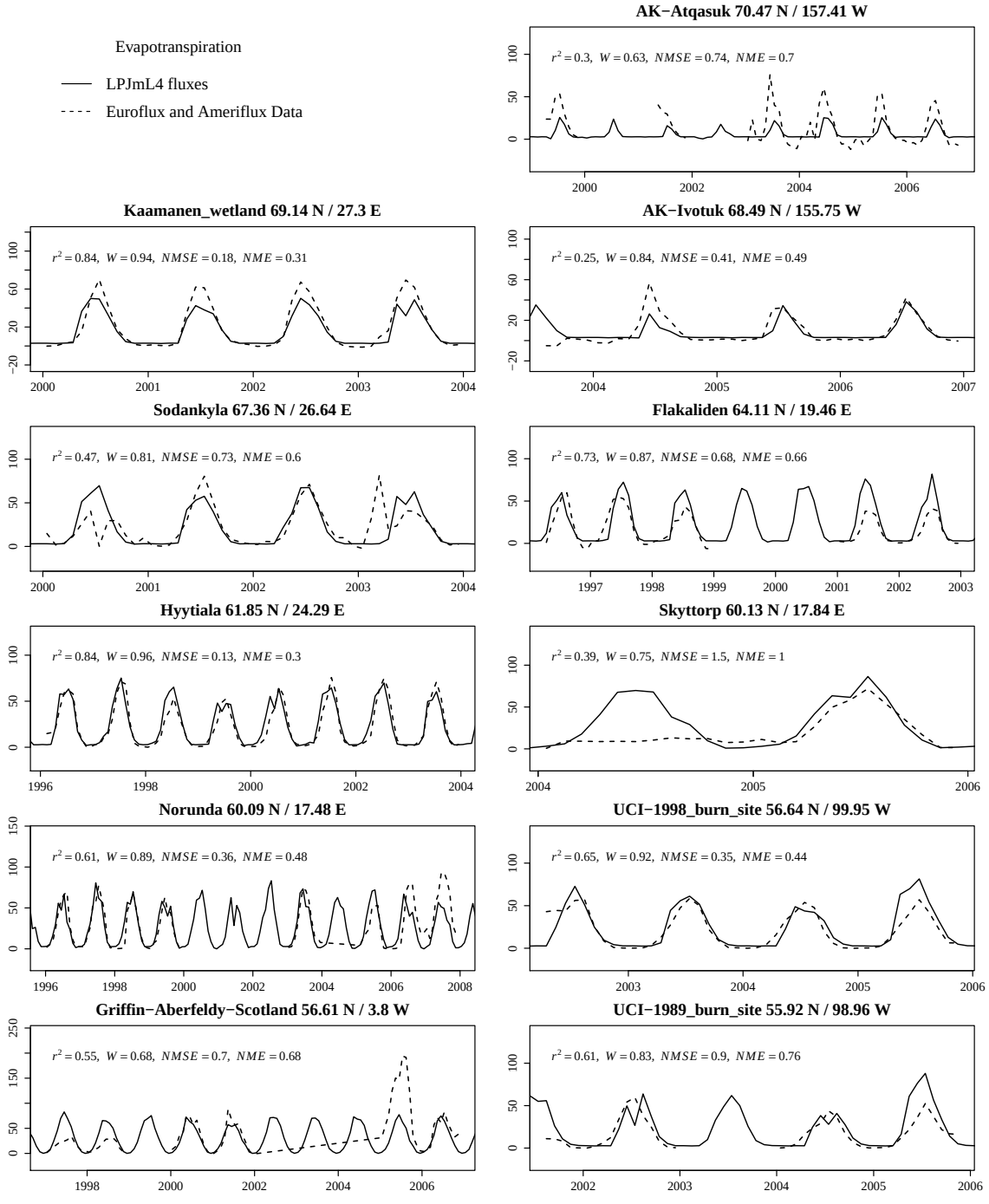

Figure S8. Comparison of Evapotranspiration fluxes with EDDY-flux measurements.

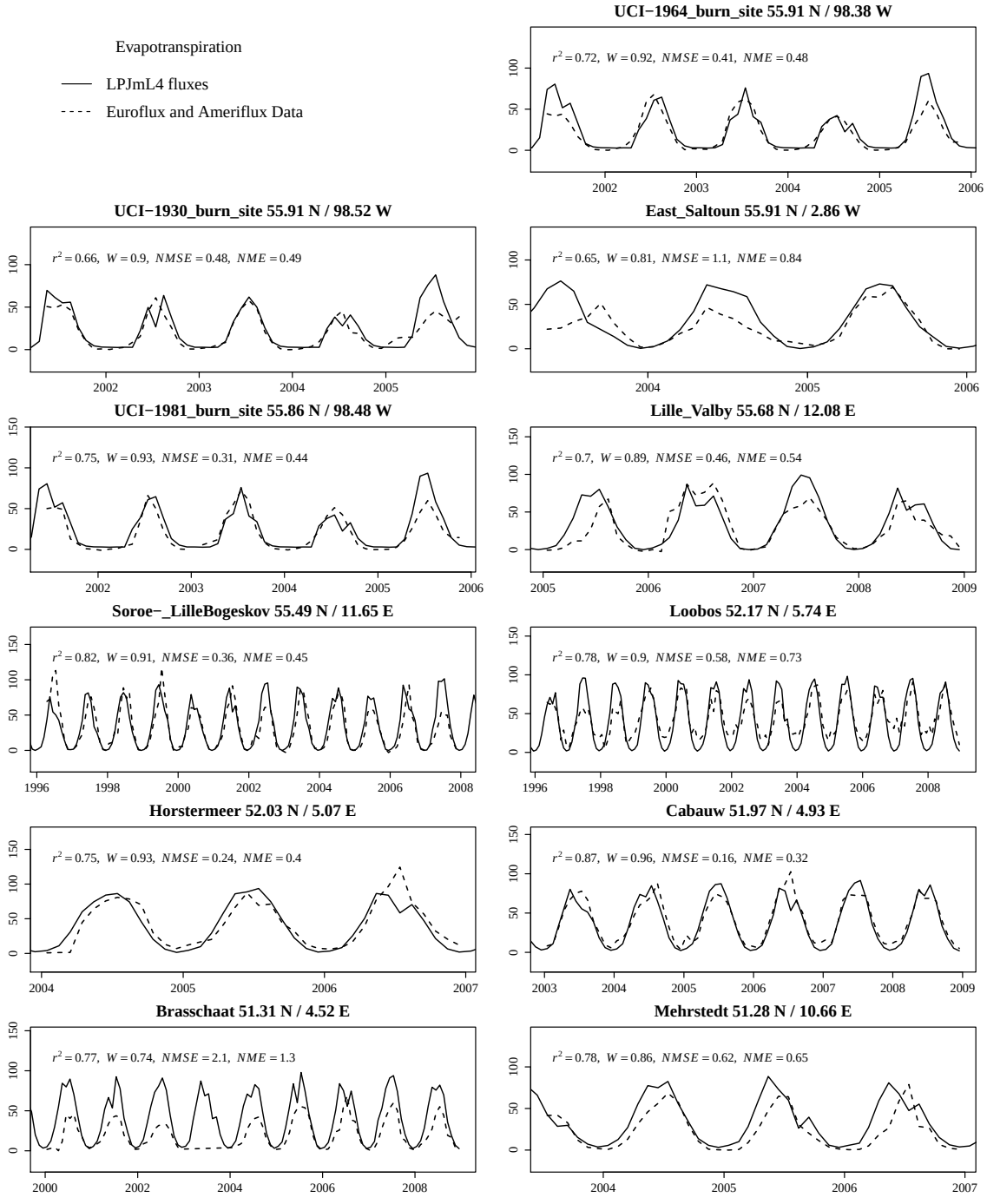

Figure S9. Comparison of Evapotranspiration fluxes with EDDY-flux measurements.

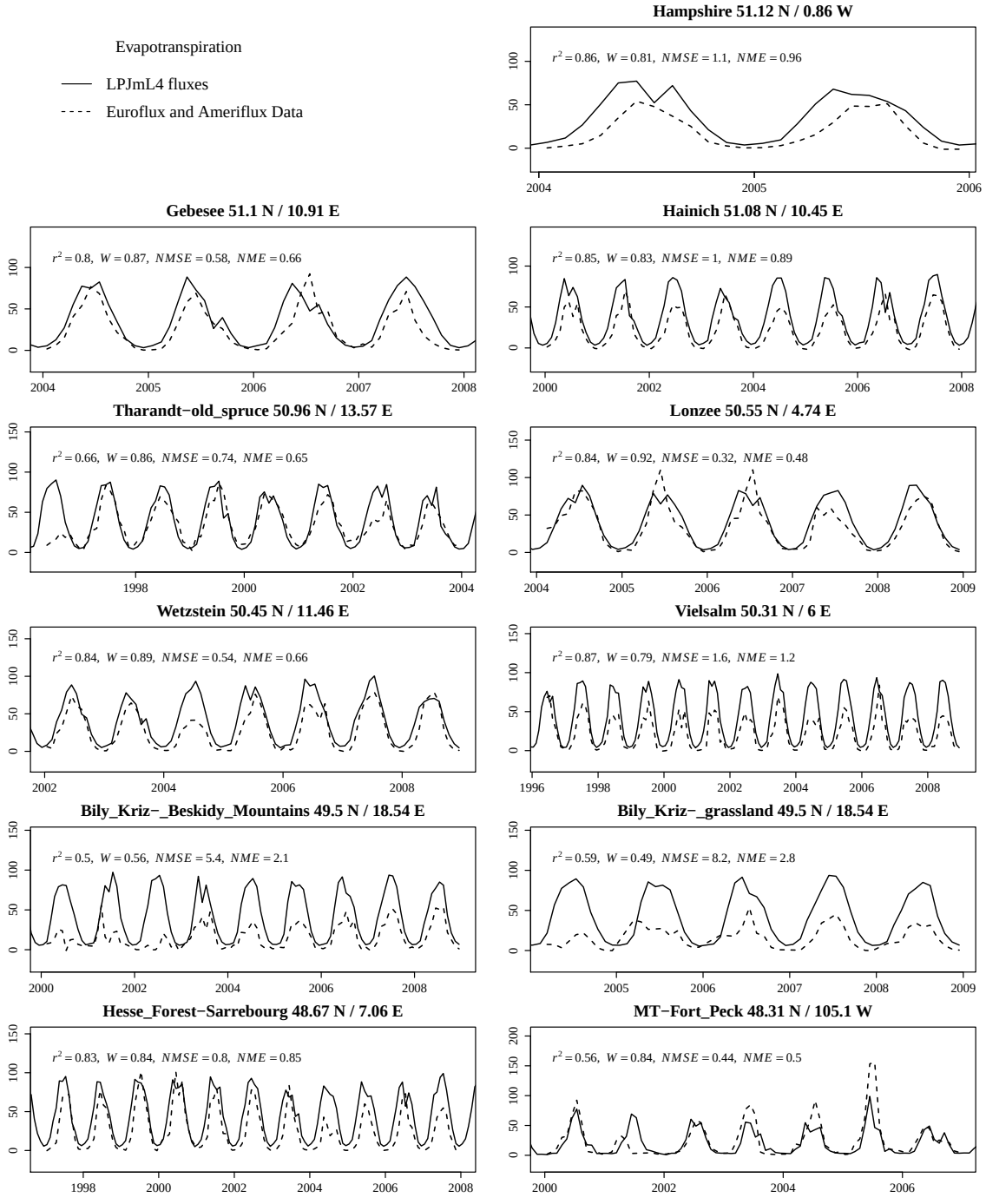

Figure S10. Comparison of Evapotranspiration fluxes with EDDY-flux measurements.

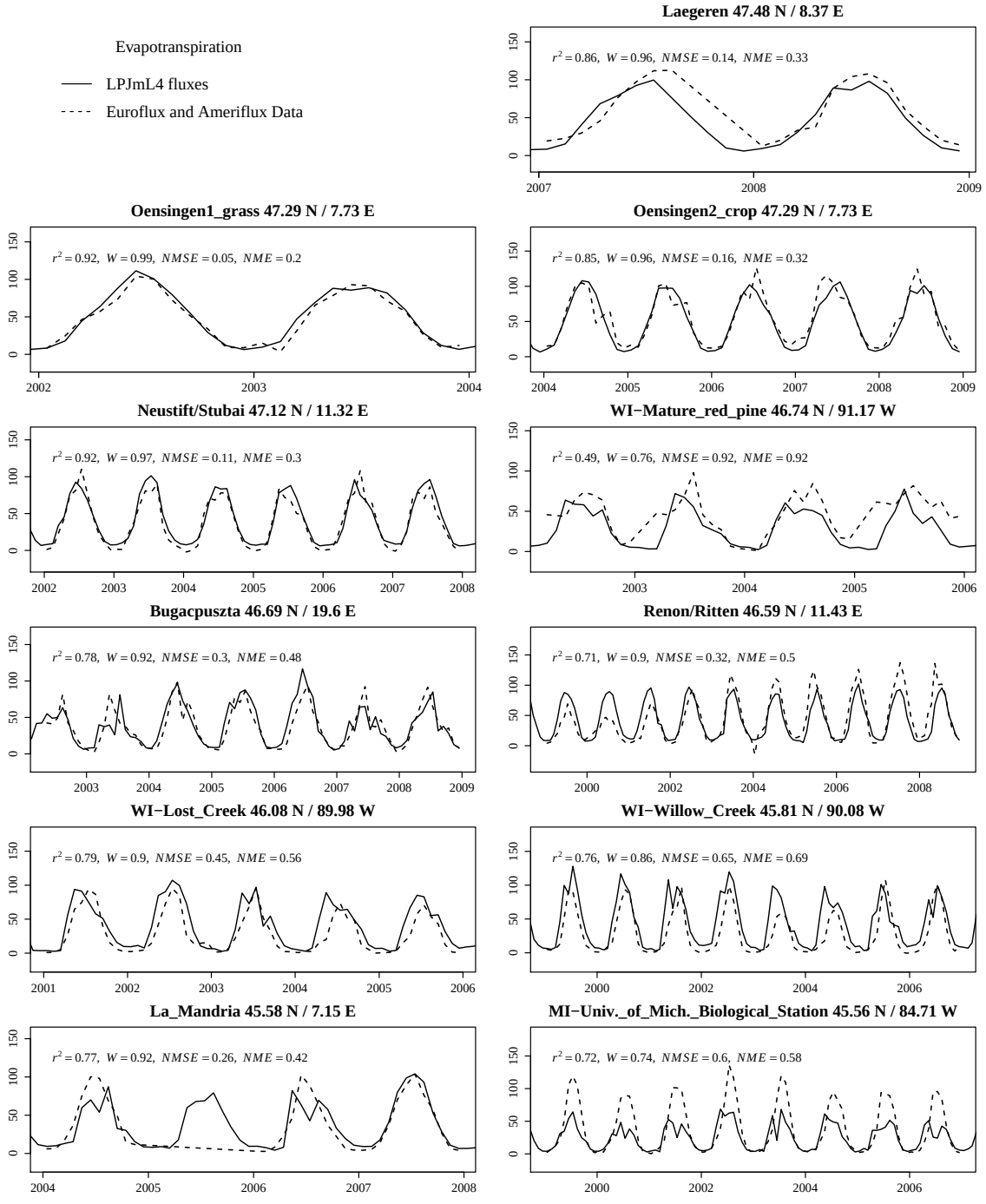

Figure S11. Comparison of Evapotranspiration fluxes with EDDY-flux measurements.

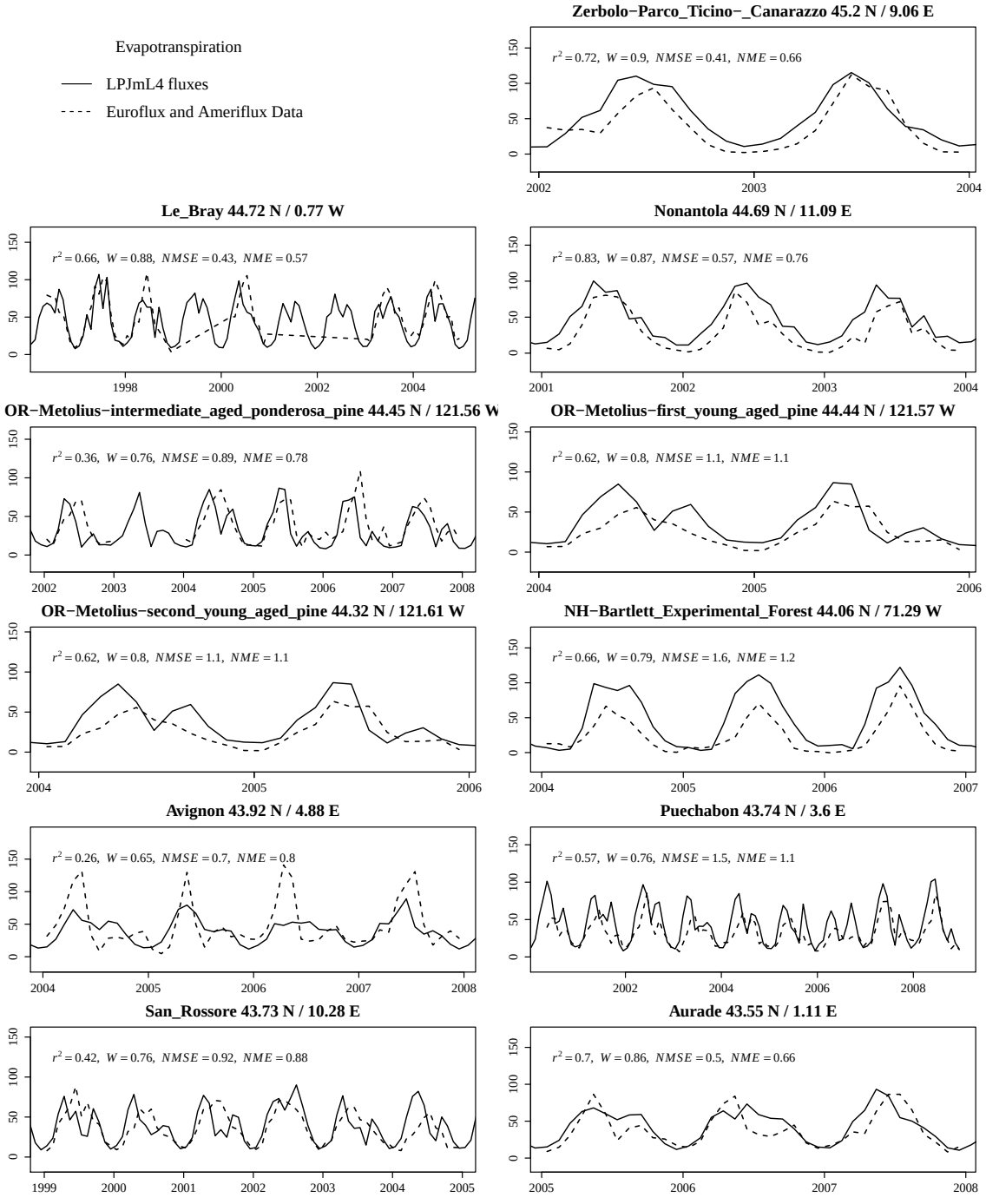

Figure S12. Comparison of Evapotranspiration fluxes with EDDY-flux measurements.

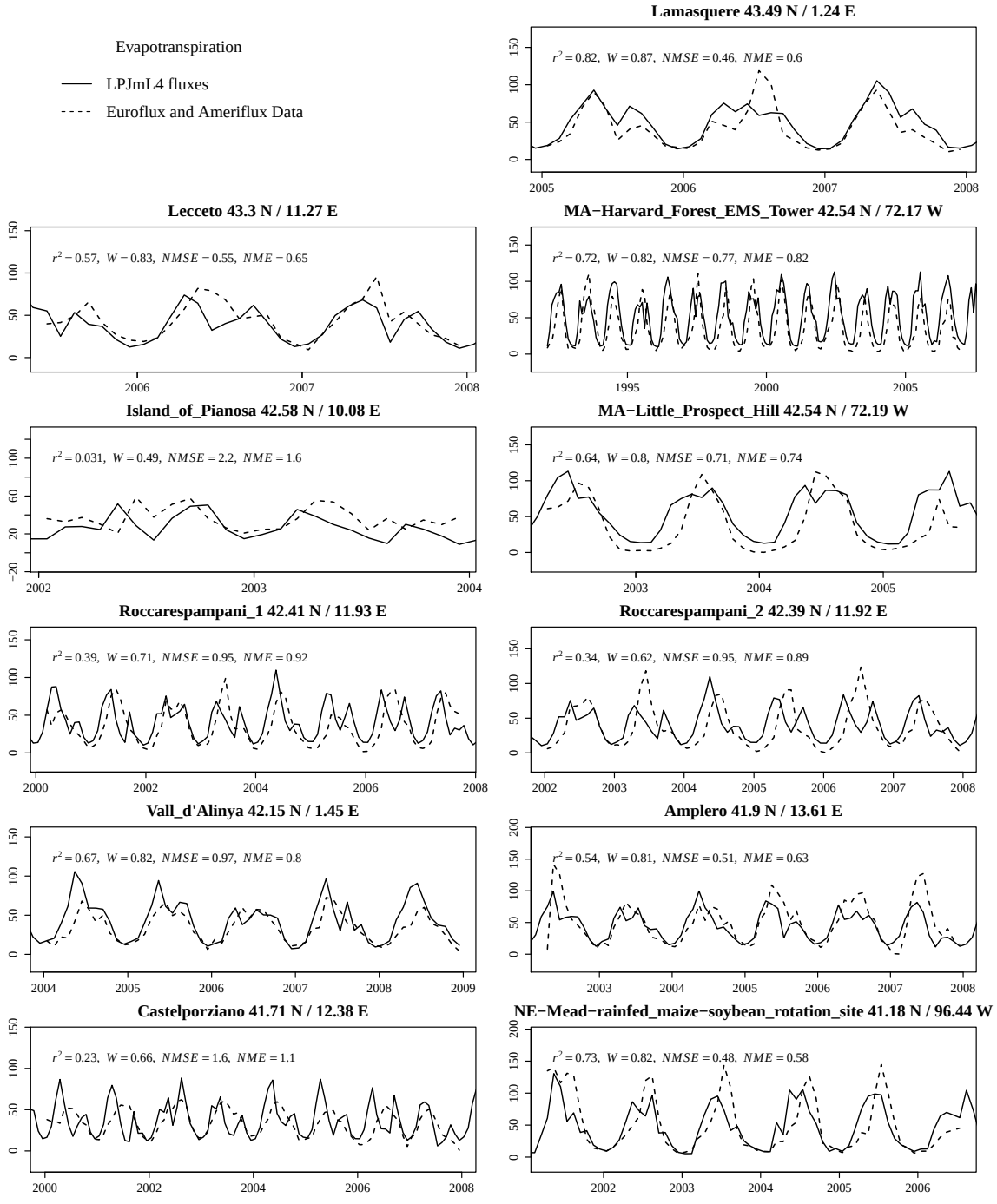

Figure S13. Comparison of Evapotranspiration fluxes with EDDY-flux measurements.

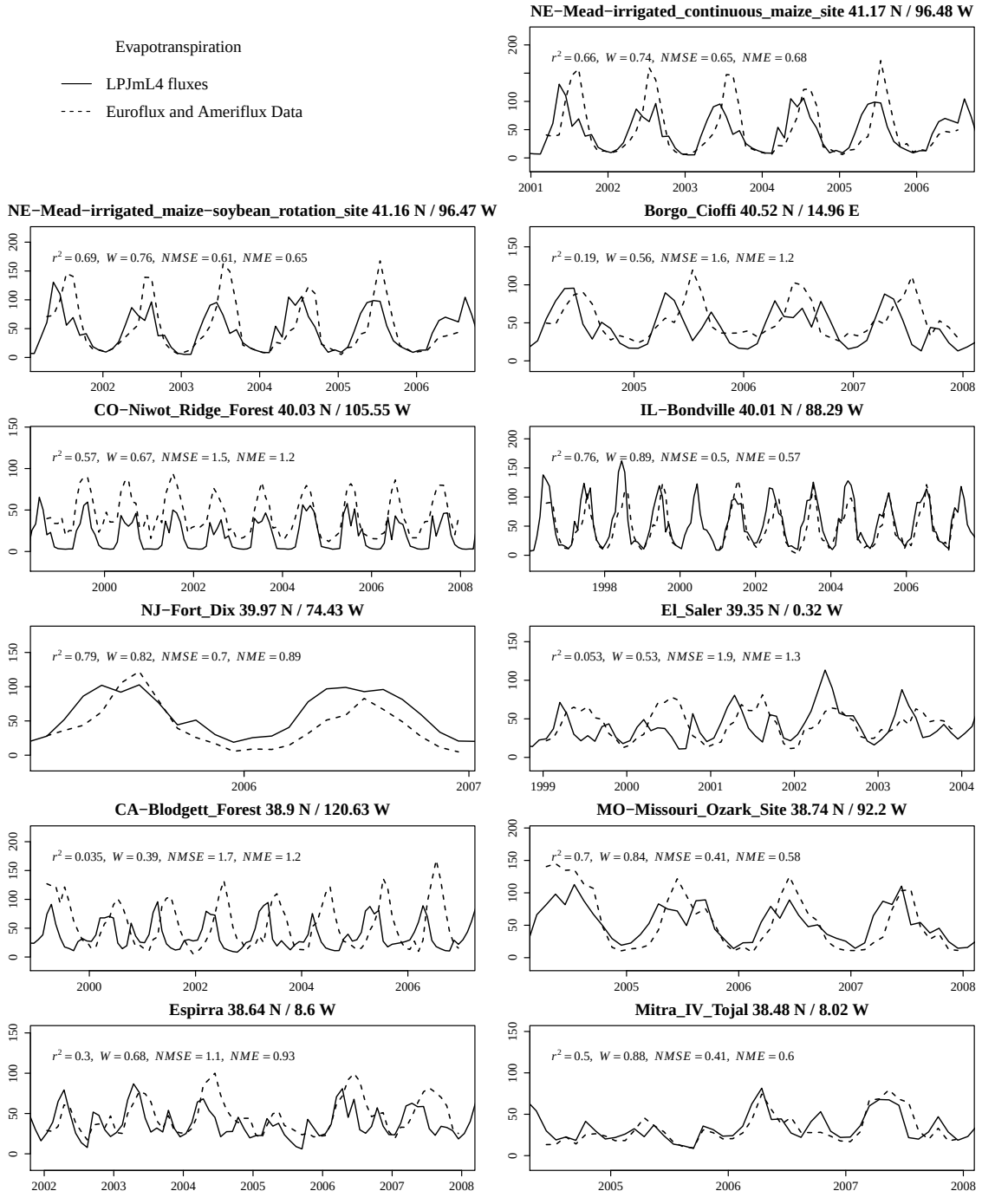

Figure S14. Comparison of Evapotranspiration fluxes with EDDY-flux measurements.

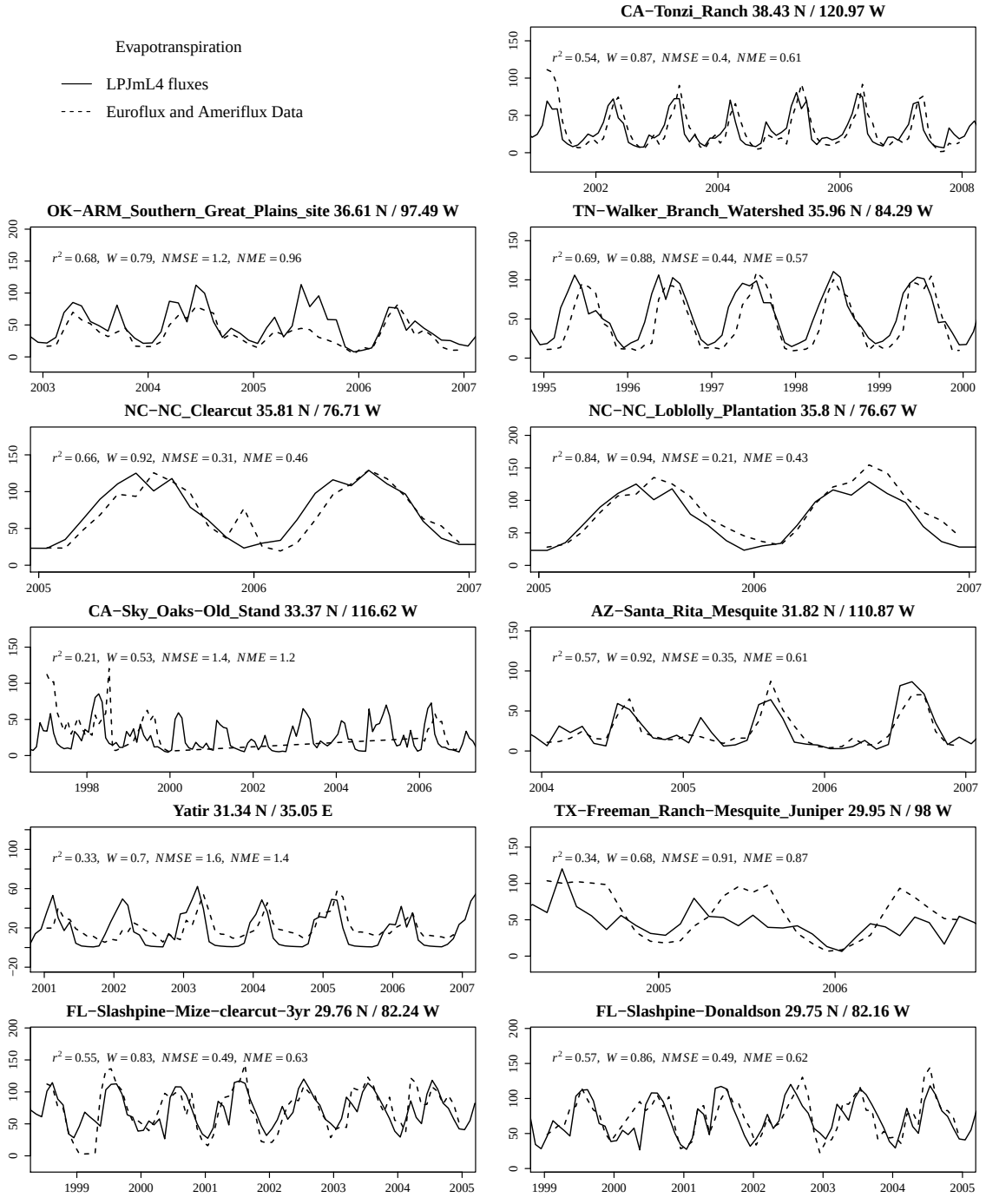

Figure S15. Comparison of Evapotranspiration fluxes with EDDY-flux measurements.

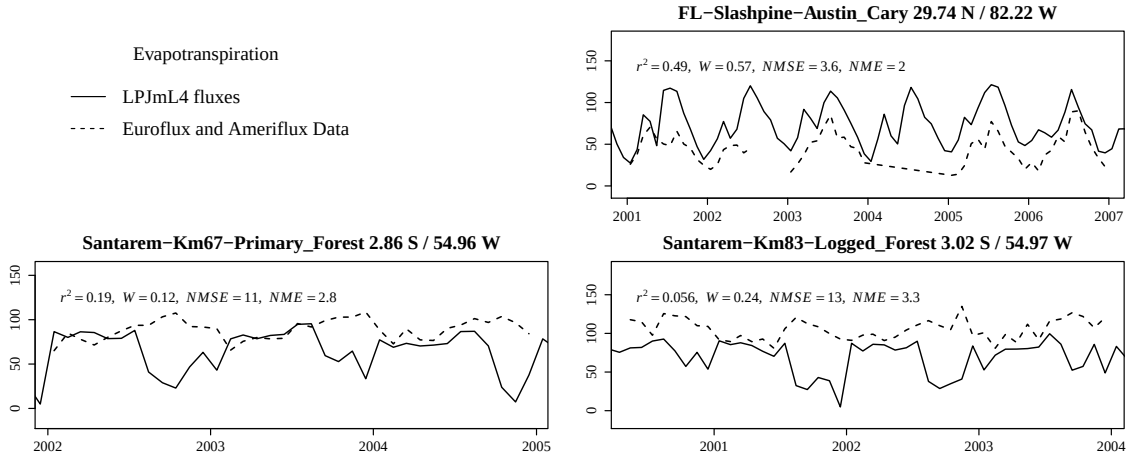

Figure S16. Comparison of Evapotranspiration fluxes with EDDY-flux measurements.

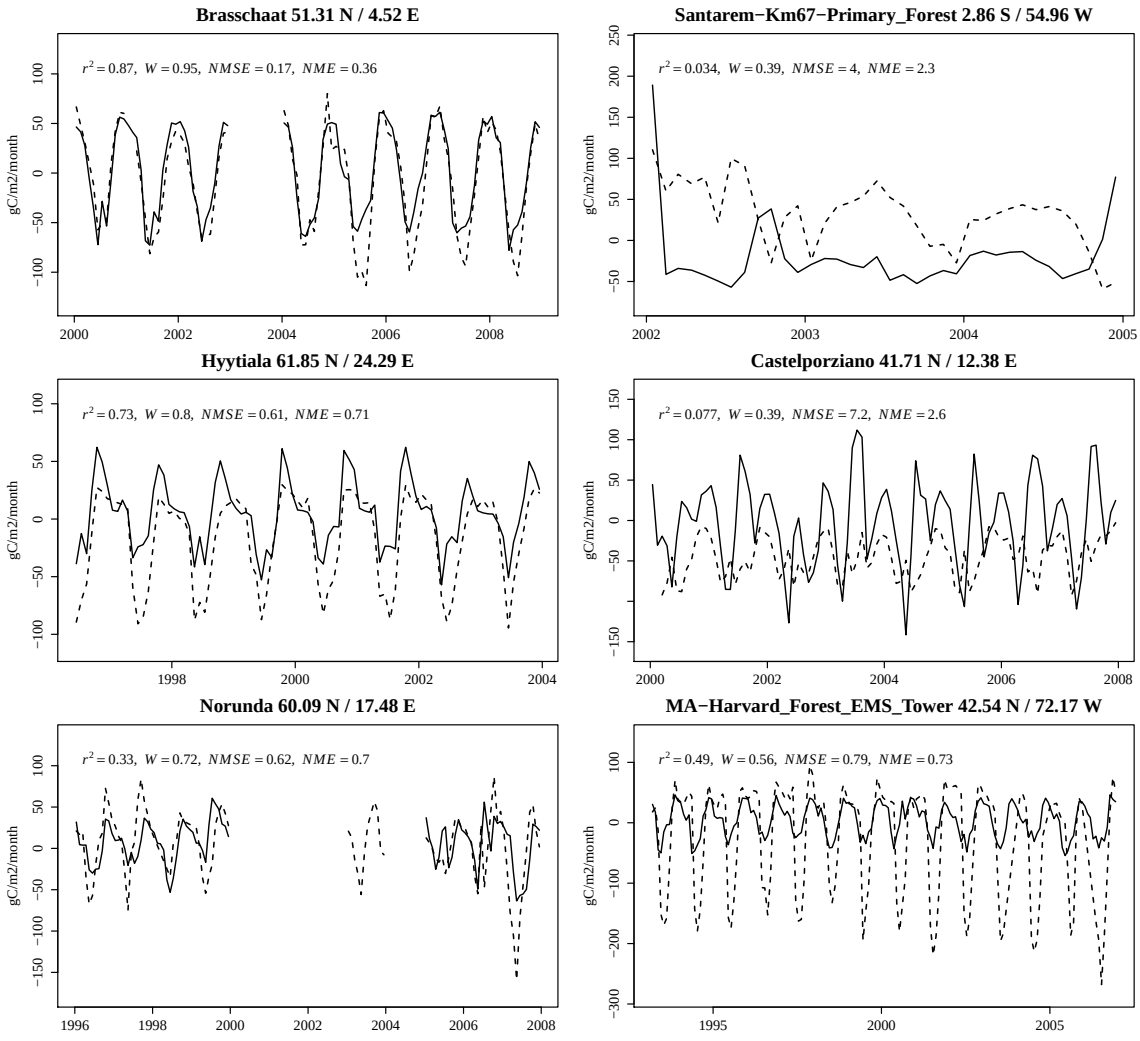

Figure S17. Comparison of NEE fluxes with EDDY-flux measurements driven by site specific meteorological data.

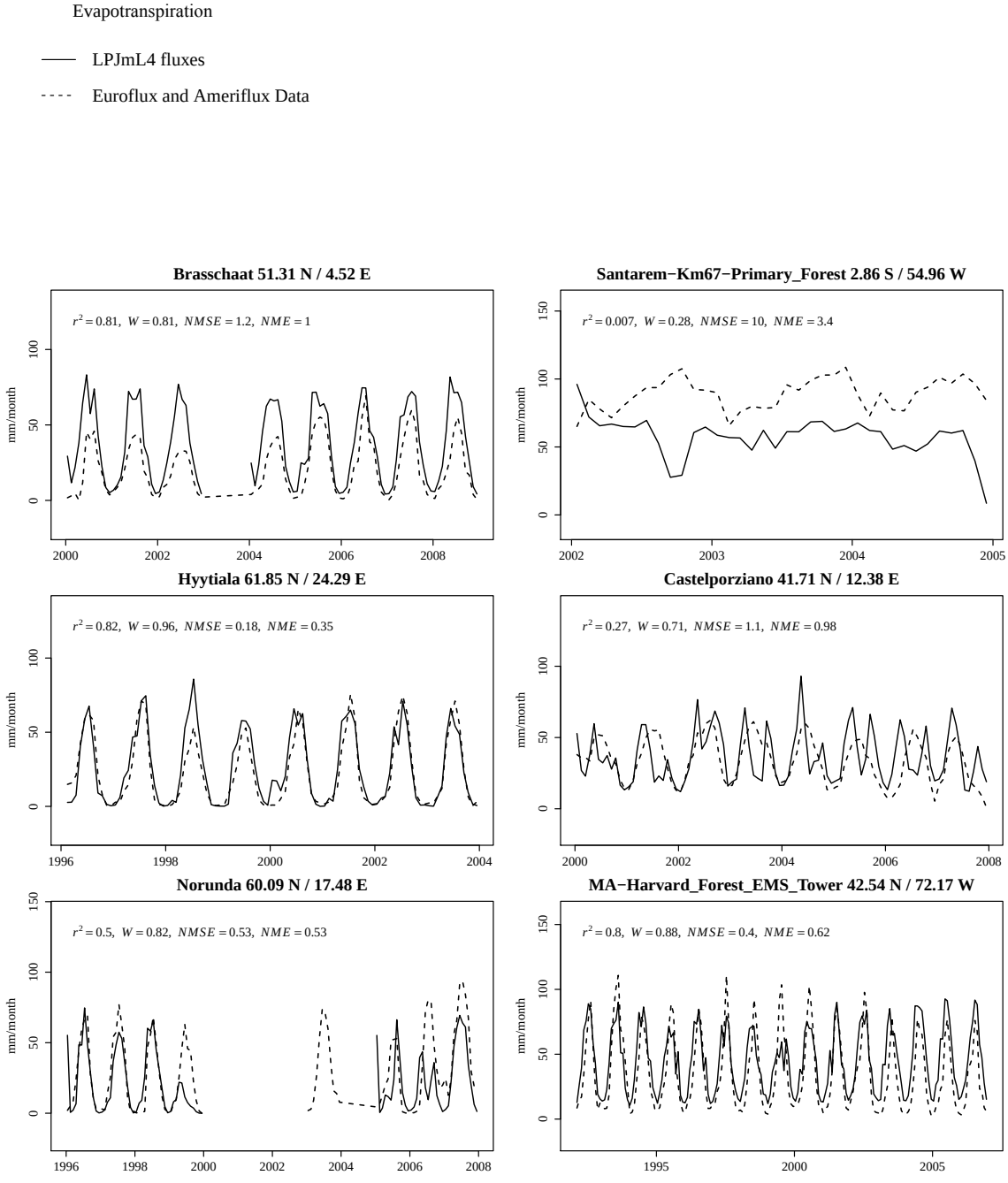

Figure S18. Comparison of Evapotranspiration fluxes with EDDY-flux measurements driven by site specific meteorological data.

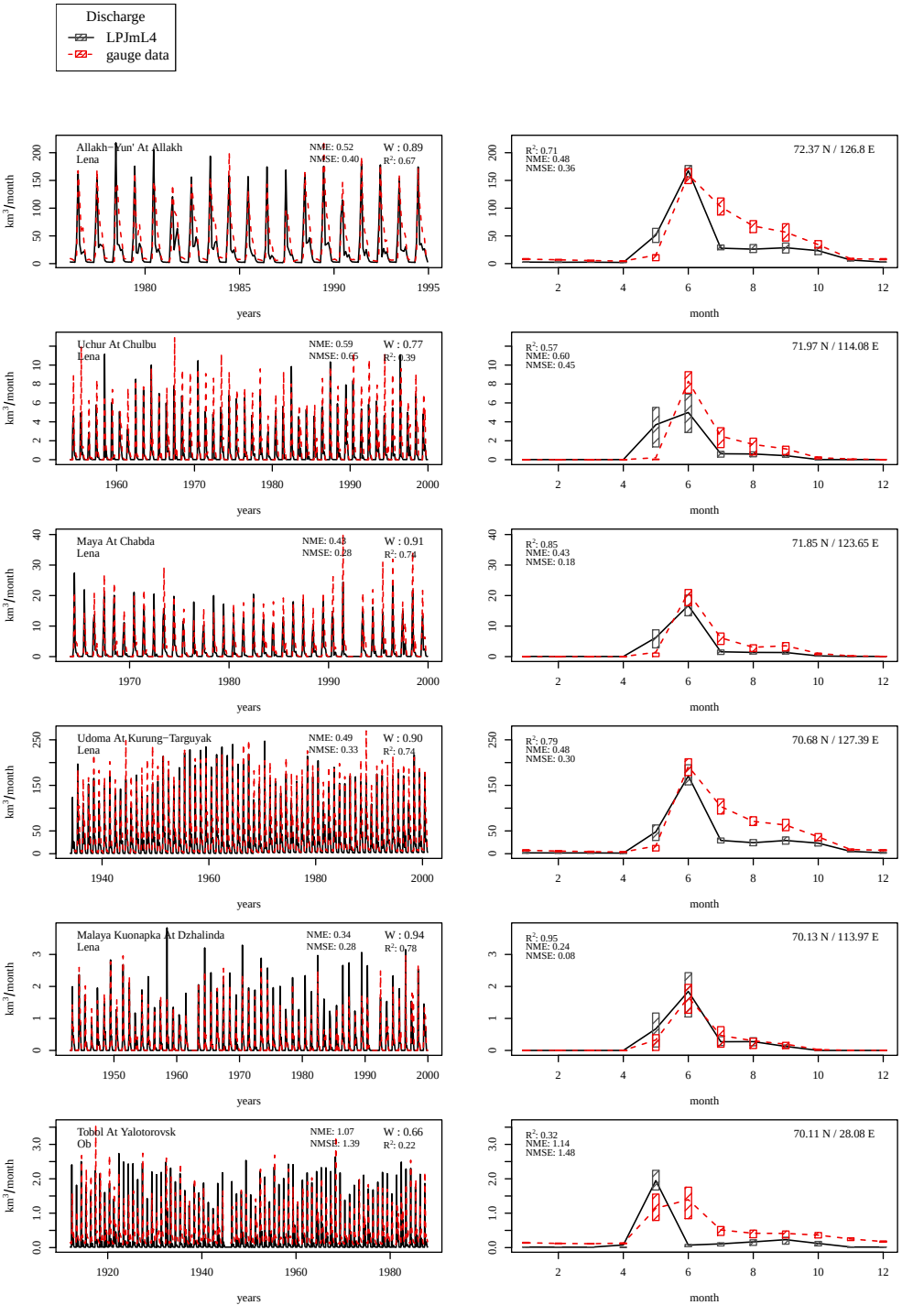

Figure S19. Evaluation of river discharge at gauging stations [1].

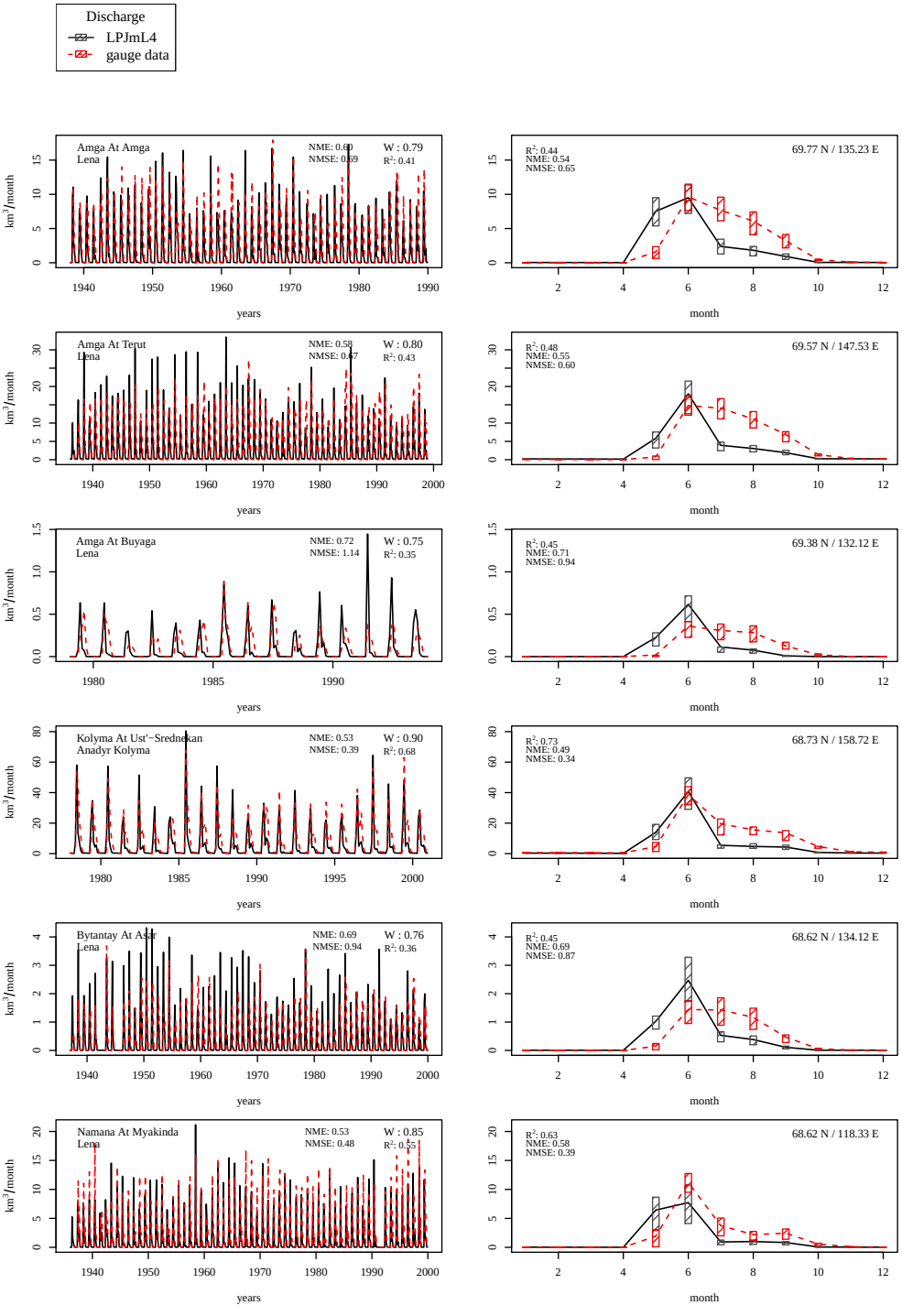

Figure S20. Evaluation of river discharge at gauging stations [2].

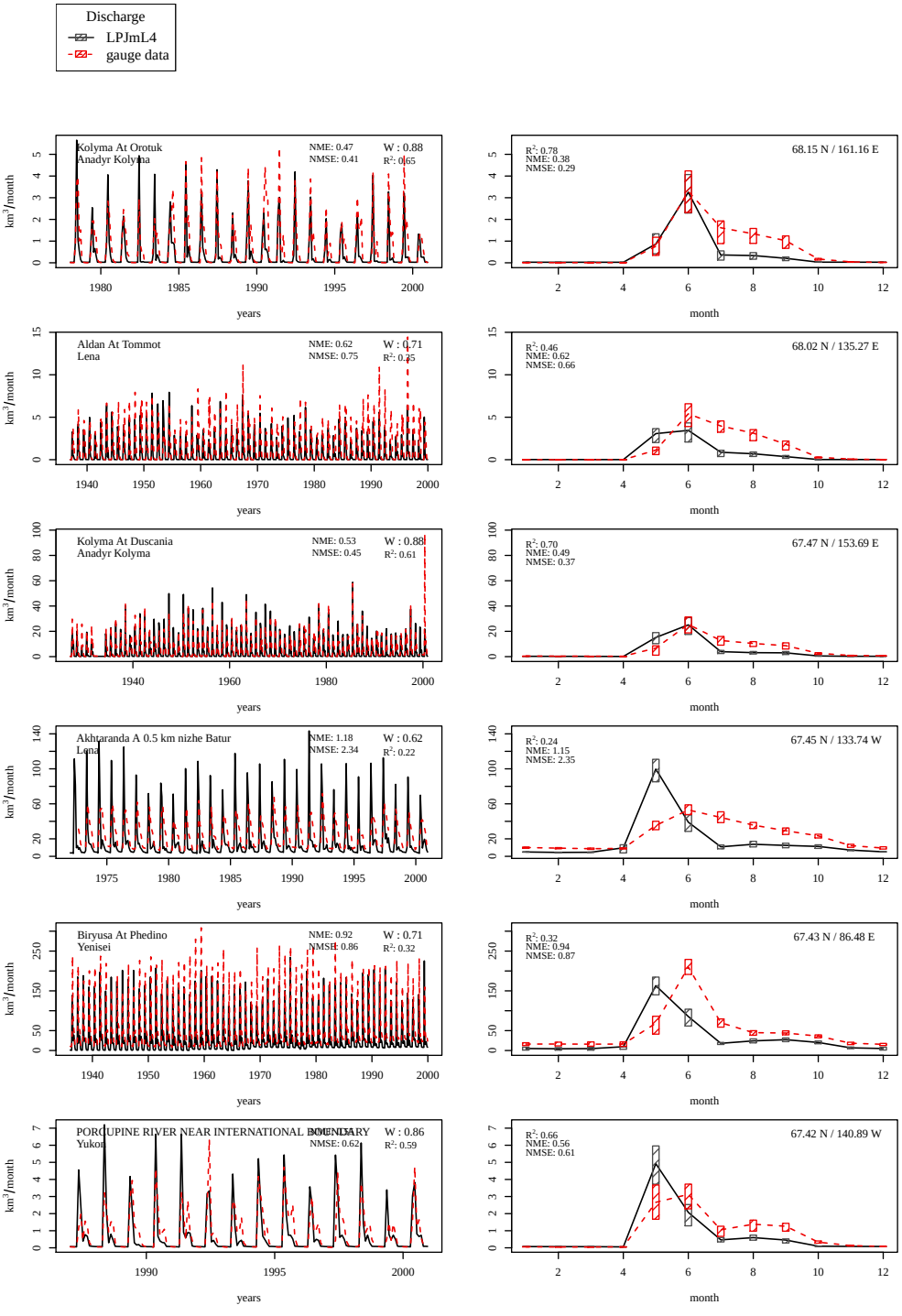

Figure S21. Evaluation of river discharge at gauging stations [3].

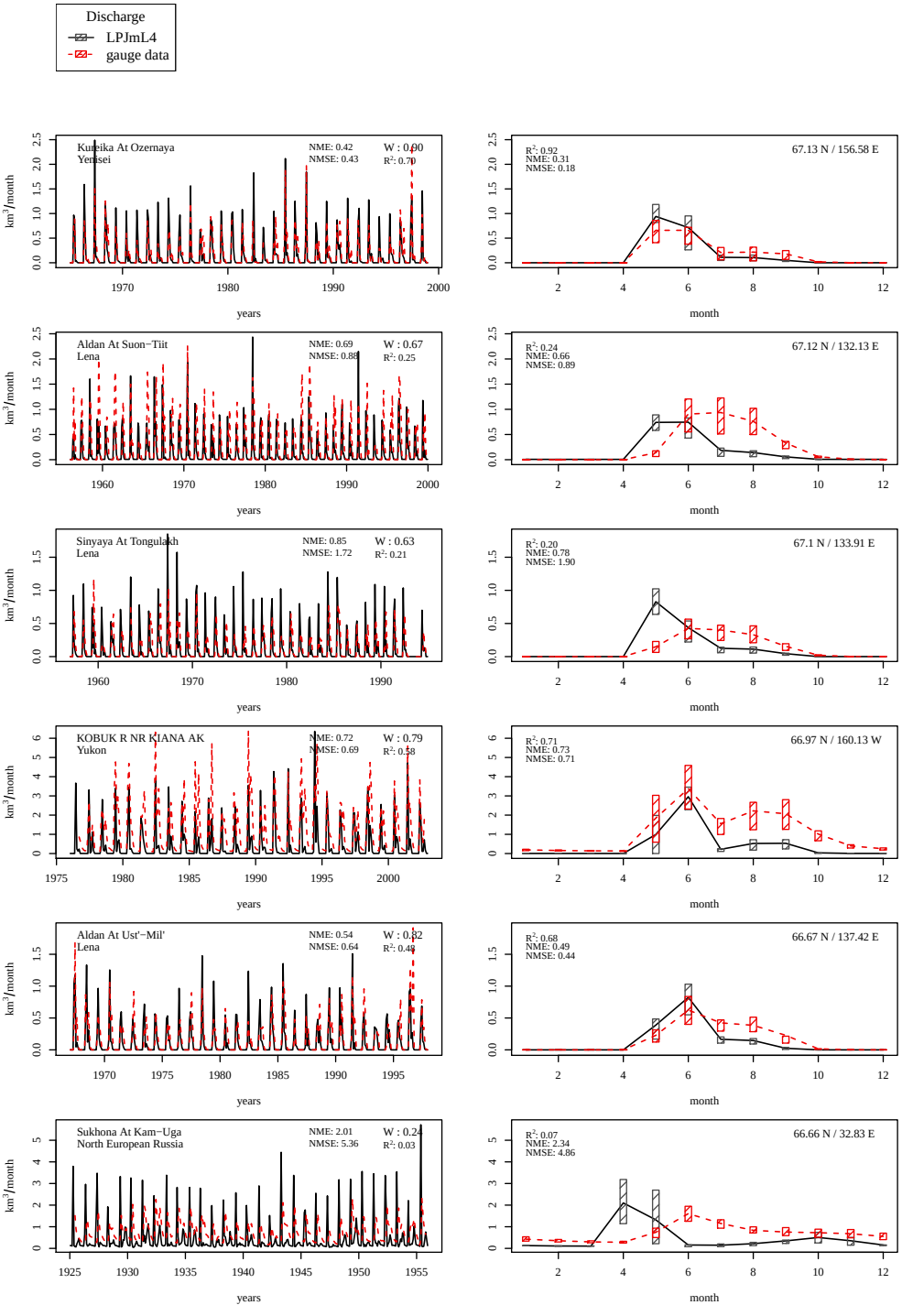

Figure S22. Evaluation of river discharge at gauging stations [4].

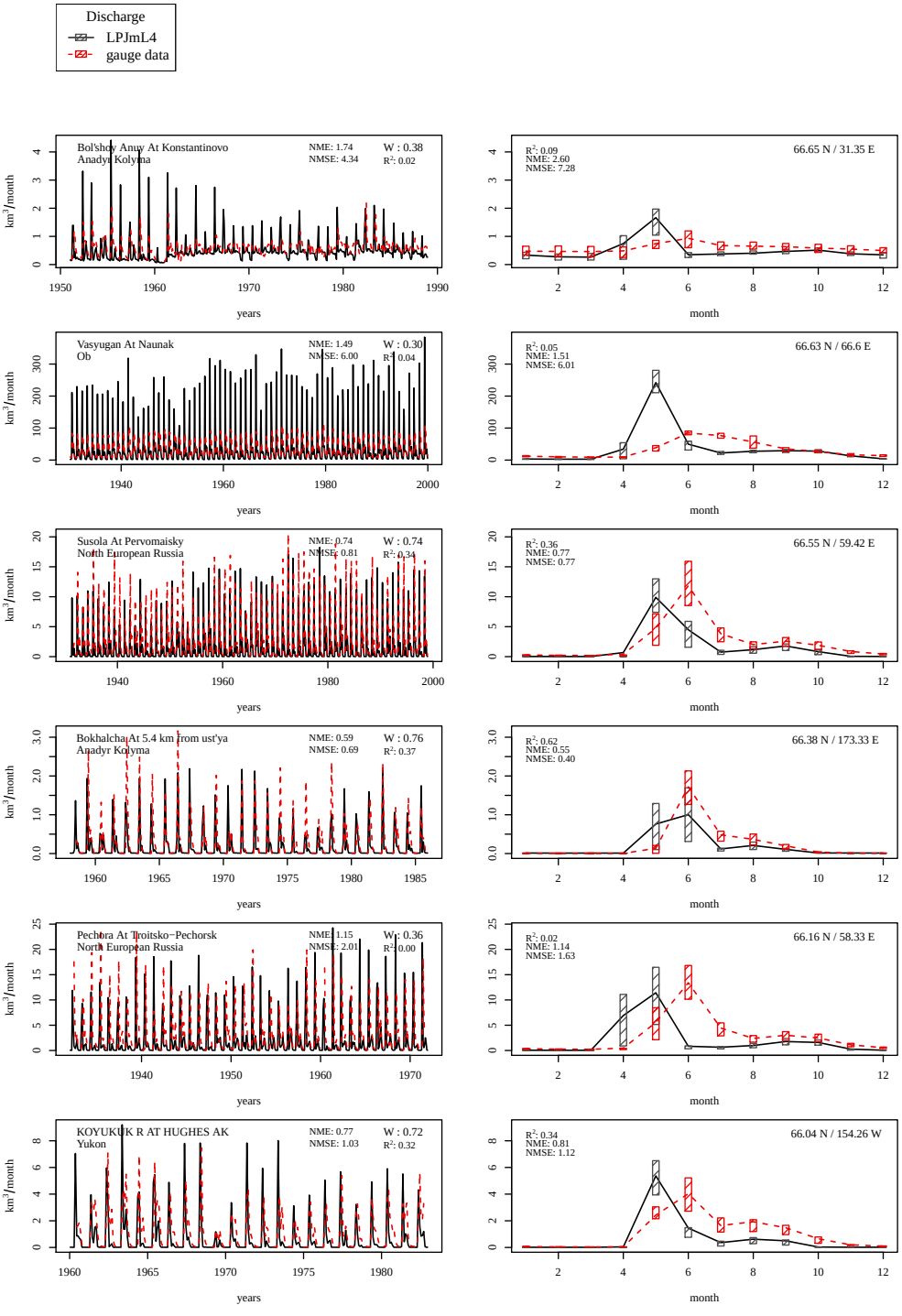

Figure S23. Evaluation of river discharge at gauging stations [5].

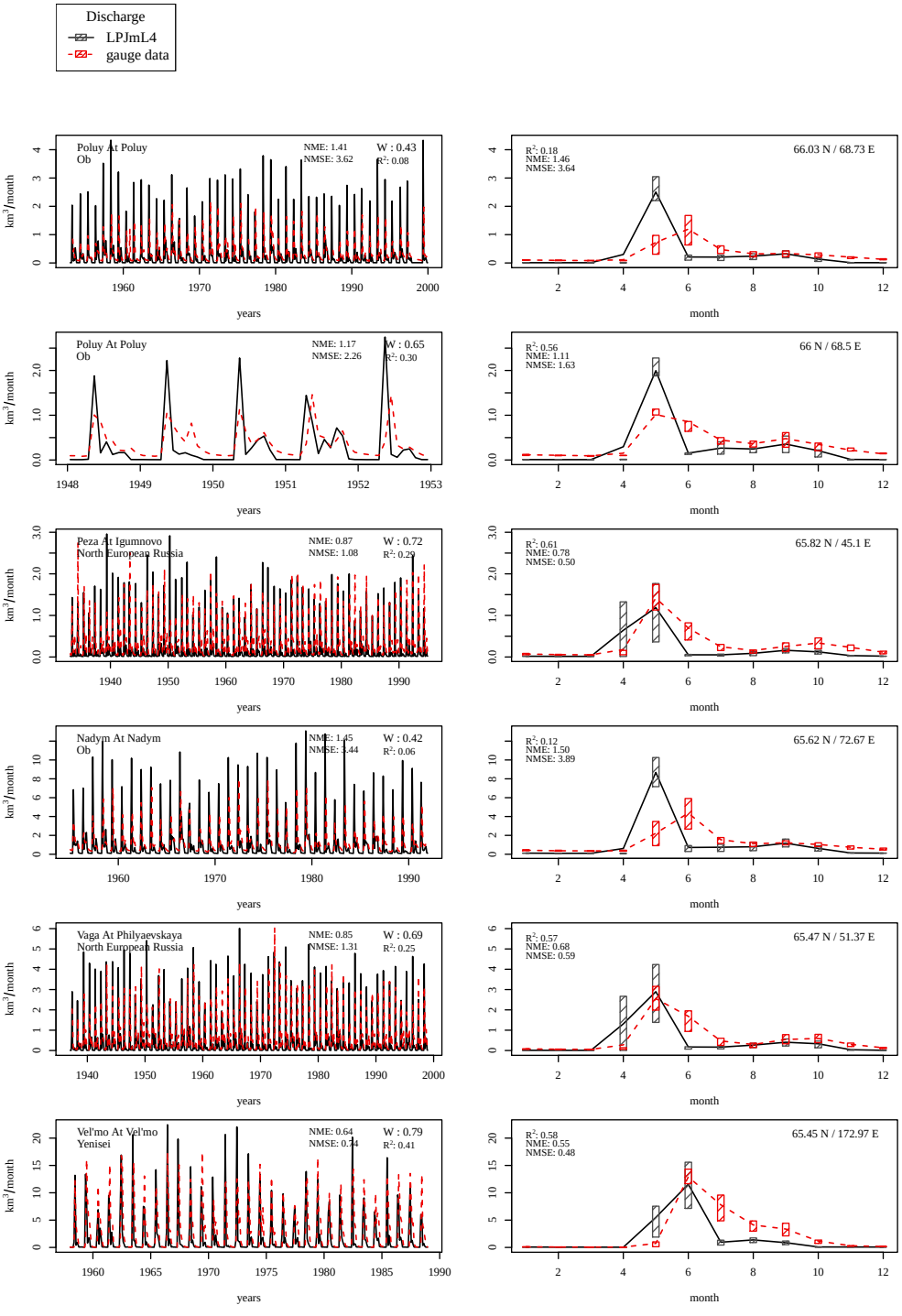

Figure S24. Evaluation of river discharge at gauging stations [6].

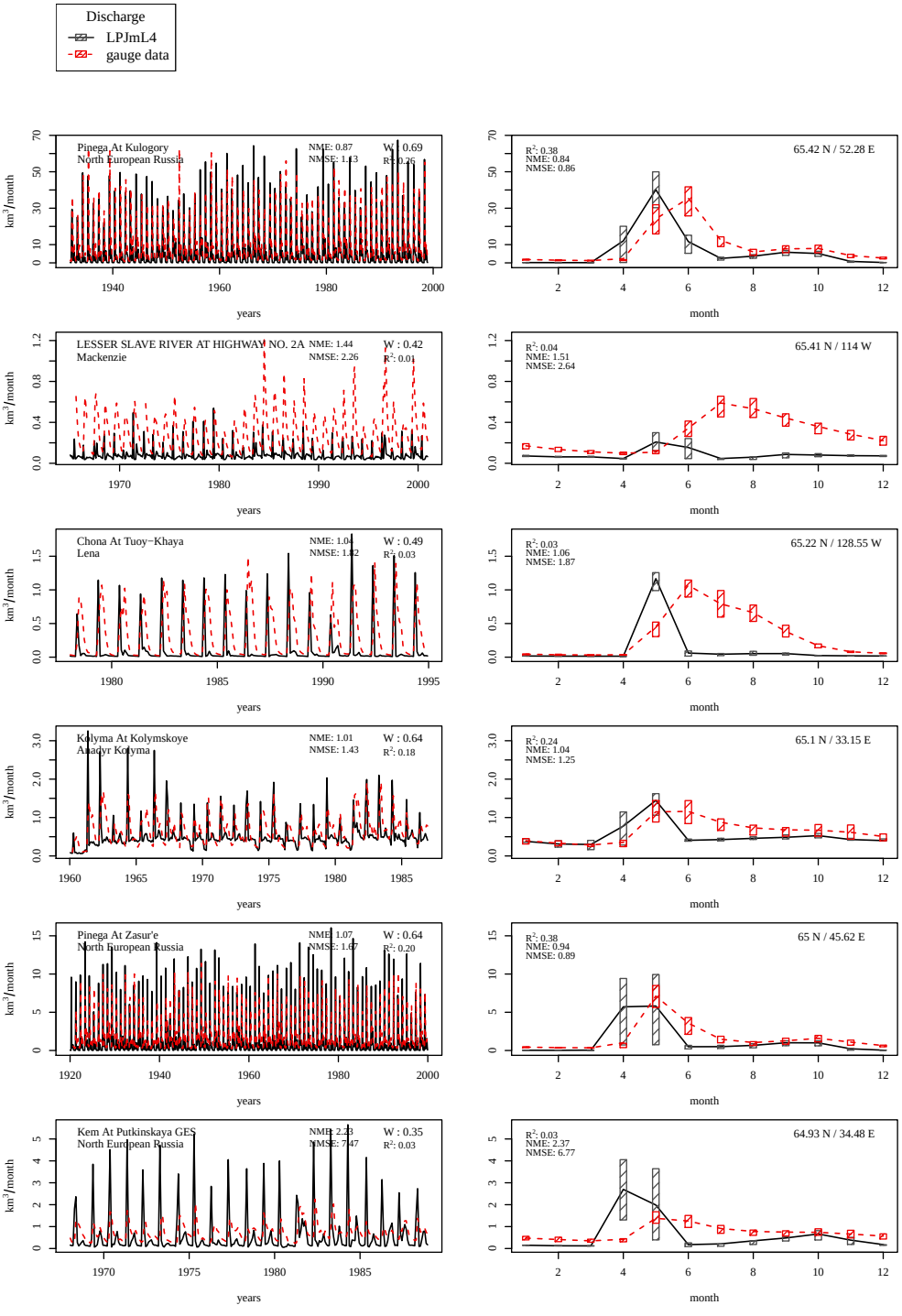

Figure S25. Evaluation of river discharge at gauging stations [7].

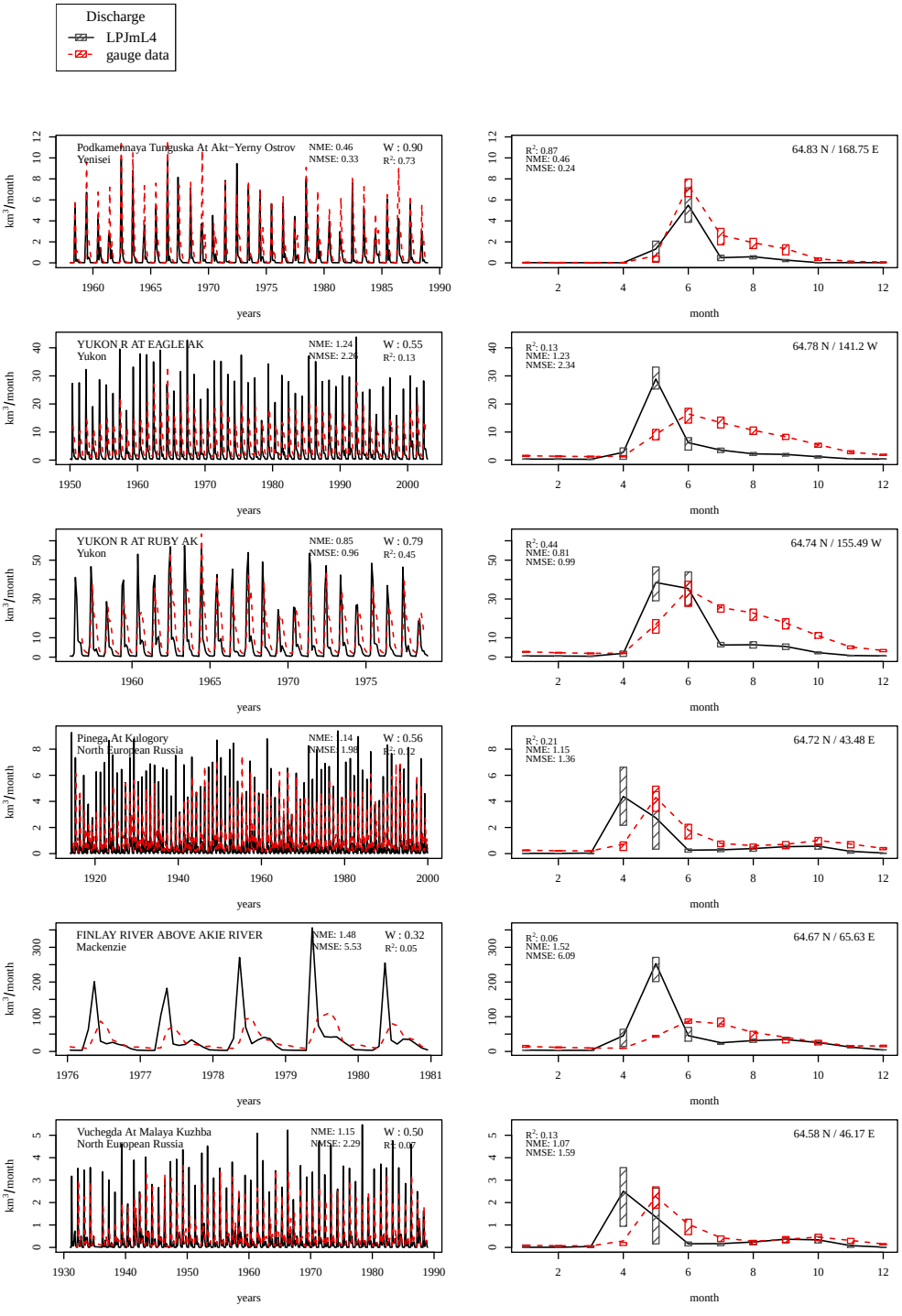

Figure S26. Evaluation of river discharge at gauging stations [8].

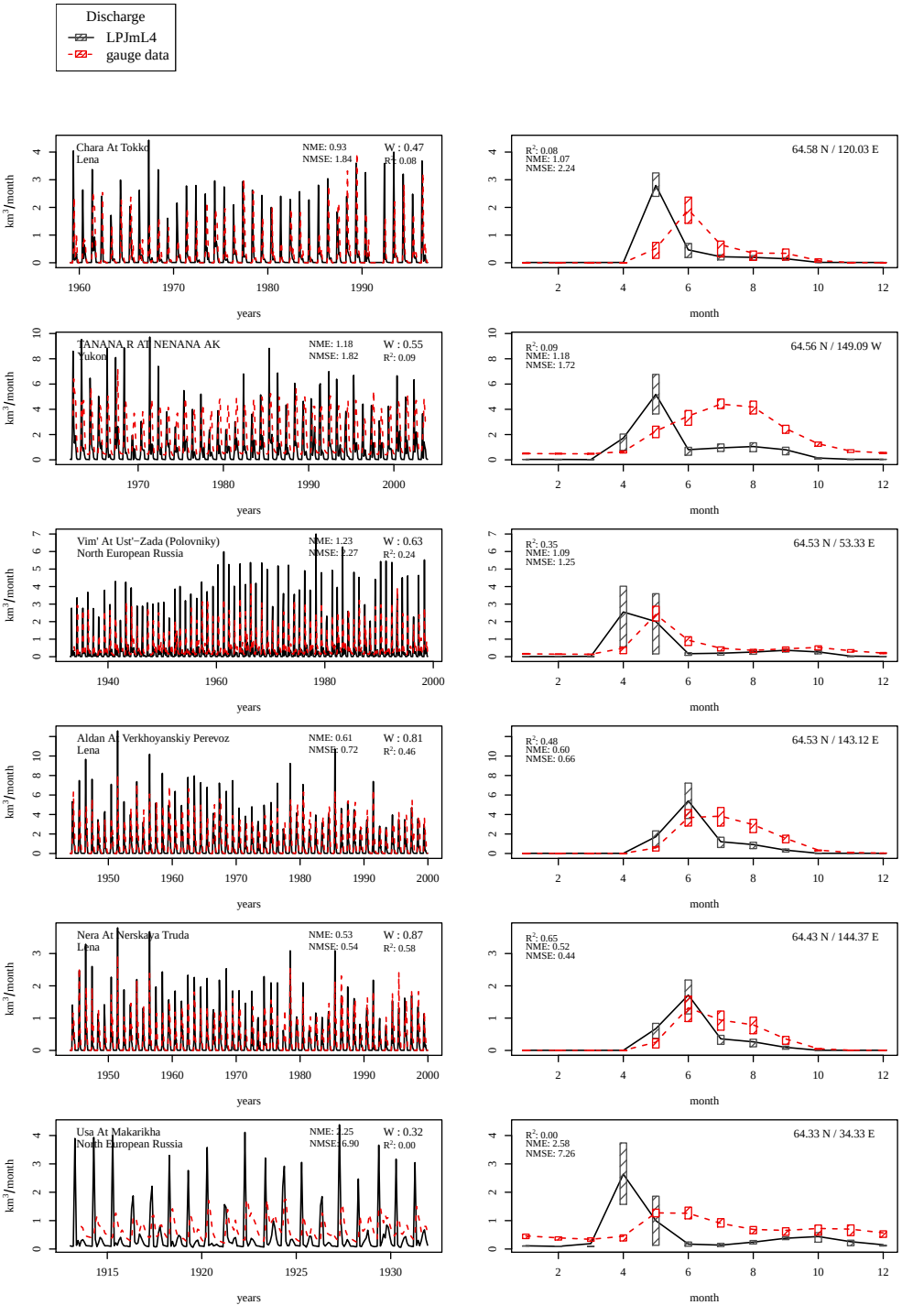

Figure S27. Evaluation of river discharge at gauging stations [9].

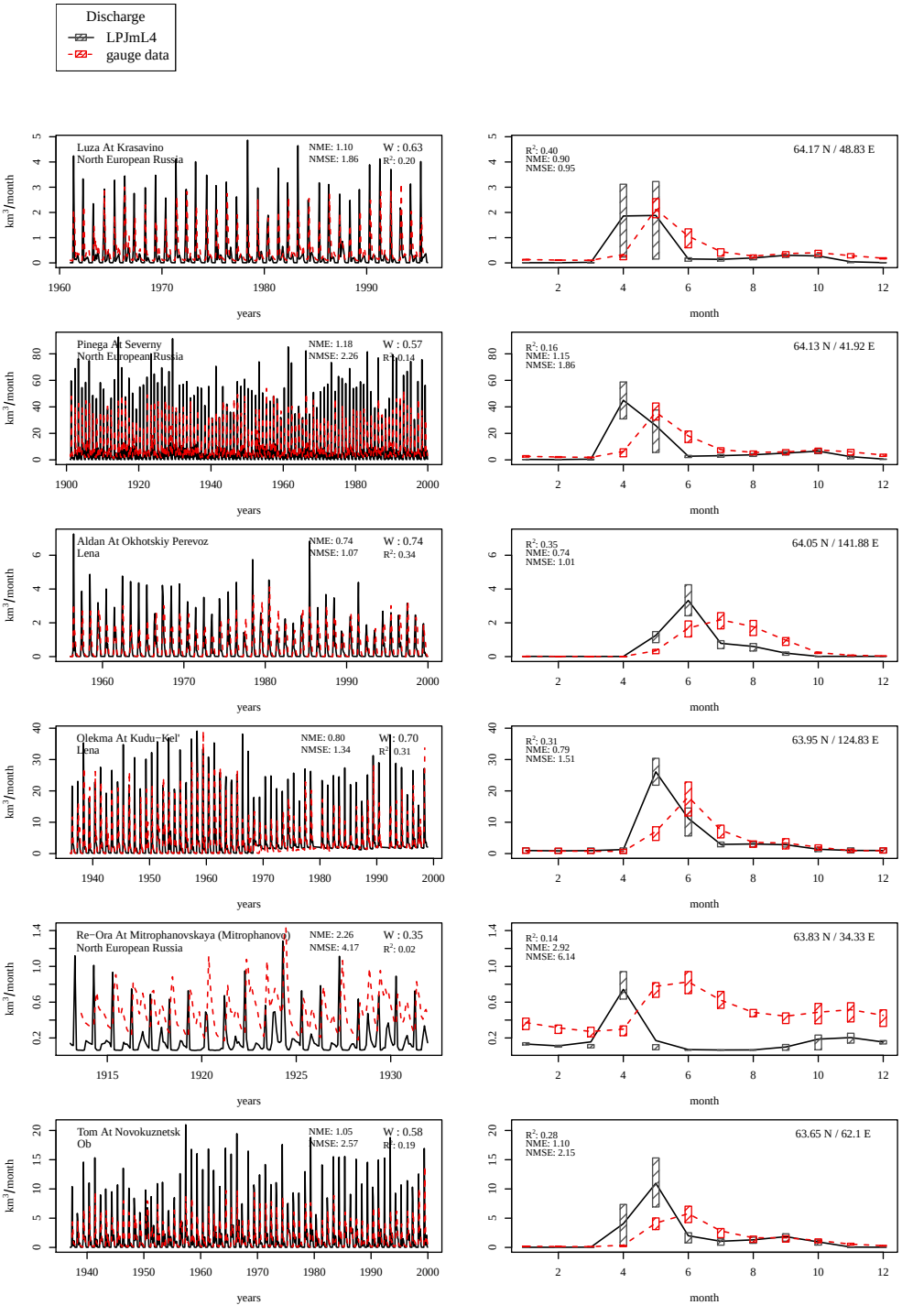

Figure S28. Evaluation of river discharge at gauging stations [10].

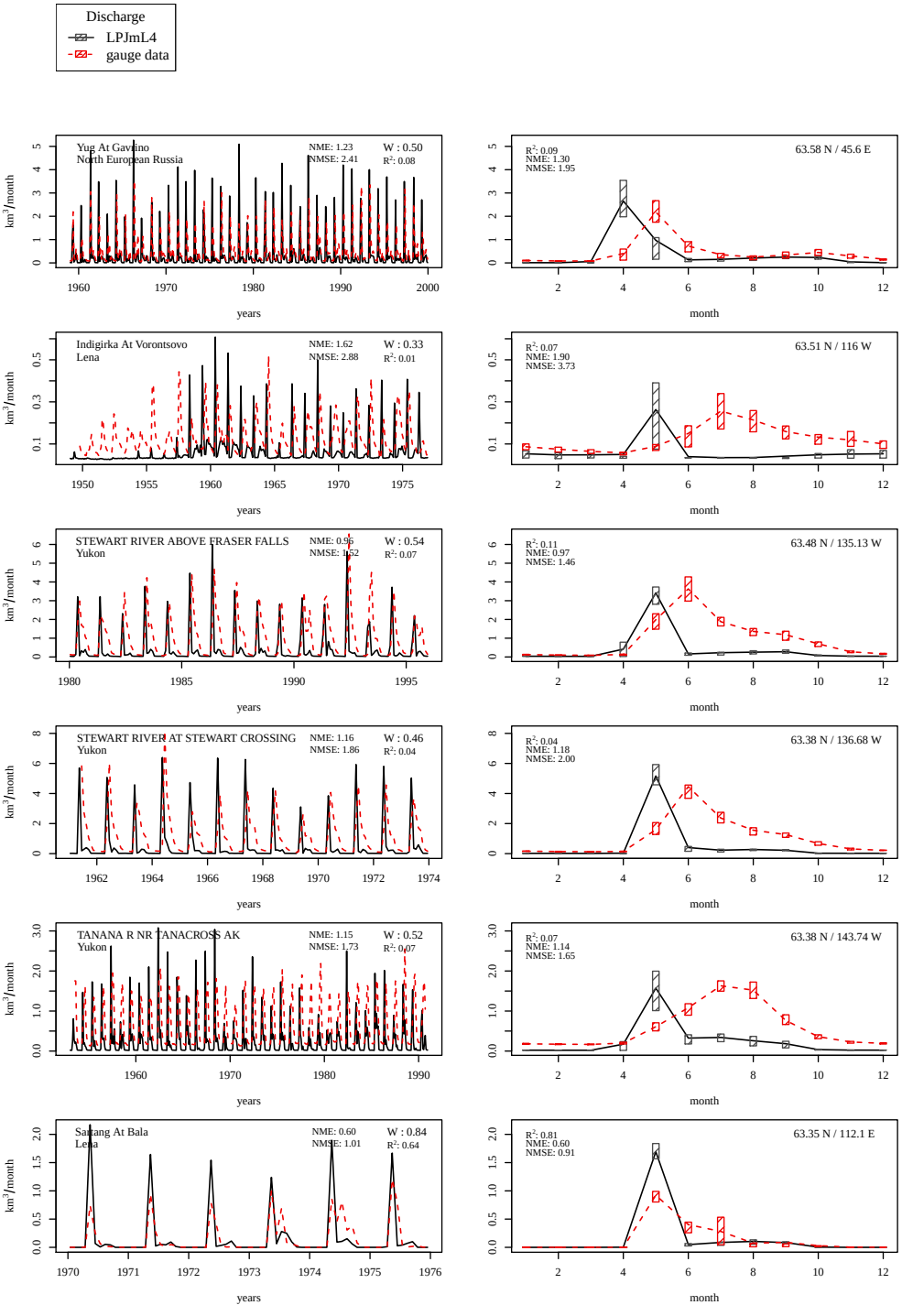

Figure S29. Evaluation of river discharge at gauging stations [11].

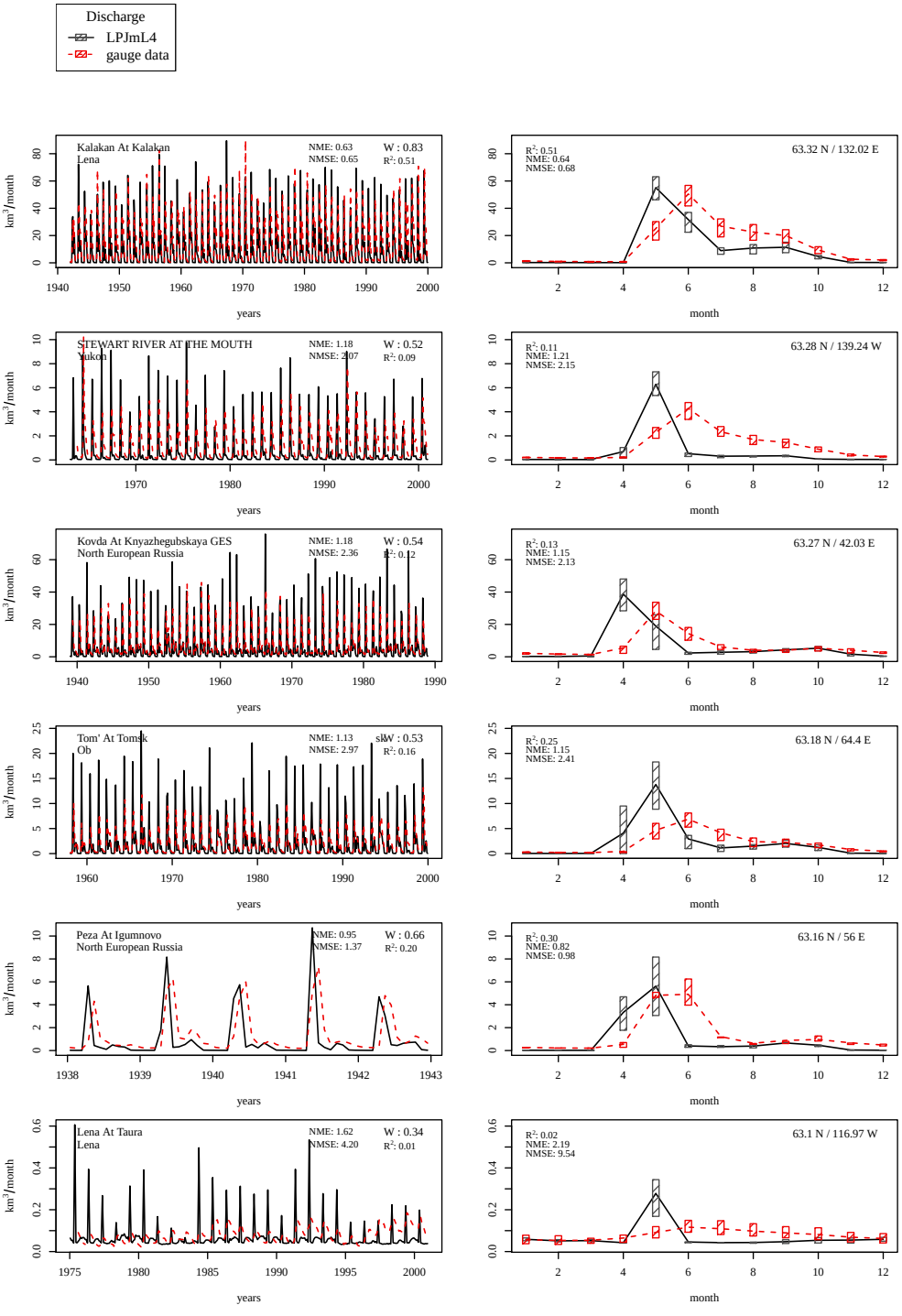

Figure S30. Evaluation of river discharge at gauging stations [12].

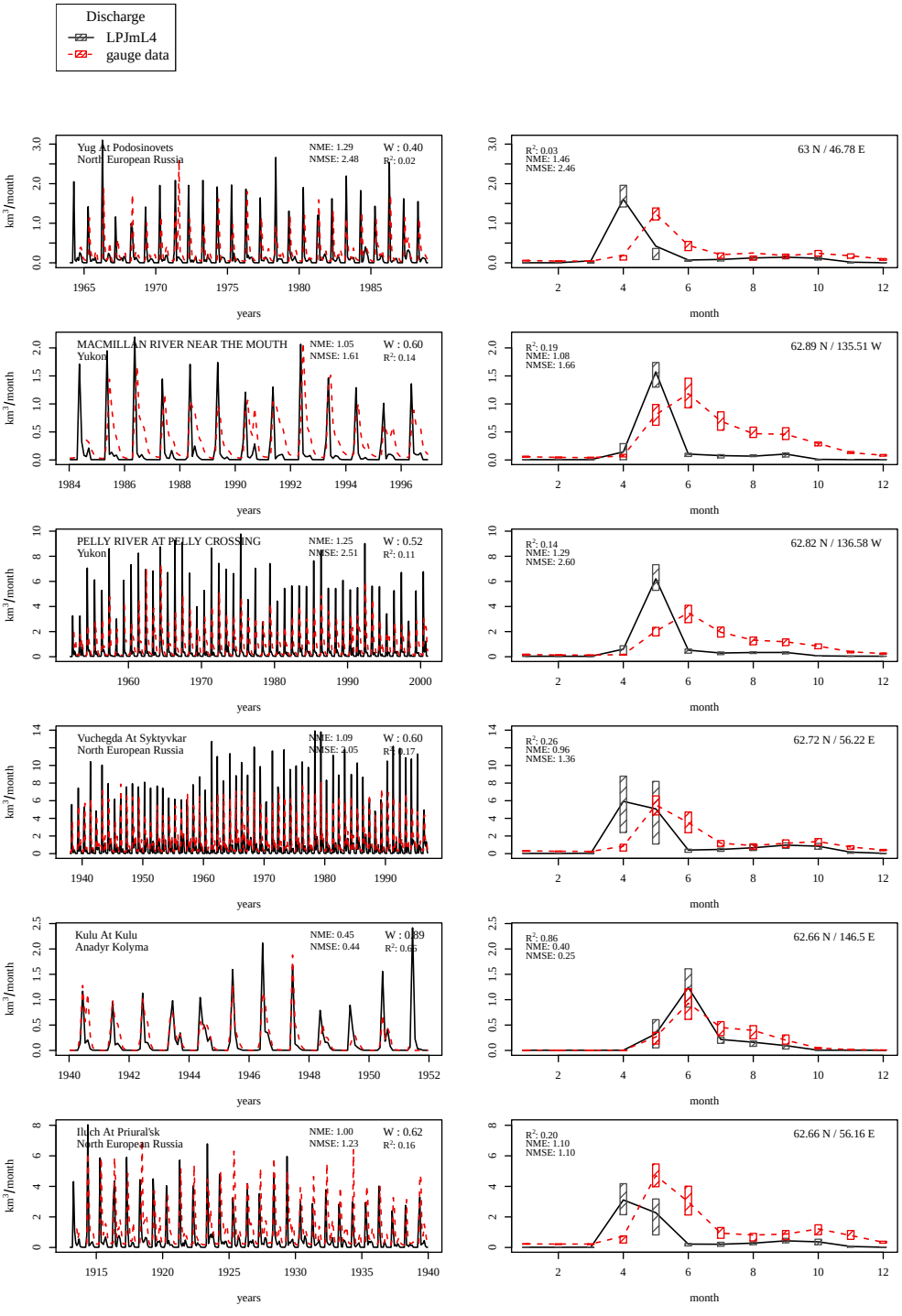

Figure S31. Evaluation of river discharge at gauging stations [13].

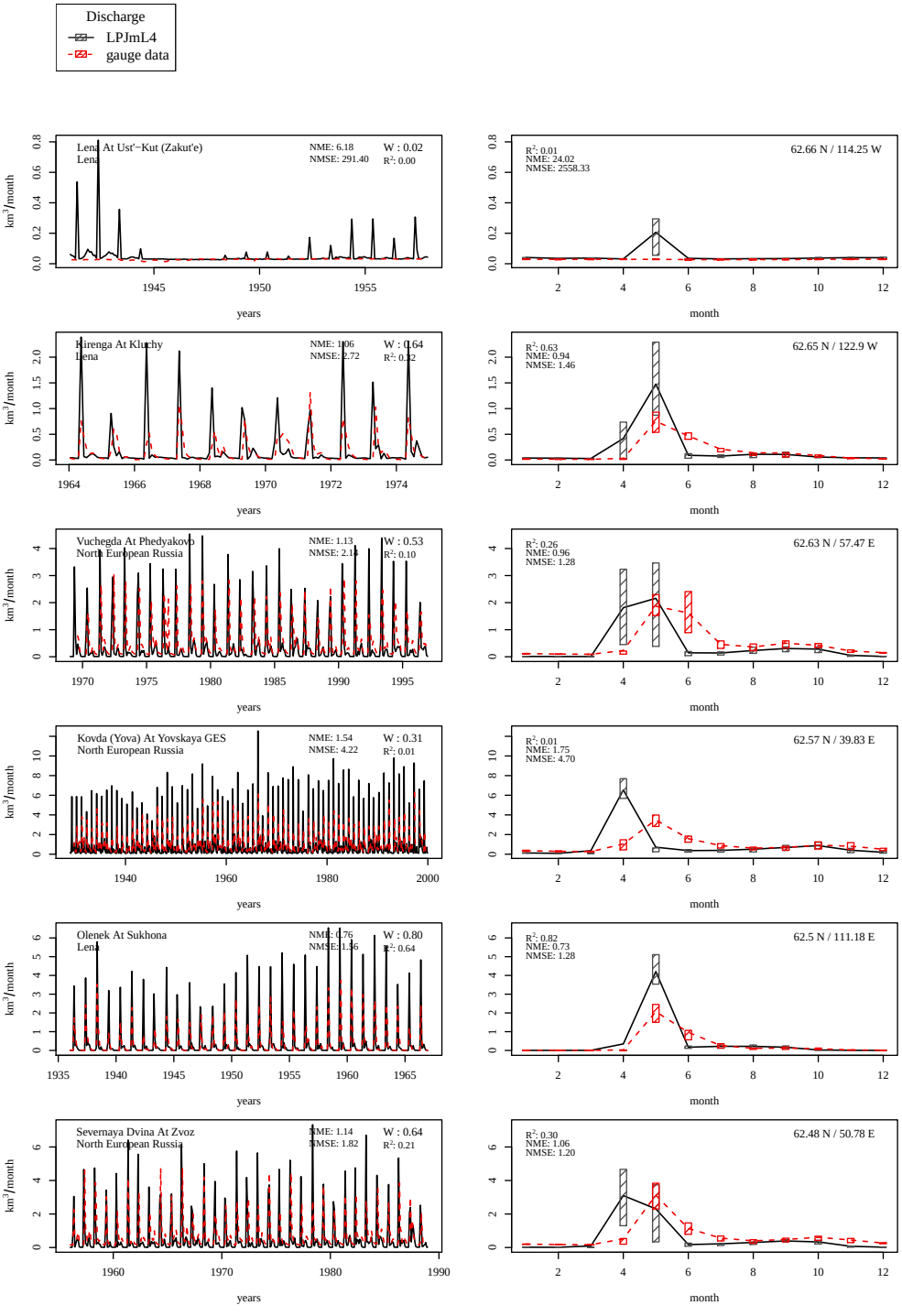

Figure S32. Evaluation of river discharge at gauging stations [14].

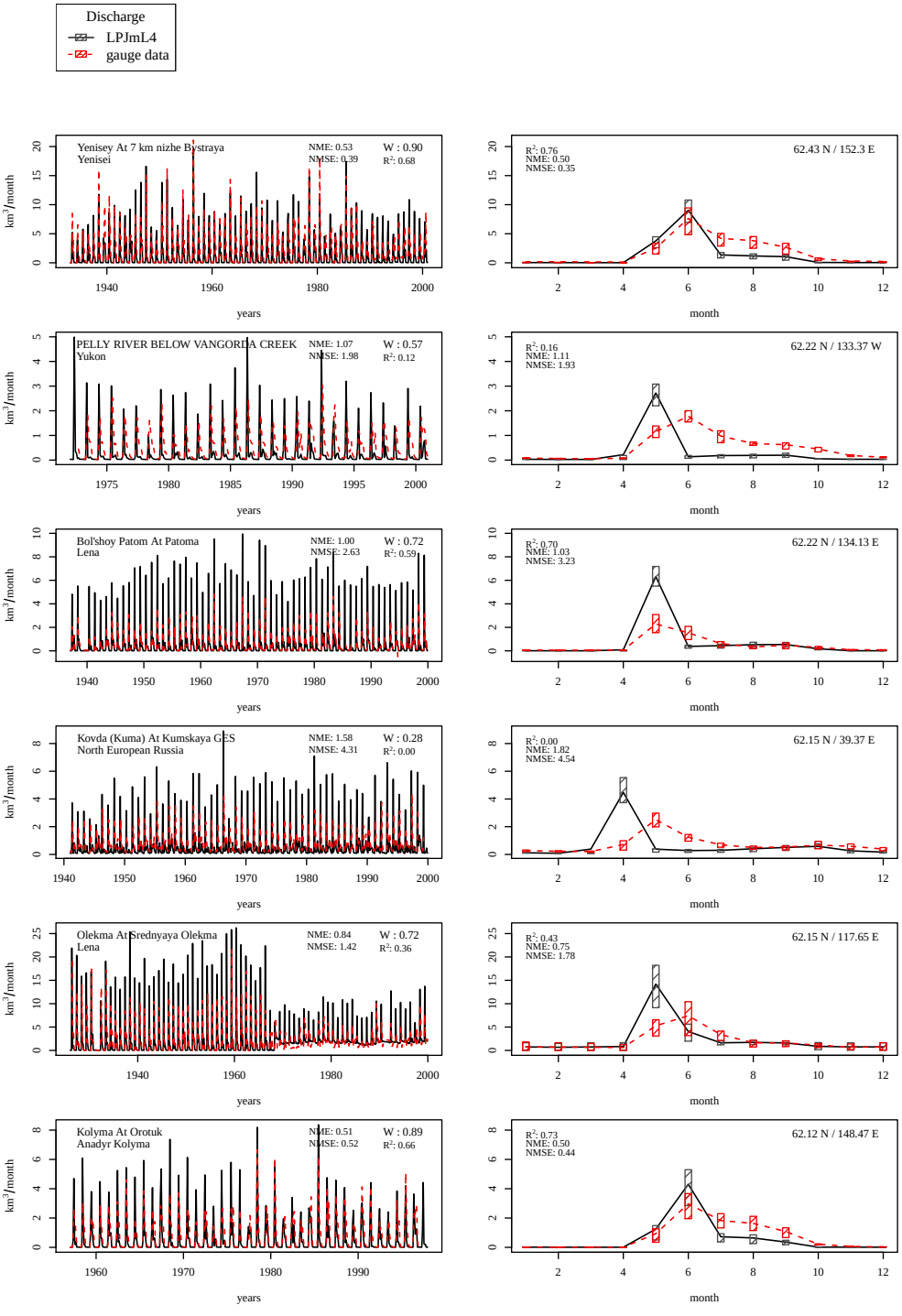

Figure S33. Evaluation of river discharge at gauging stations [15].

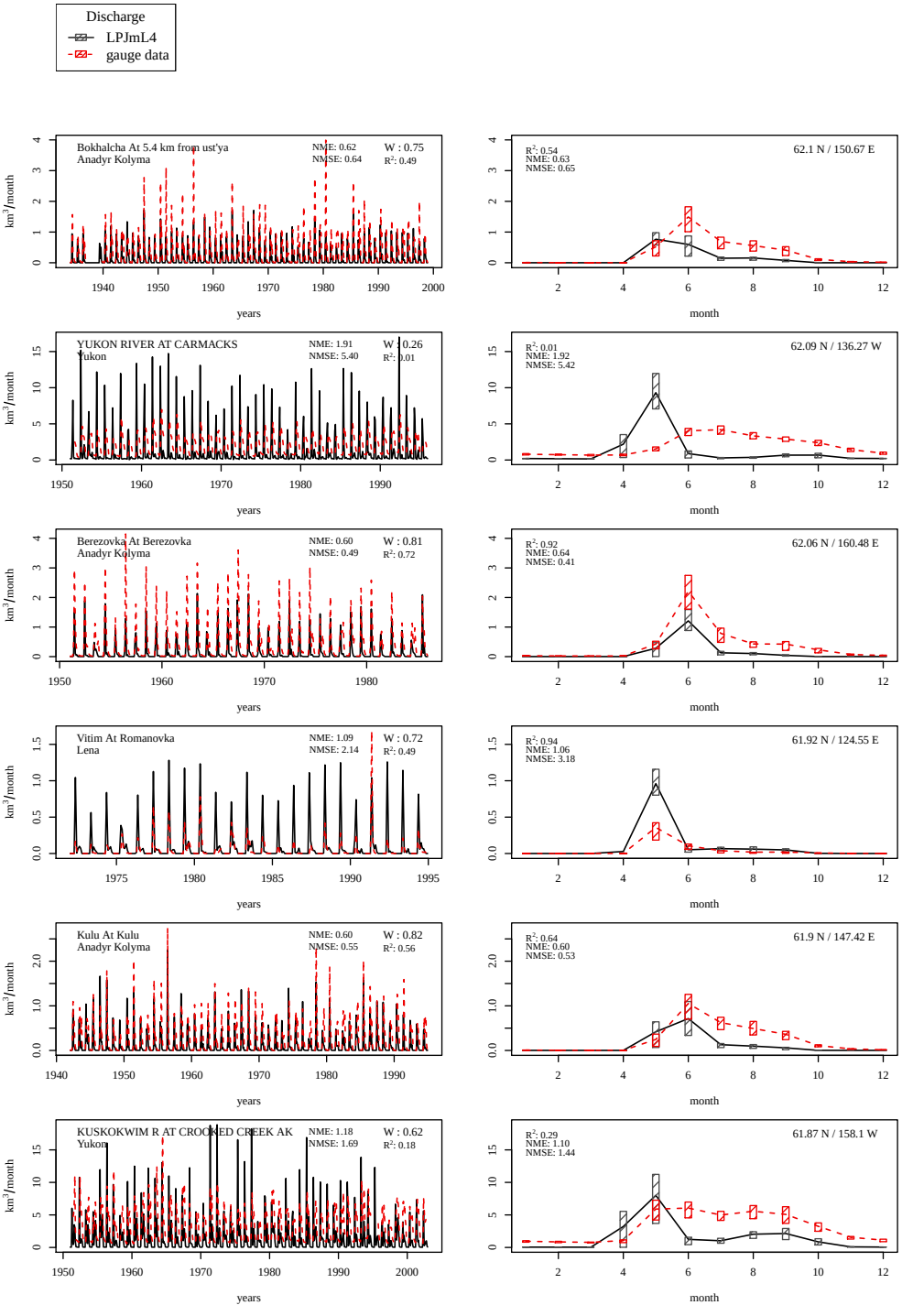

Figure S34. Evaluation of river discharge at gauging stations [16].

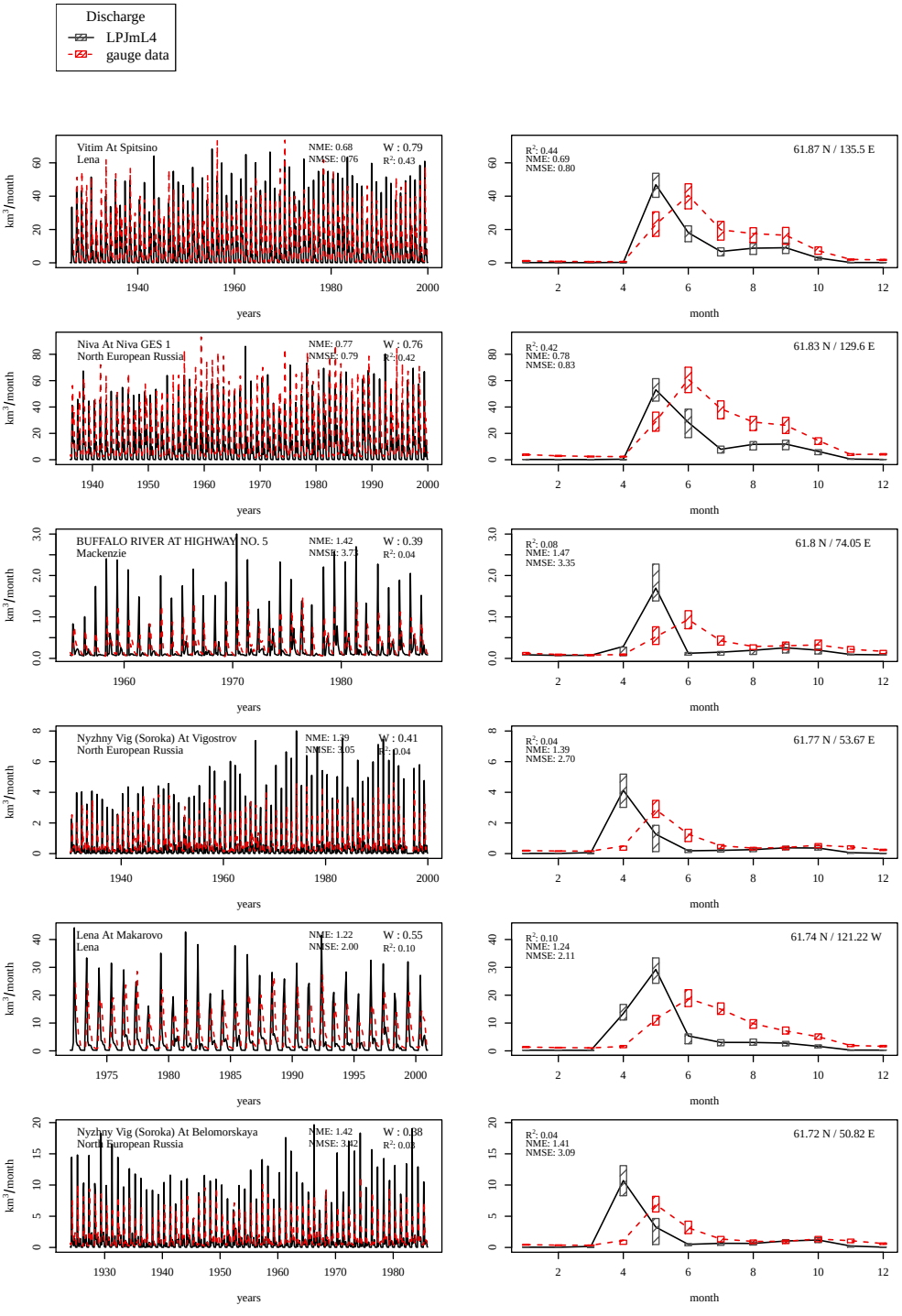

Figure S35. Evaluation of river discharge at gauging stations [17].

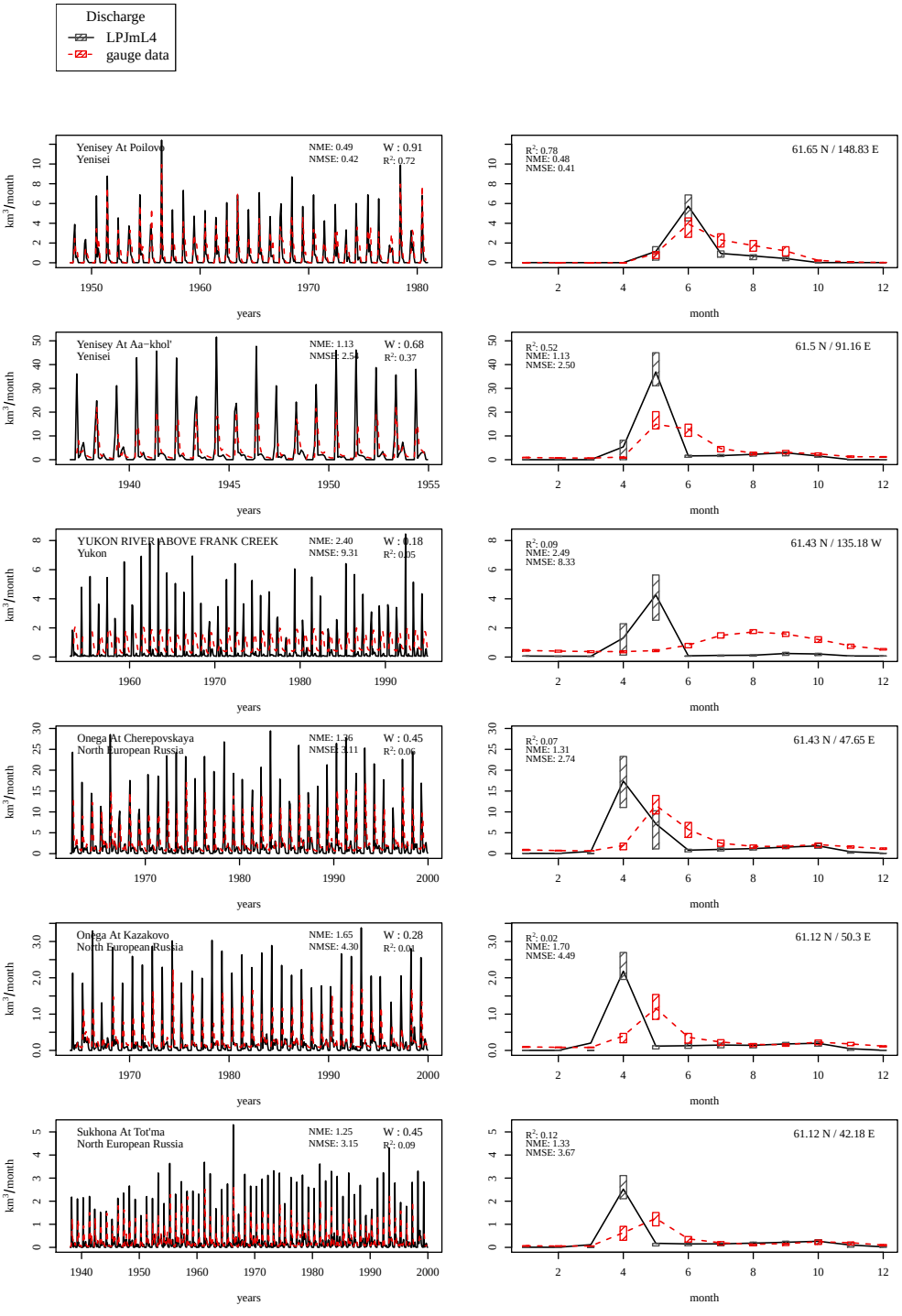

Figure S36. Evaluation of river discharge at gauging stations [18].

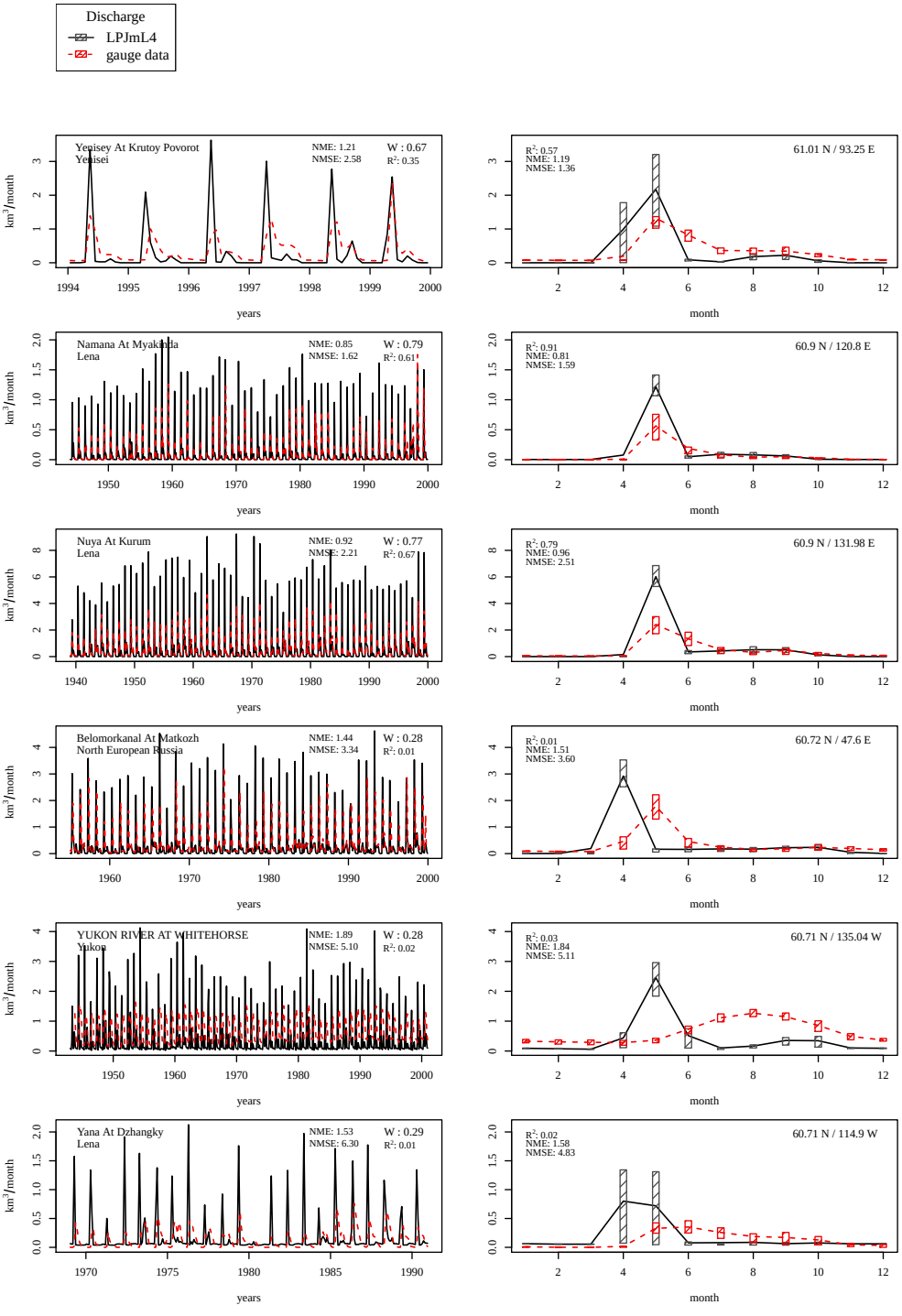

Figure S37. Evaluation of river discharge at gauging stations [19].

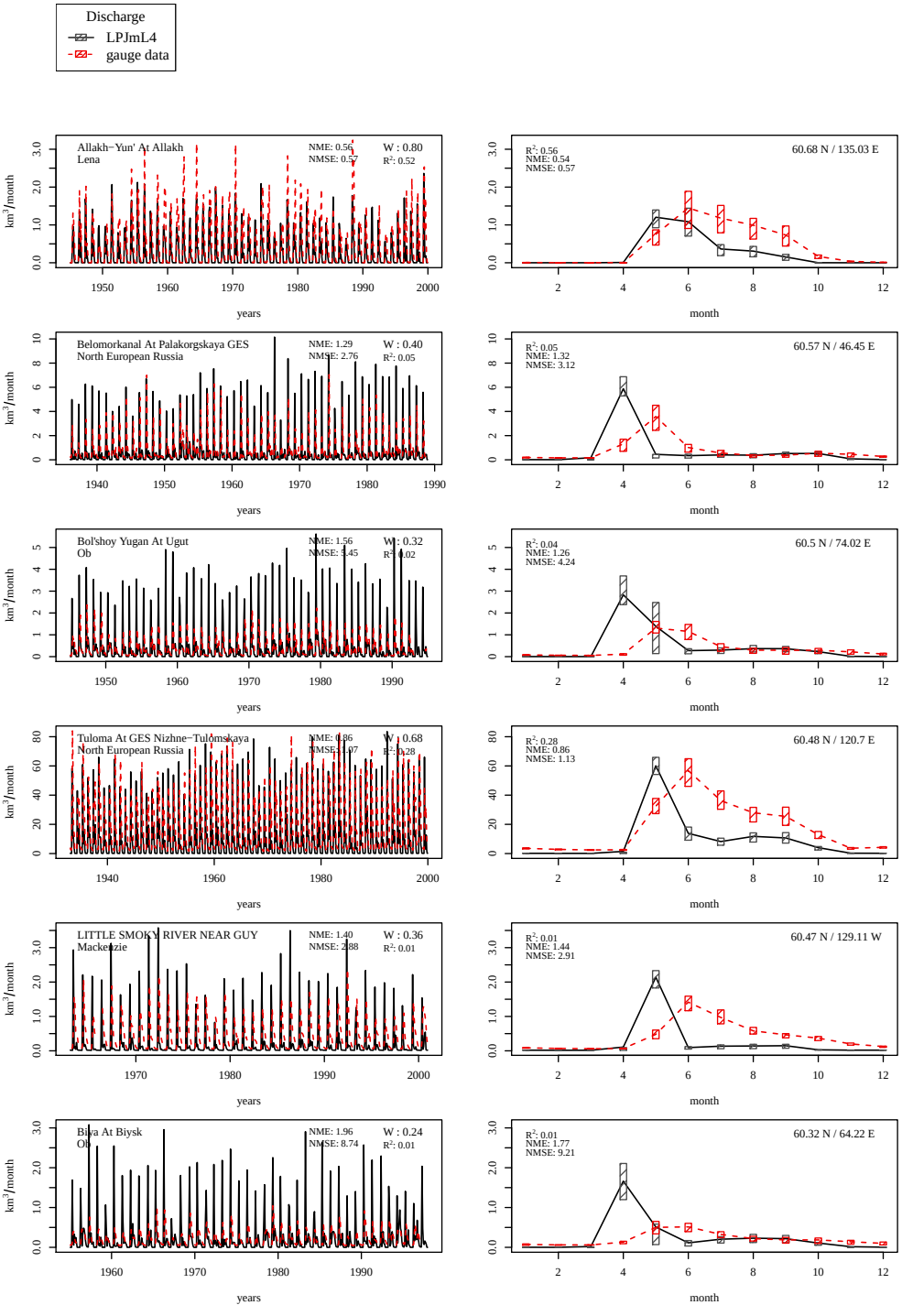

Figure S38. Evaluation of river discharge at gauging stations [20].

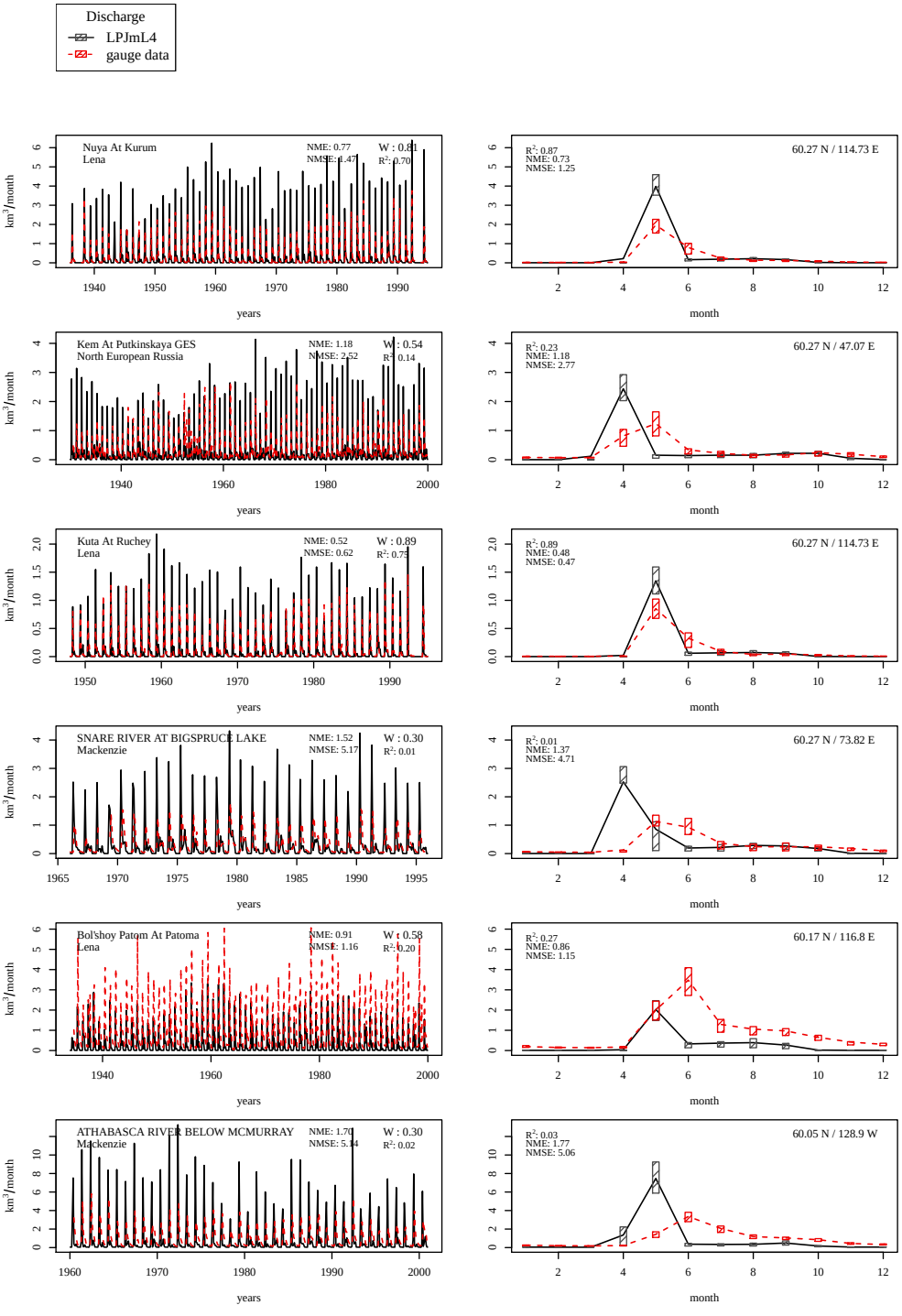

Figure S39. Evaluation of river discharge at gauging stations [21].

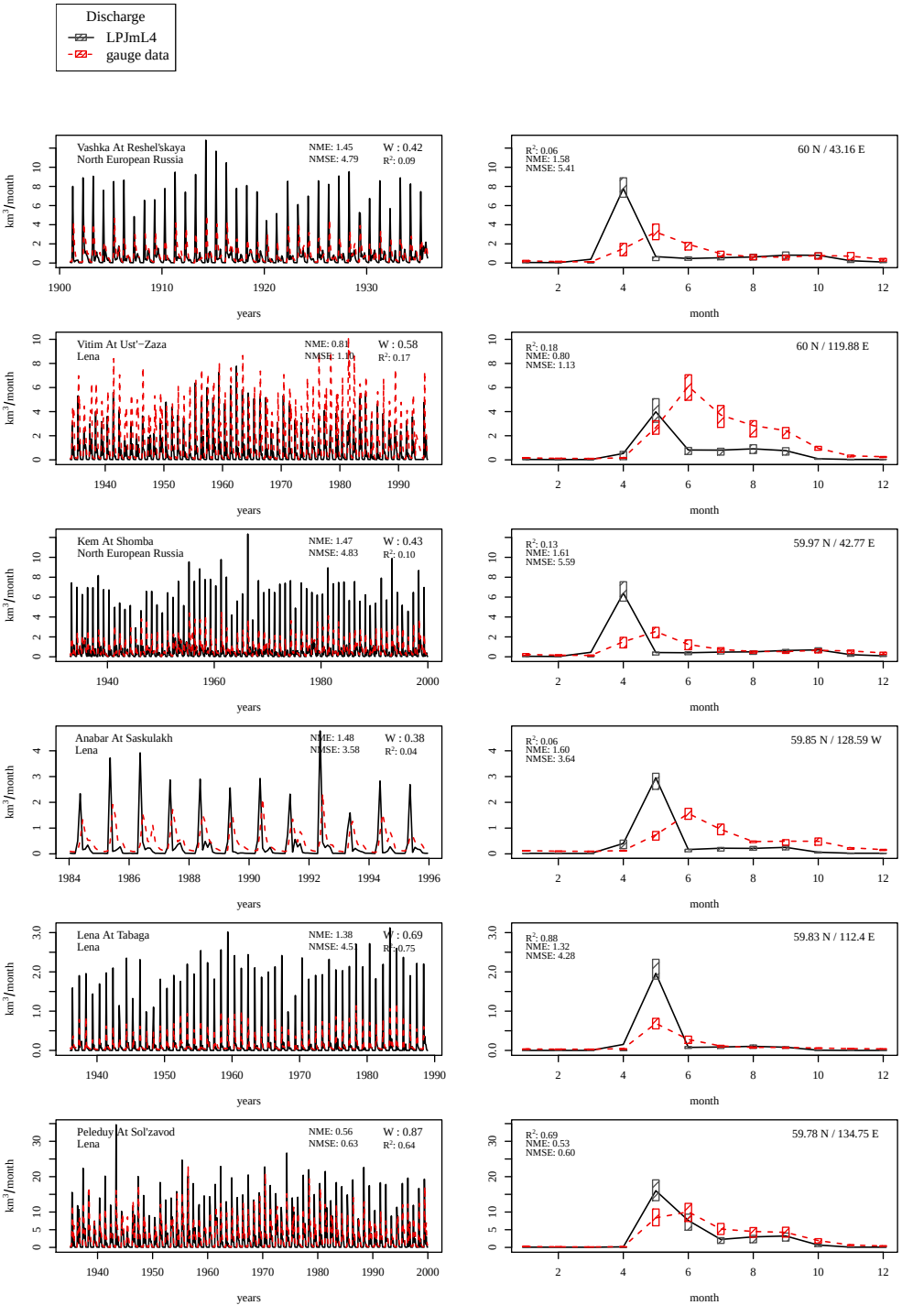

Figure S40. Evaluation of river discharge at gauging stations [22].

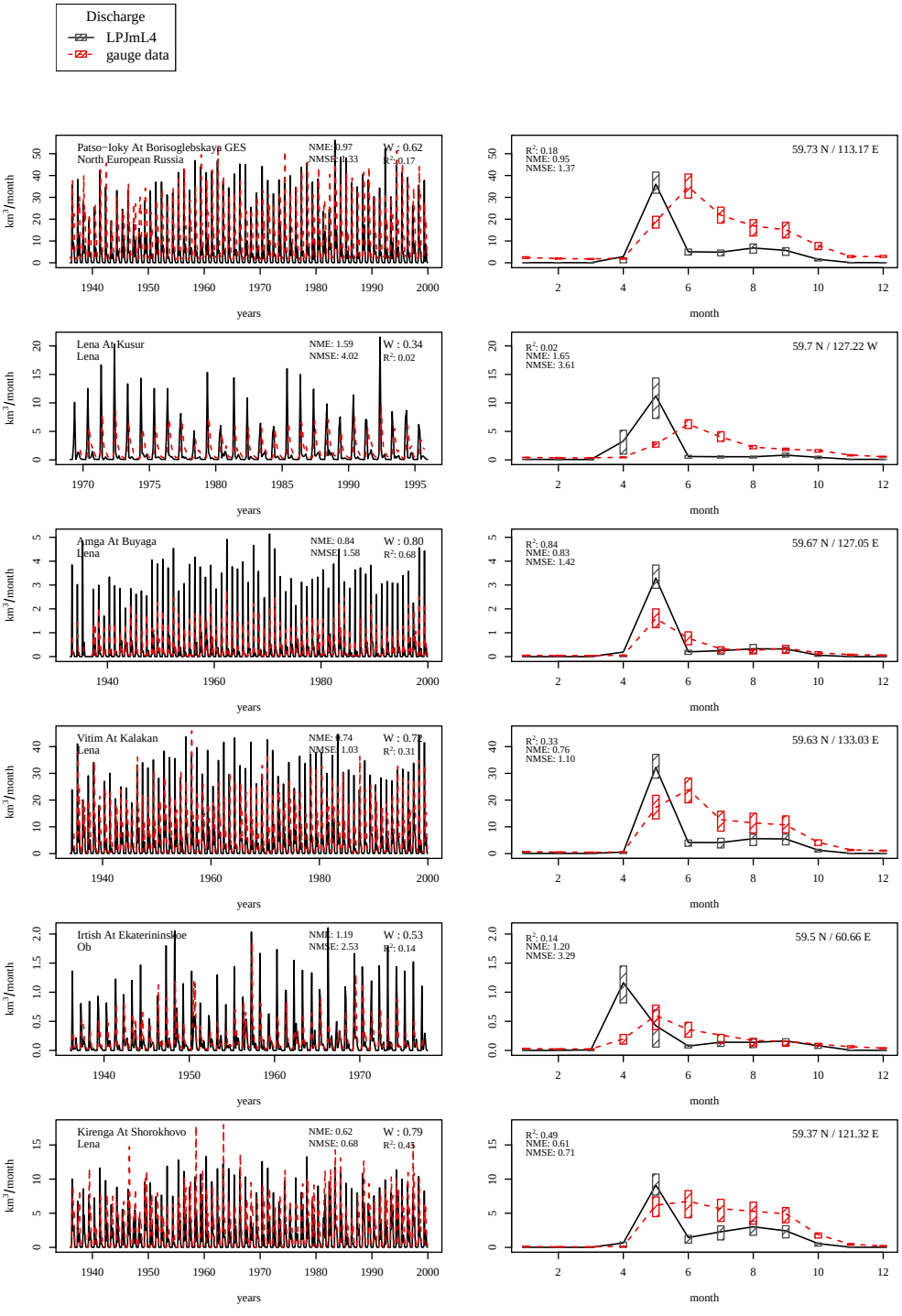

Figure S41. Evaluation of river discharge at gauging stations [23].

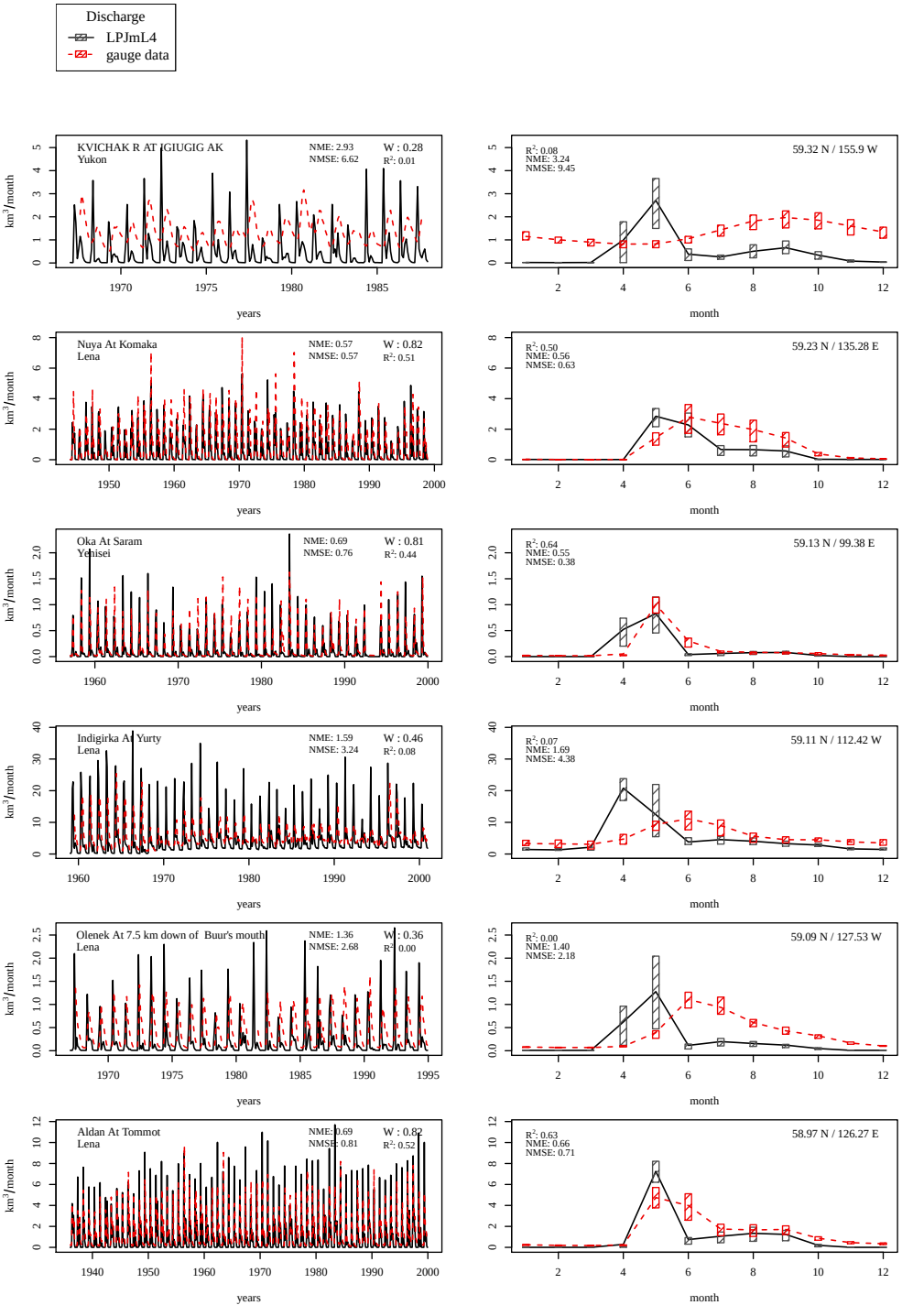

Figure S42. Evaluation of river discharge at gauging stations [24].

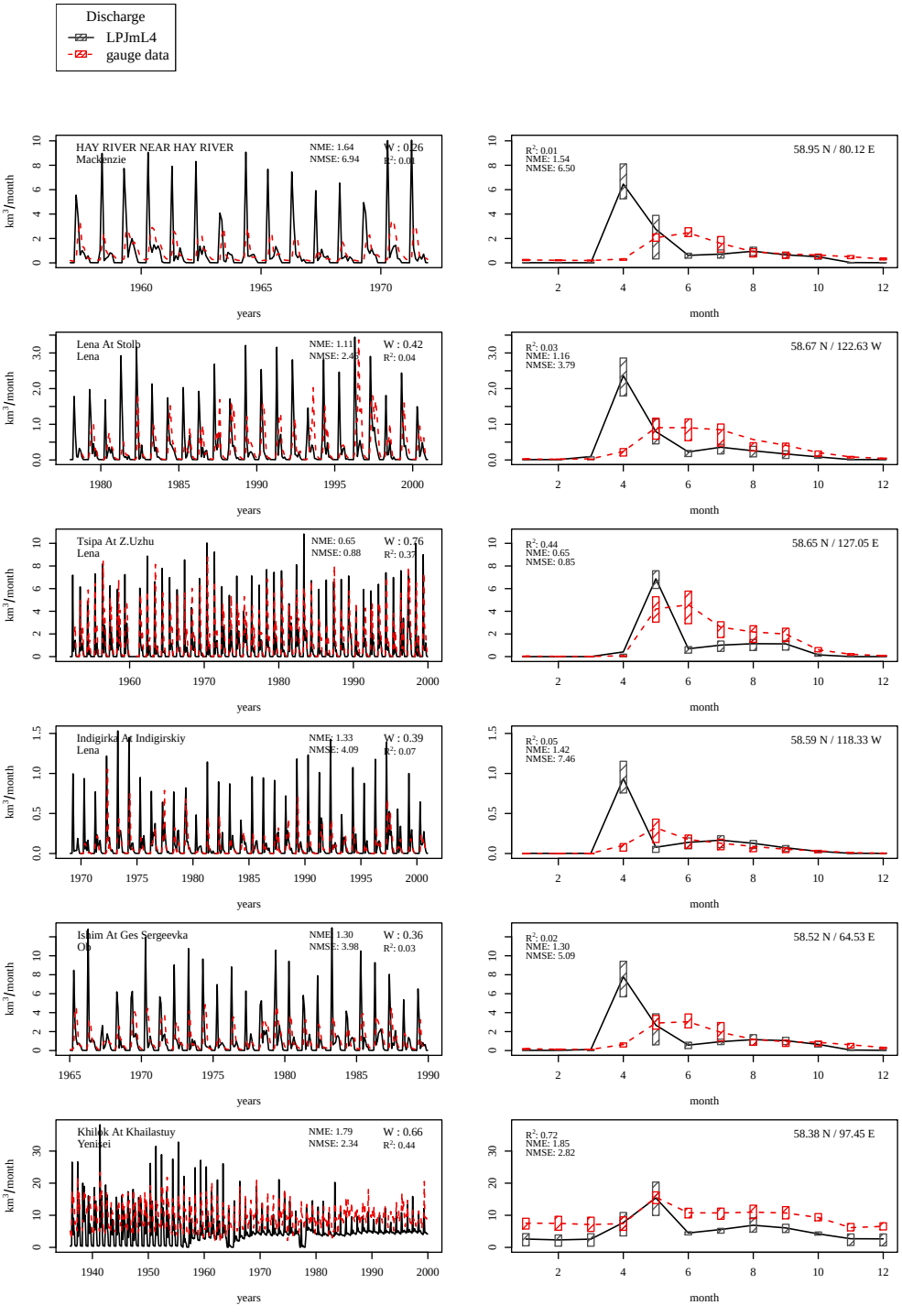

Figure S43. Evaluation of river discharge at gauging stations [25].

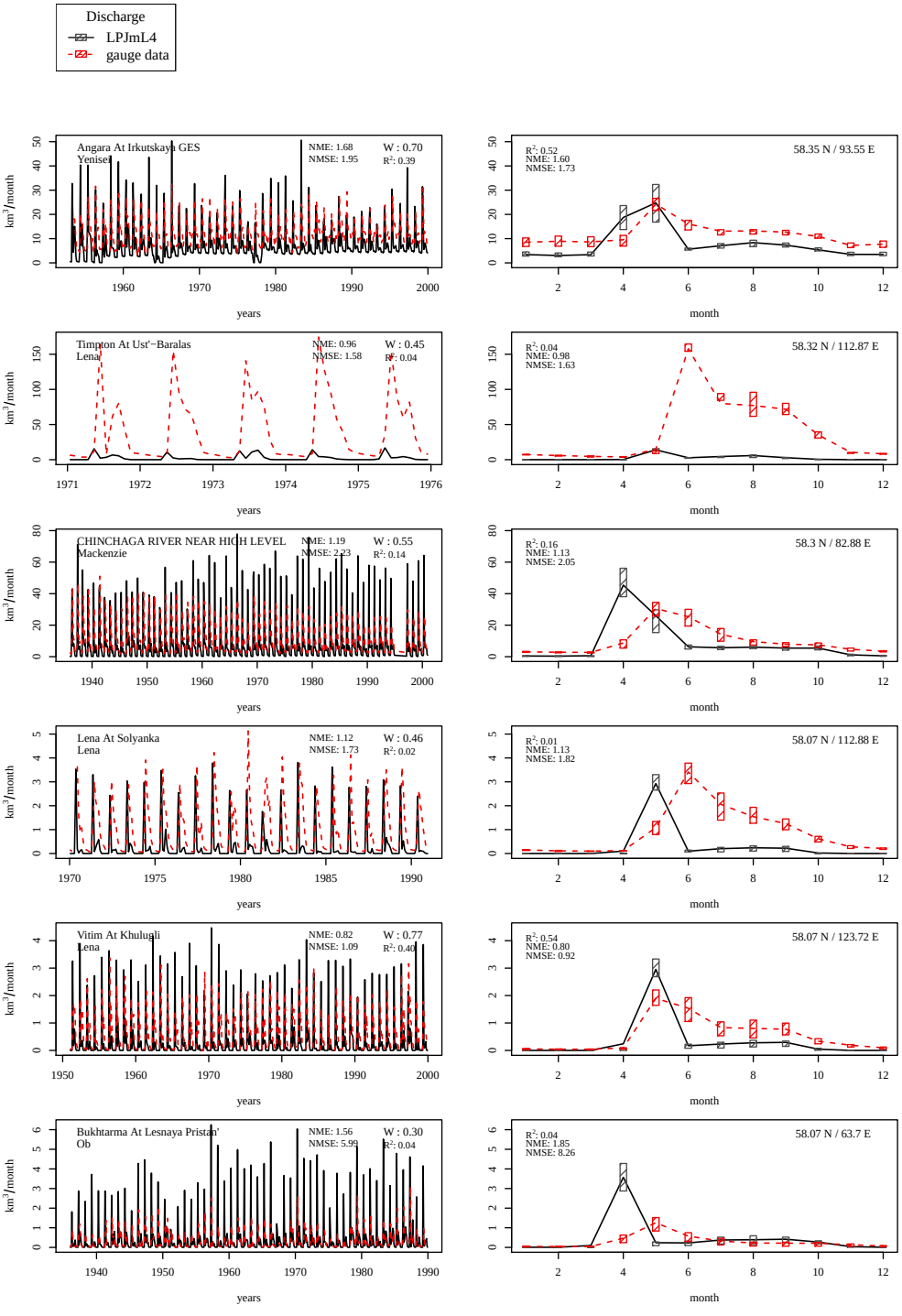

Figure S44. Evaluation of river discharge at gauging stations [26].

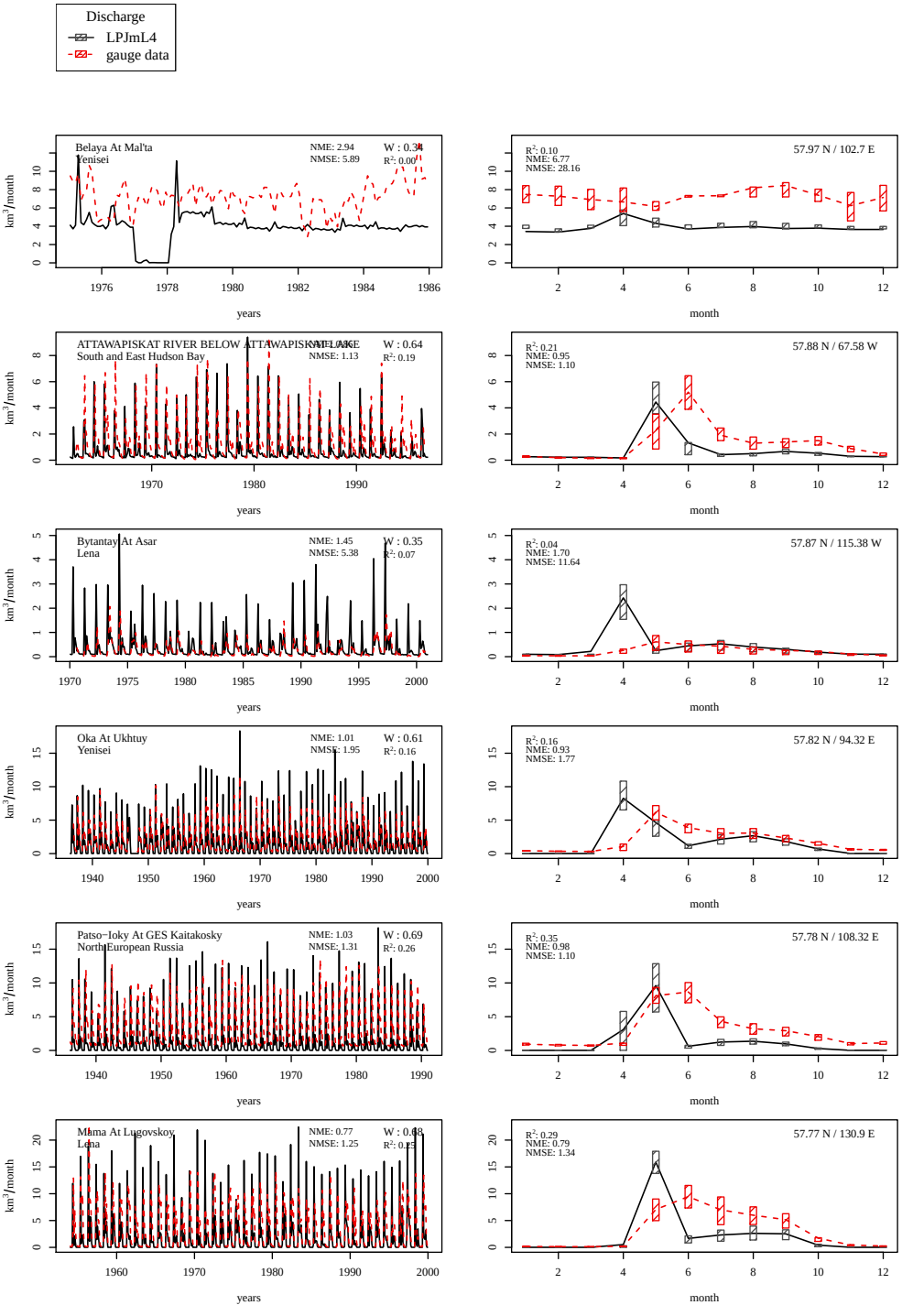

Figure S45. Evaluation of river discharge at gauging stations [27].

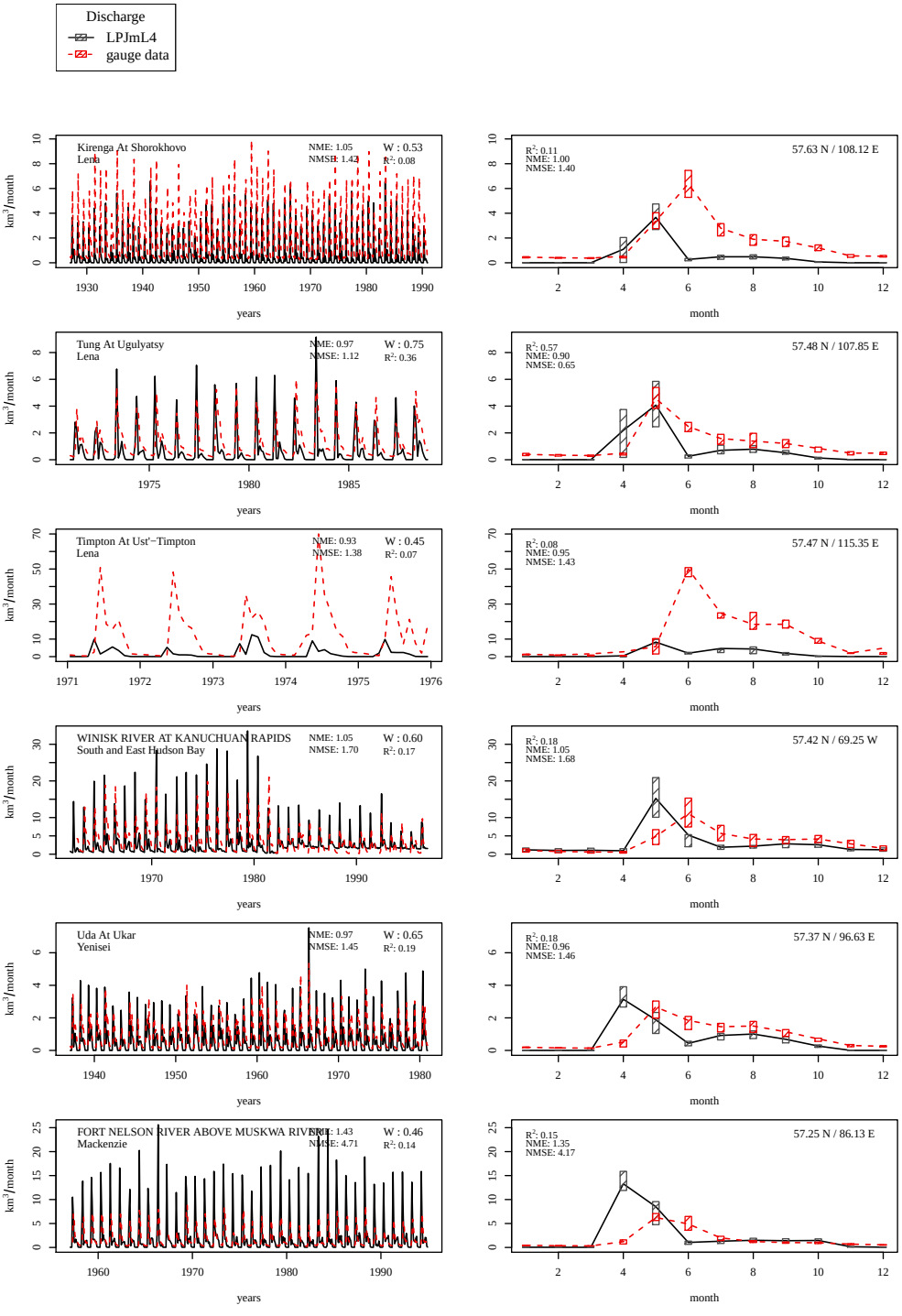

Figure S46. Evaluation of river discharge at gauging stations [28].

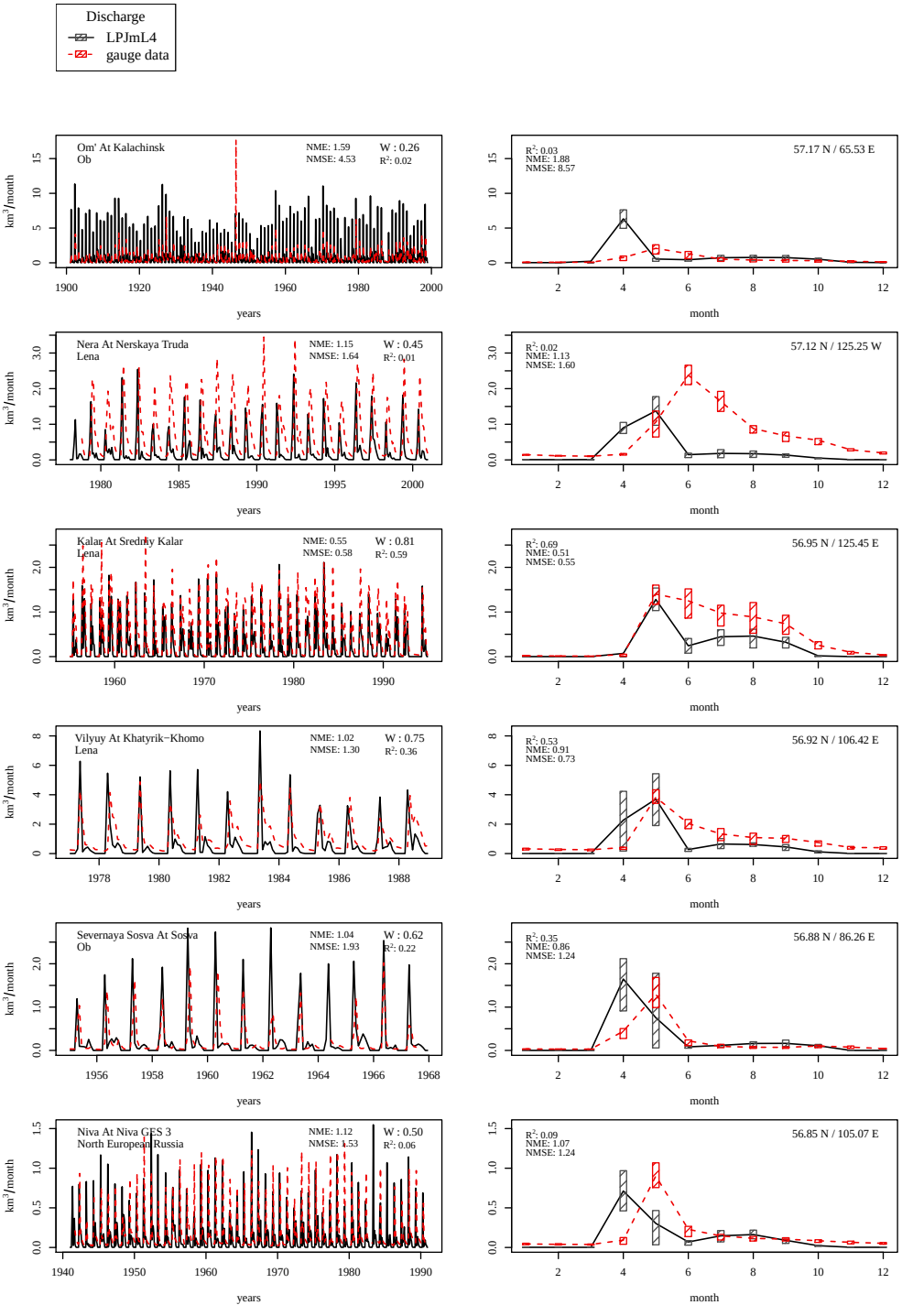

Figure S47. Evaluation of river discharge at gauging stations [29].

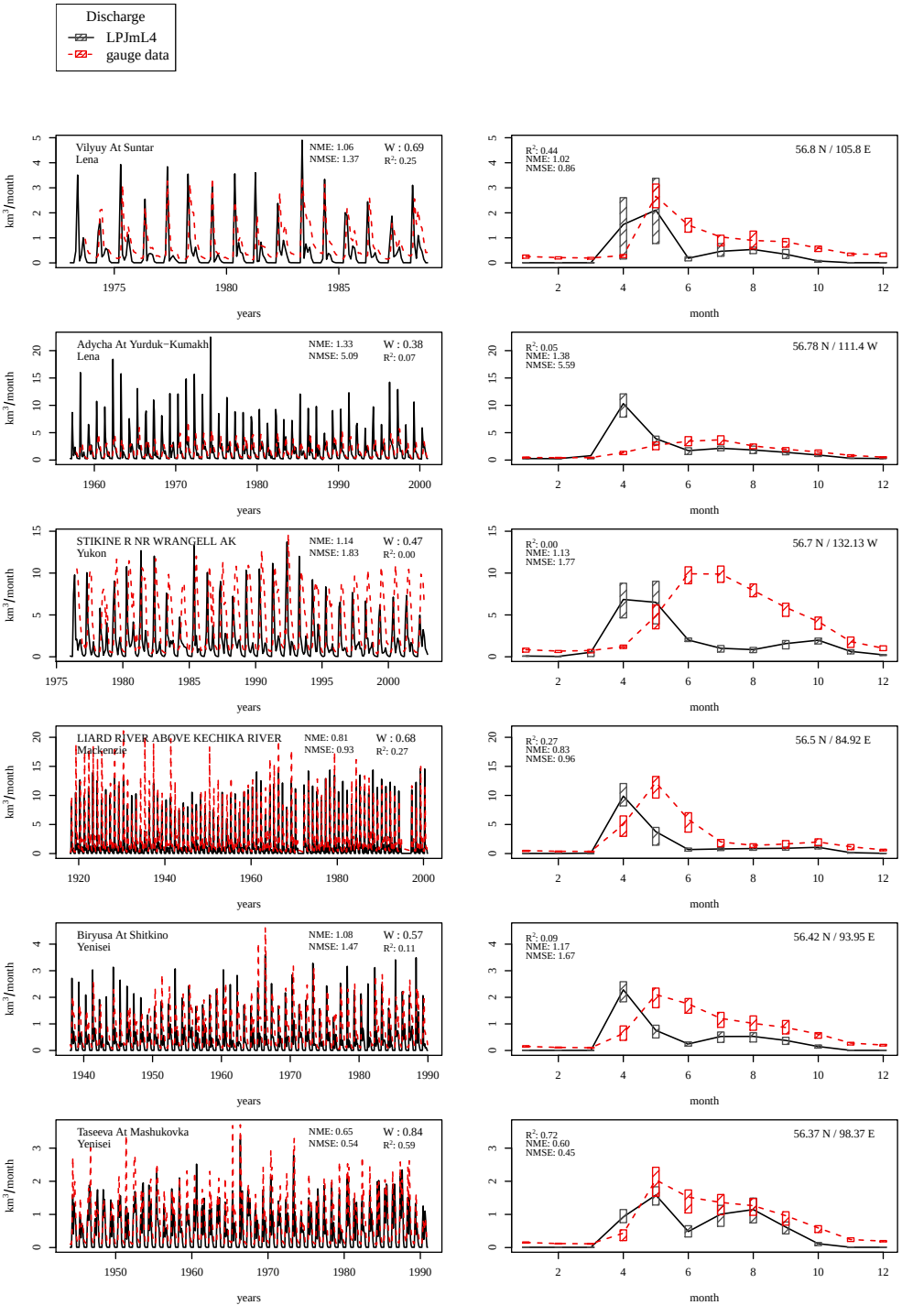

Figure S48. Evaluation of river discharge at gauging stations [30].

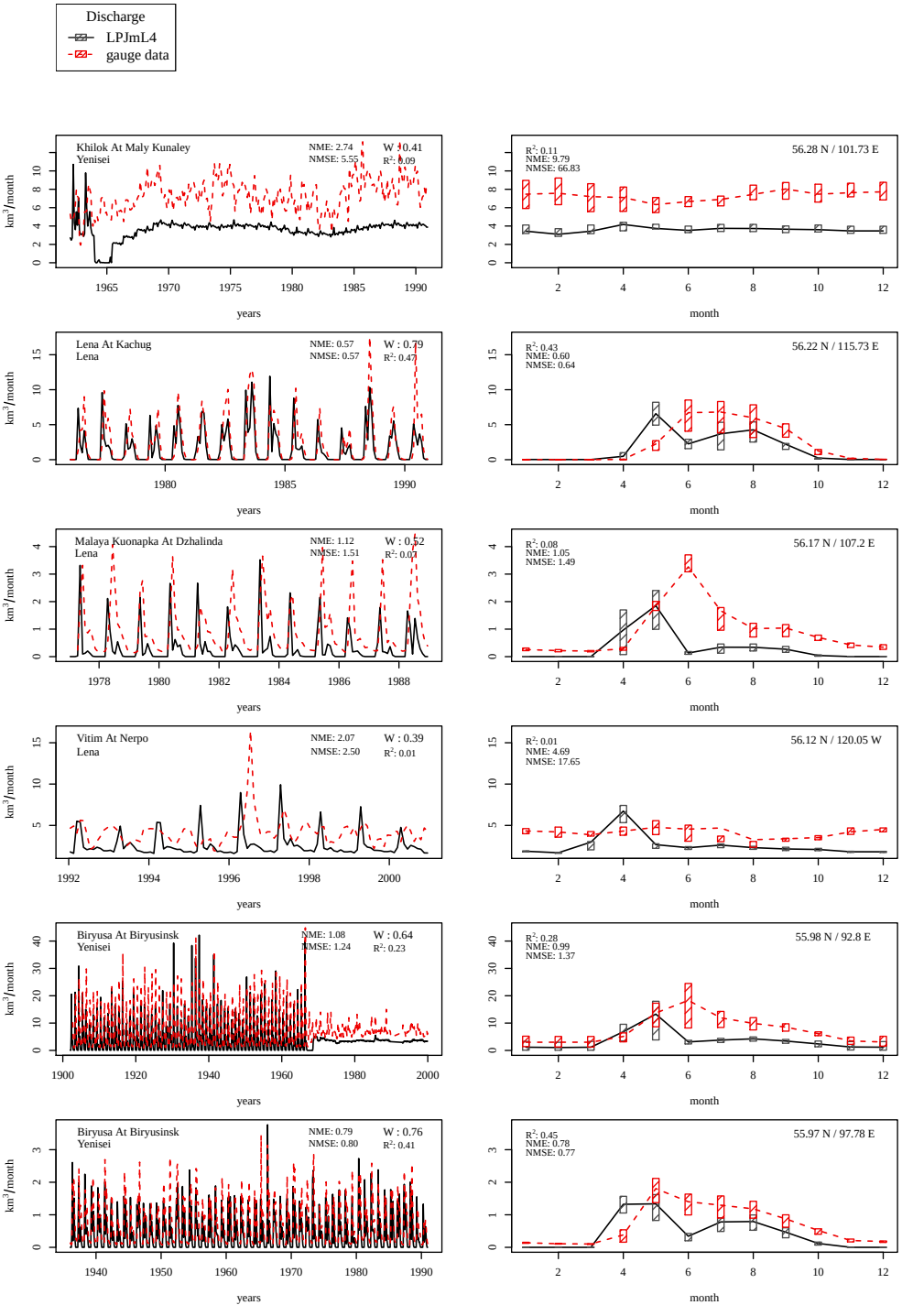

Figure S49. Evaluation of river discharge at gauging stations [31].

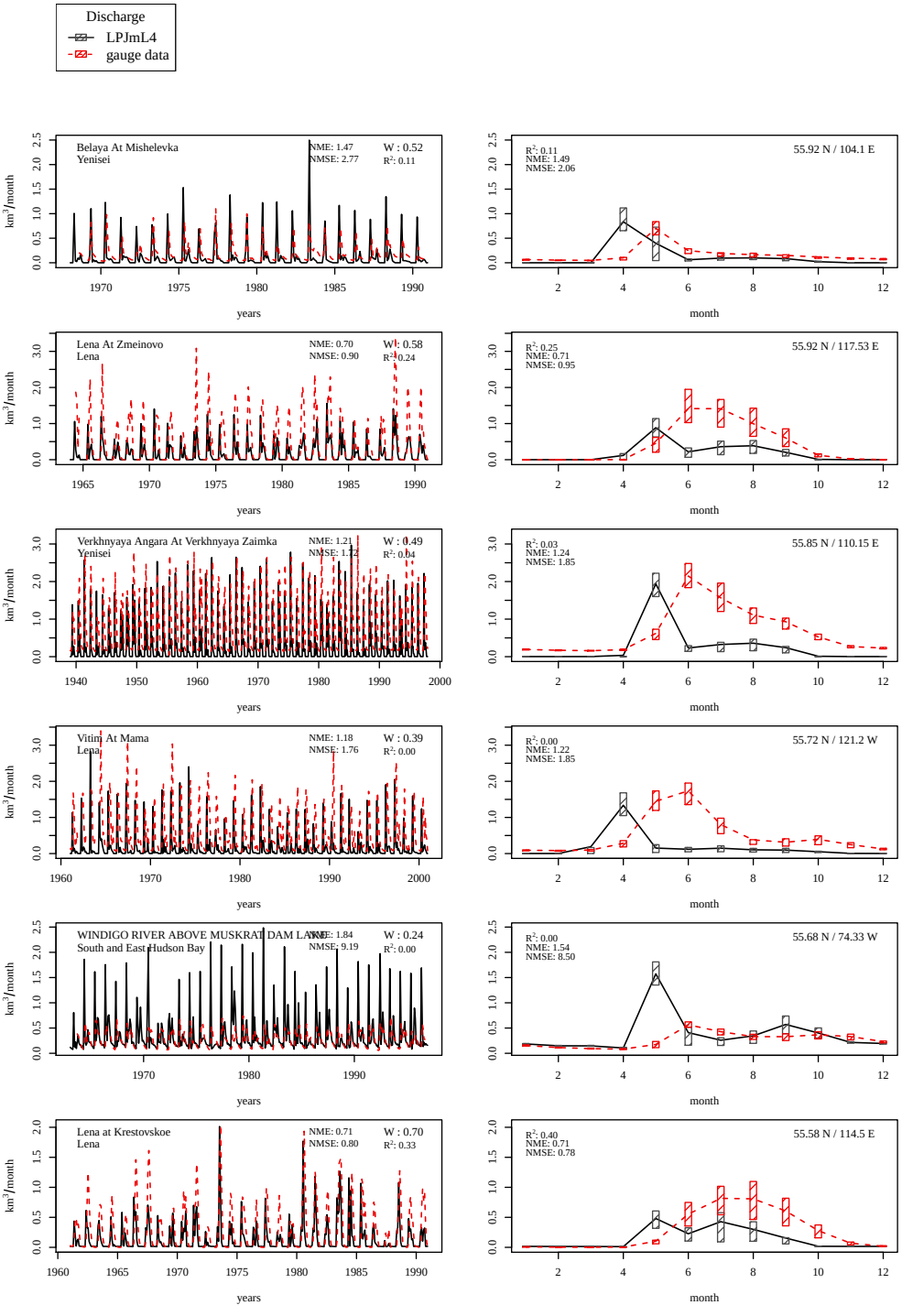

Figure S50. Evaluation of river discharge at gauging stations [32].

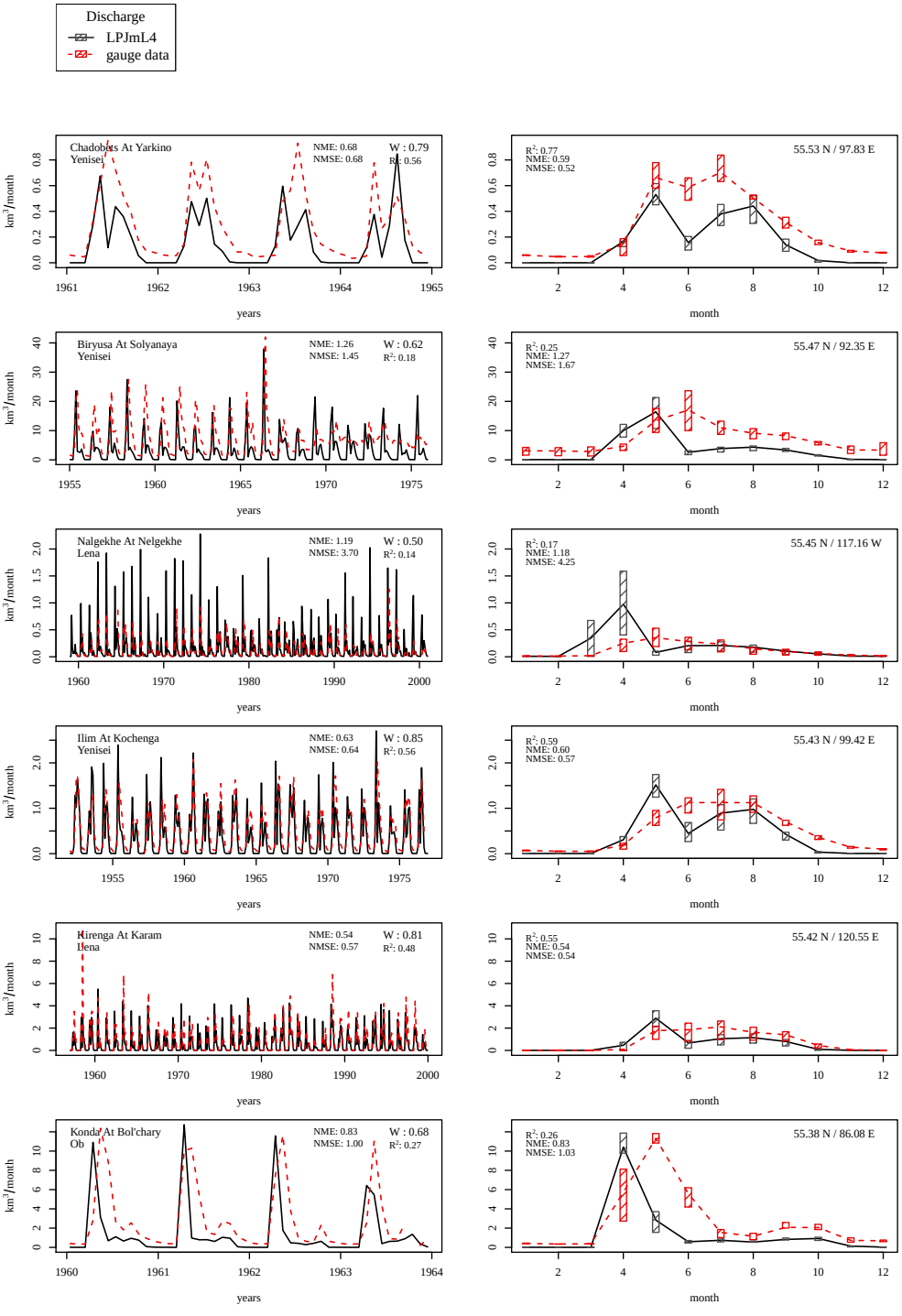

Figure S51. Evaluation of river discharge at gauging stations [33].

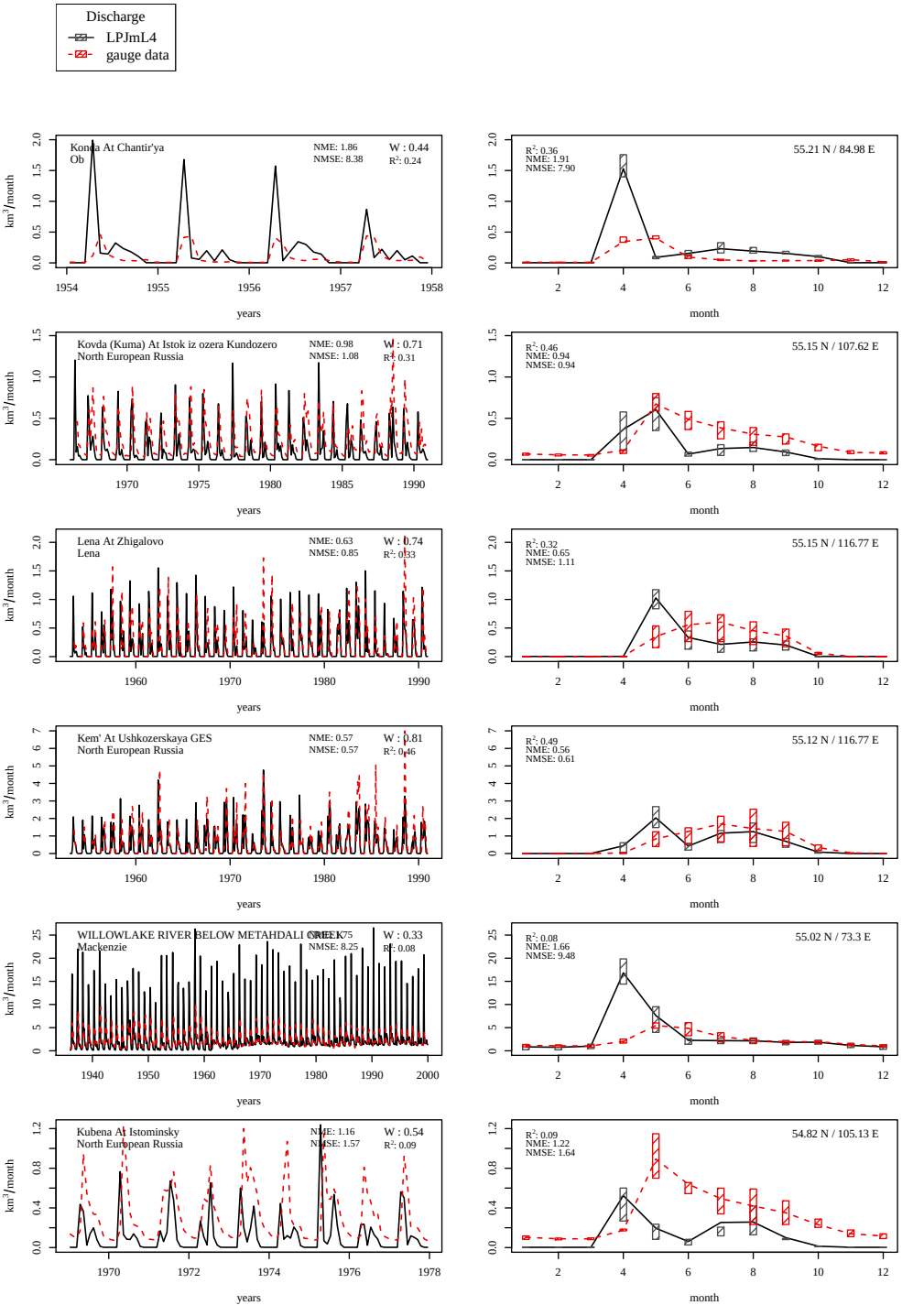

Figure S52. Evaluation of river discharge at gauging stations [34].

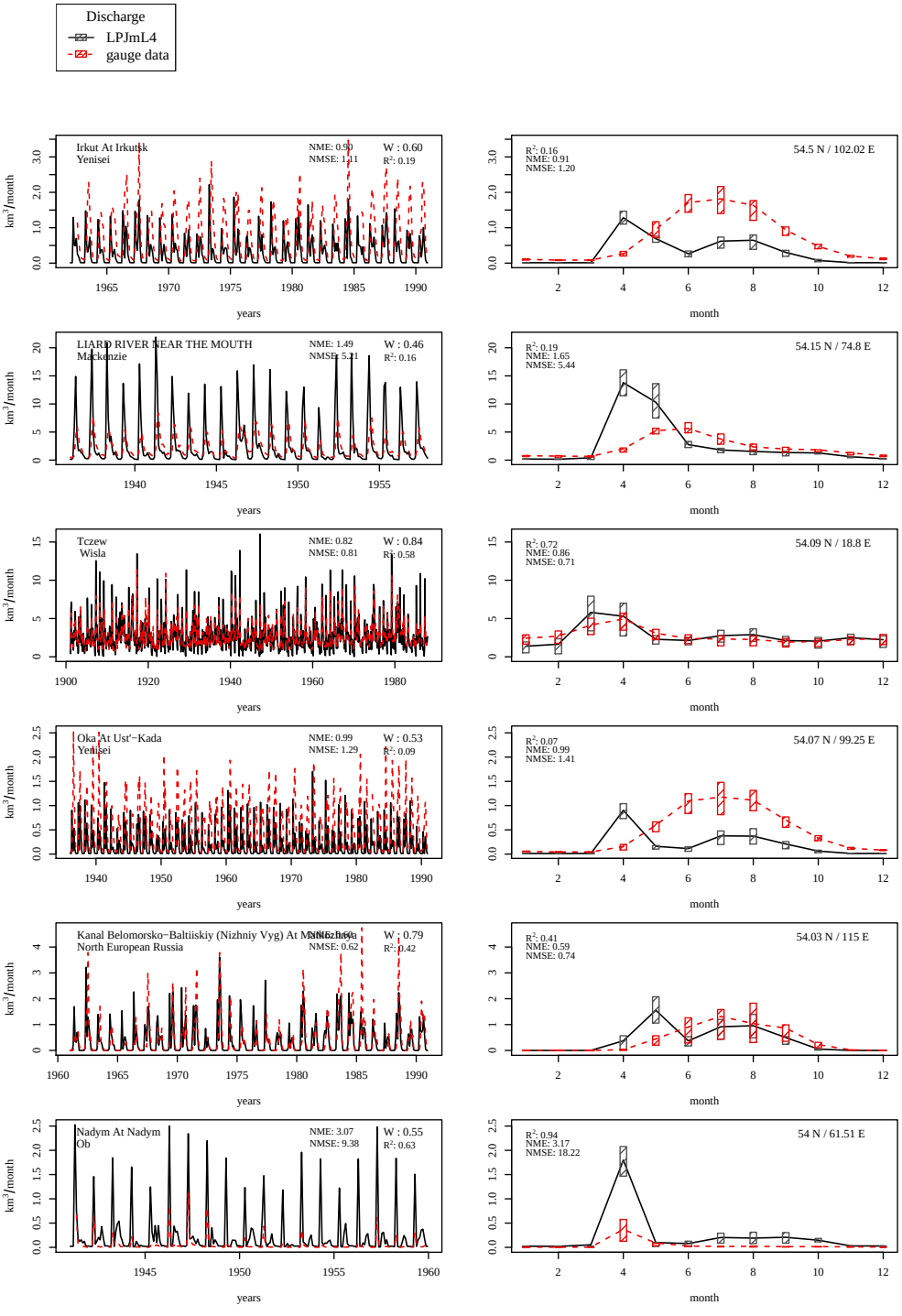

Figure S53. Evaluation of river discharge at gauging stations [35].

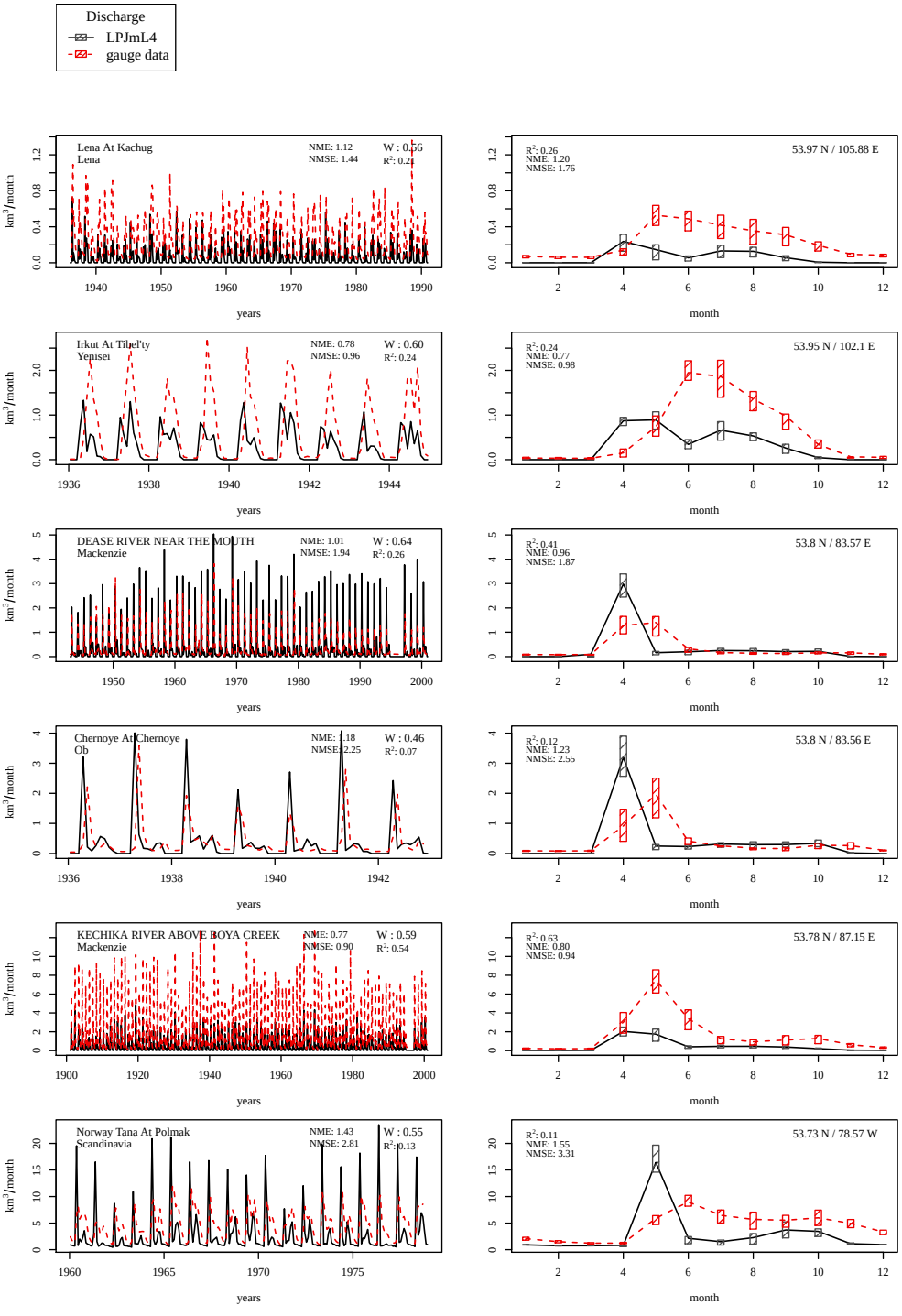

Figure S54. Evaluation of river discharge at gauging stations [36].

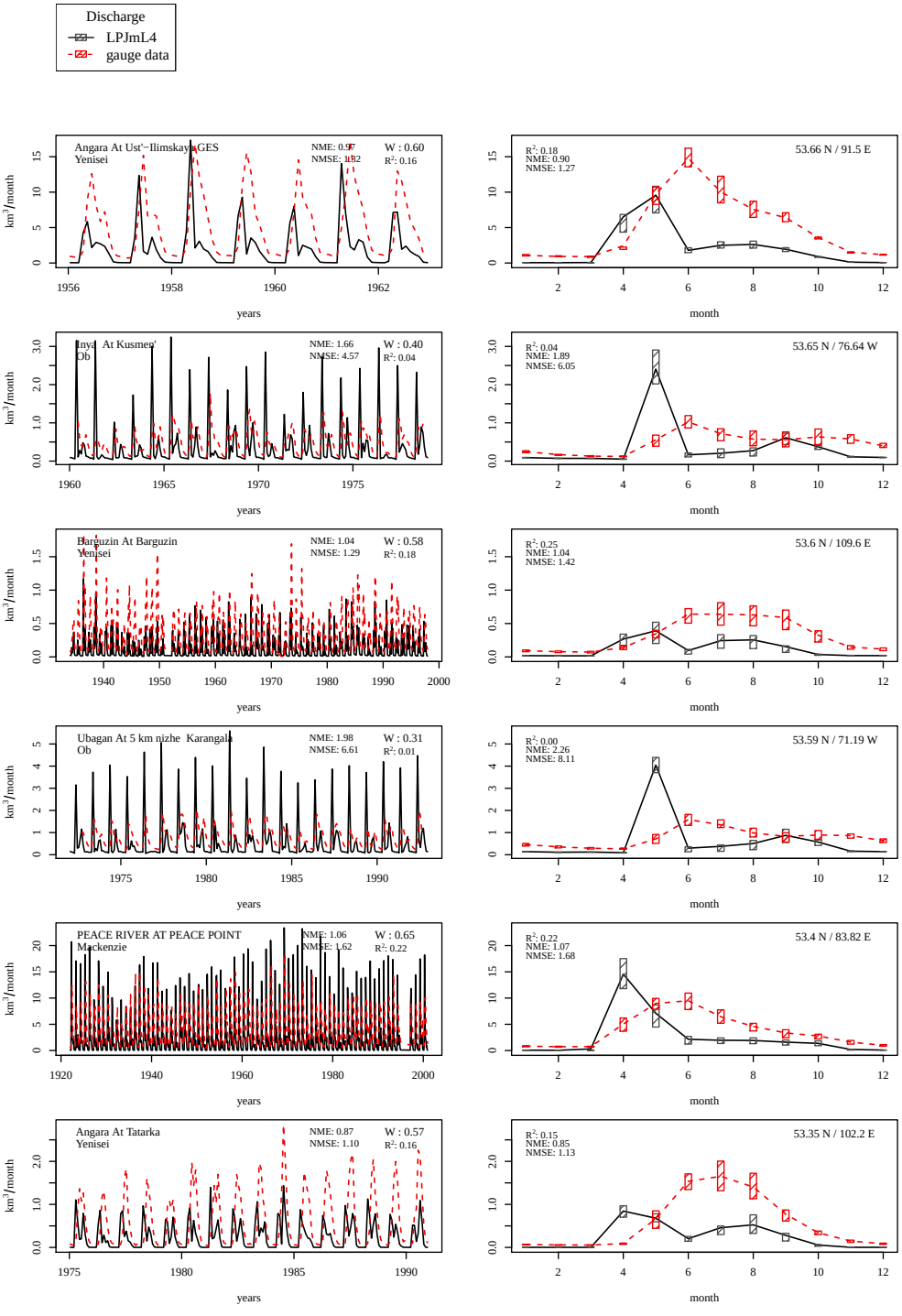

Figure S55. Evaluation of river discharge at gauging stations [37].

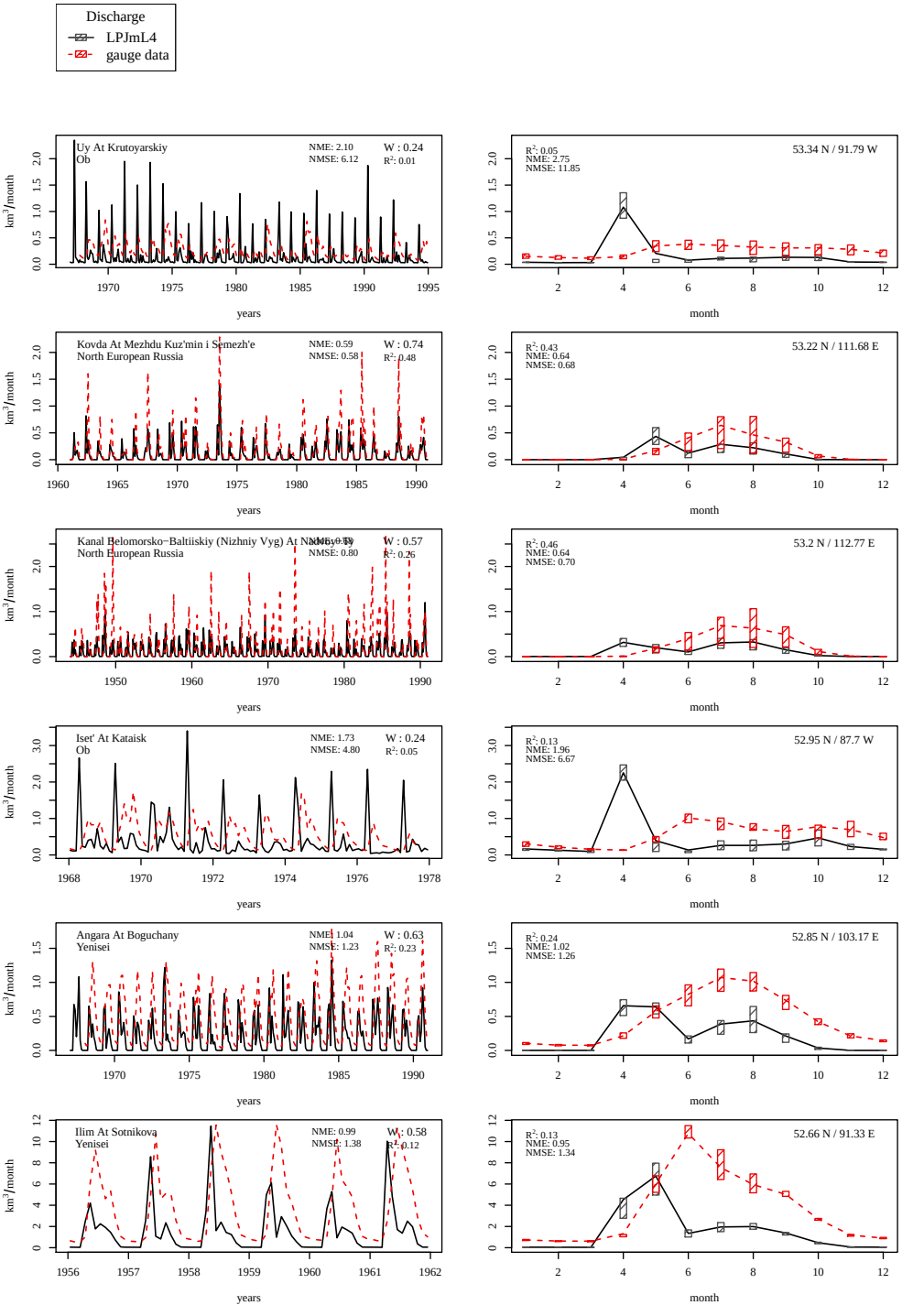

Figure S56. Evaluation of river discharge at gauging stations [38].

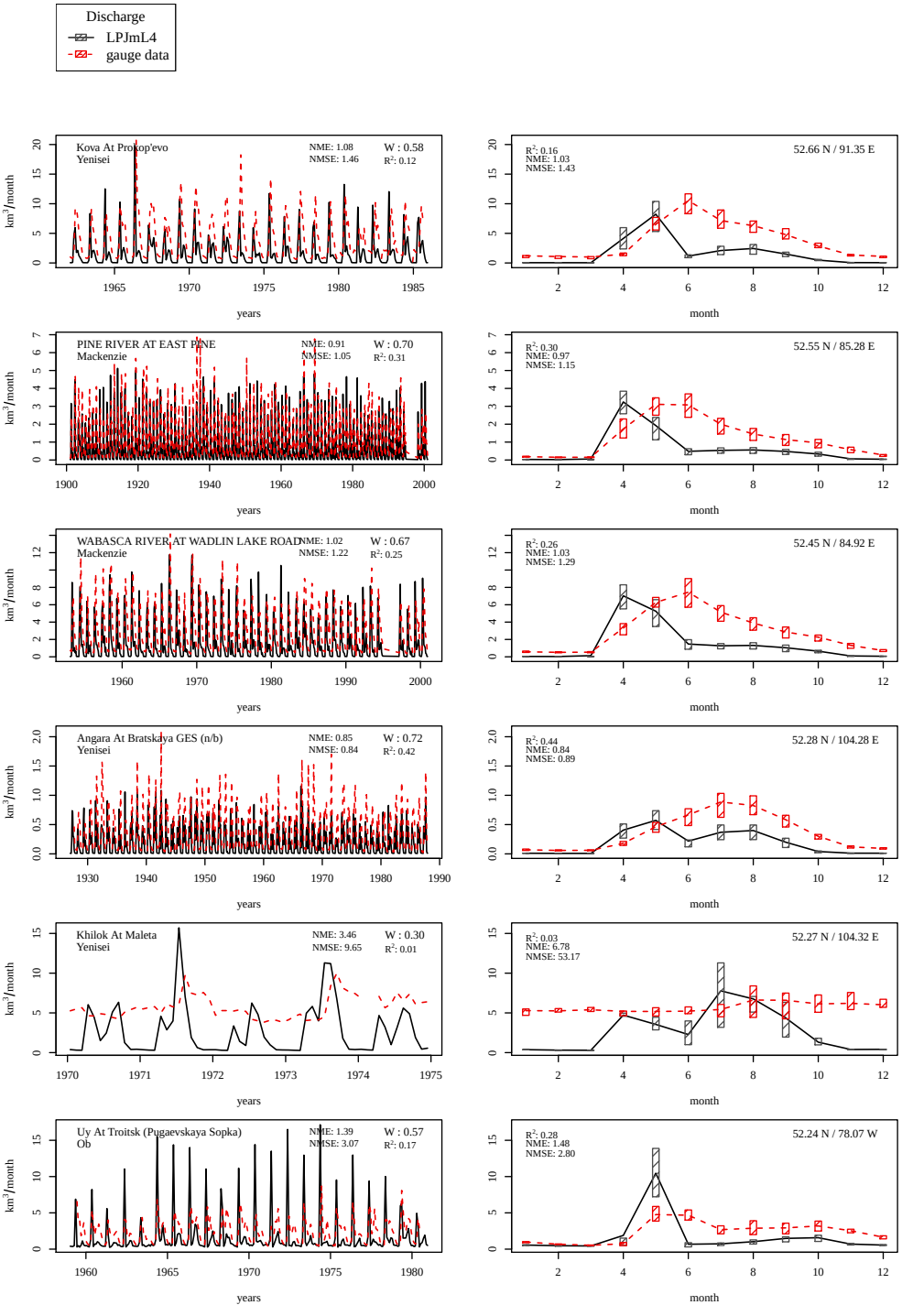

Figure S57. Evaluation of river discharge at gauging stations [39].

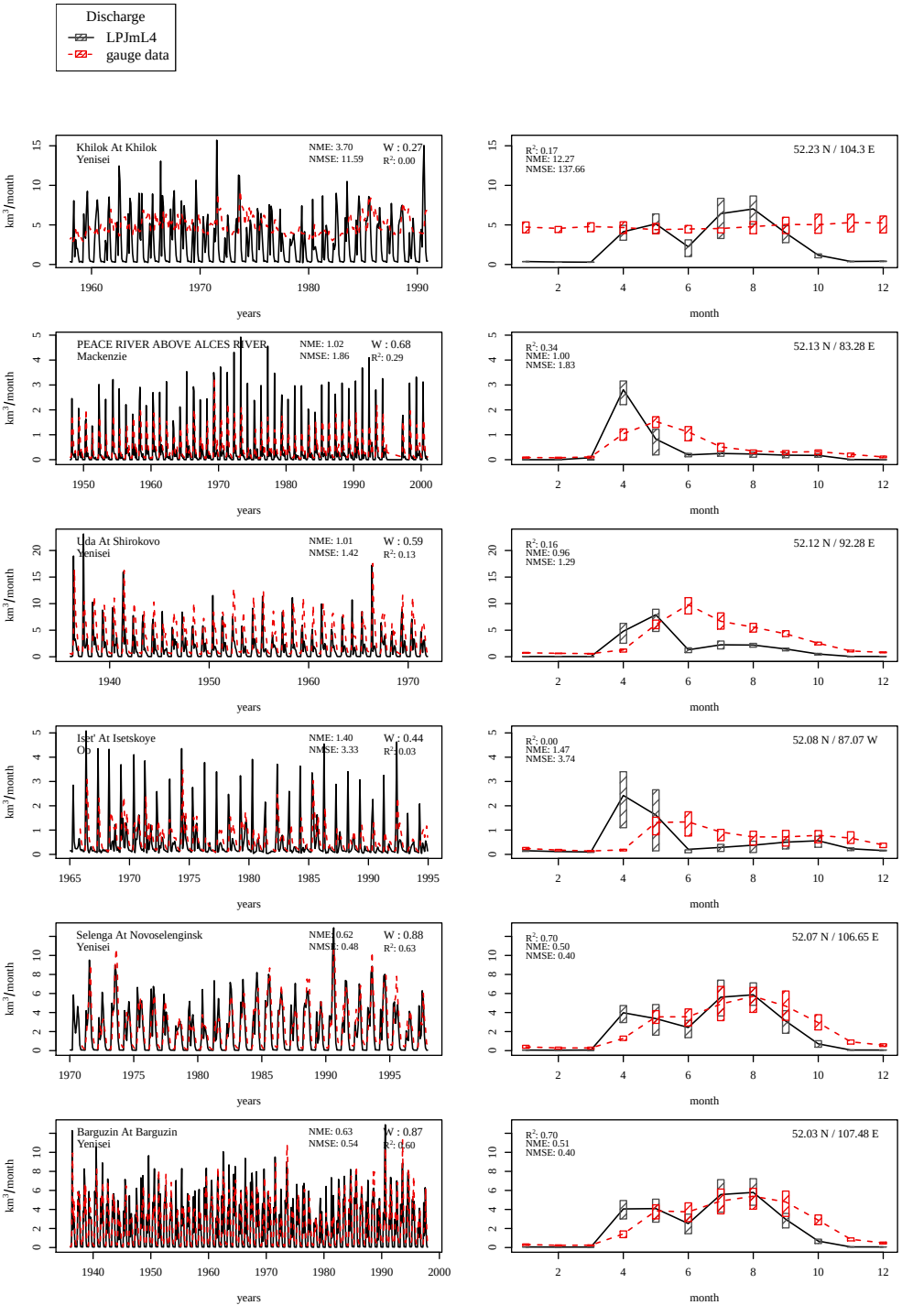

Figure S58. Evaluation of river discharge at gauging stations [40].

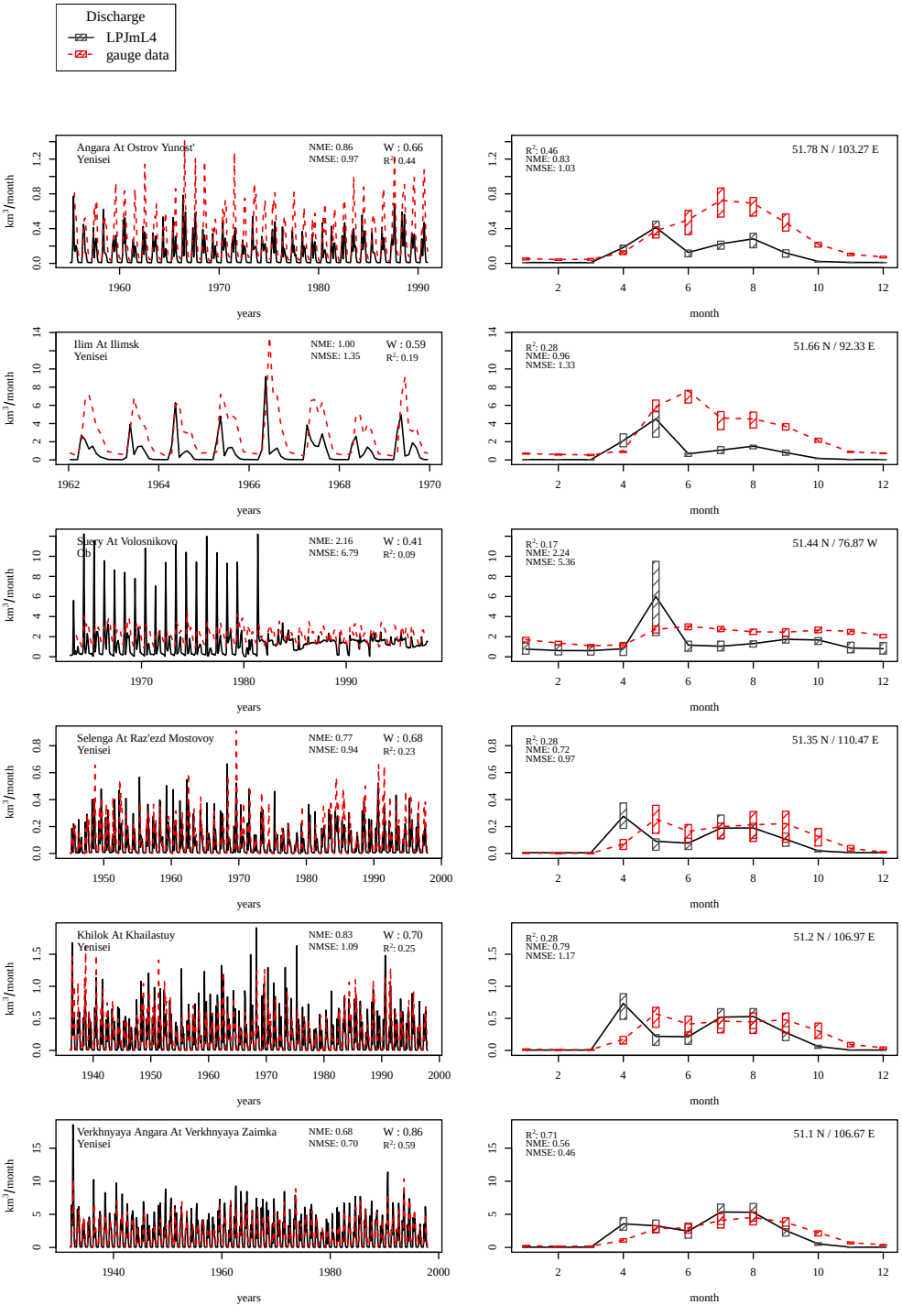

Figure S59. Evaluation of river discharge at gauging stations [41].

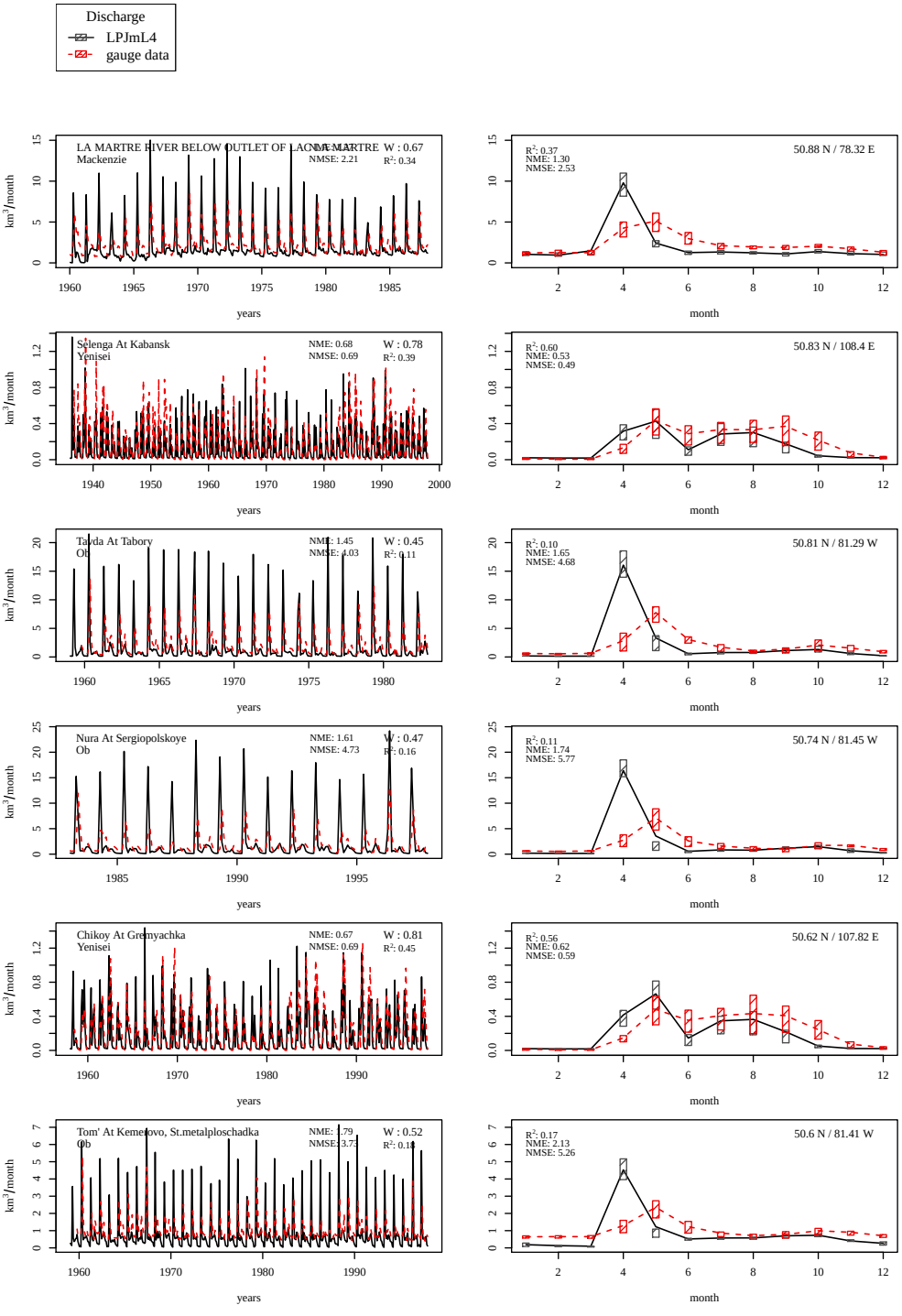

Figure S60. Evaluation of river discharge at gauging stations [42].

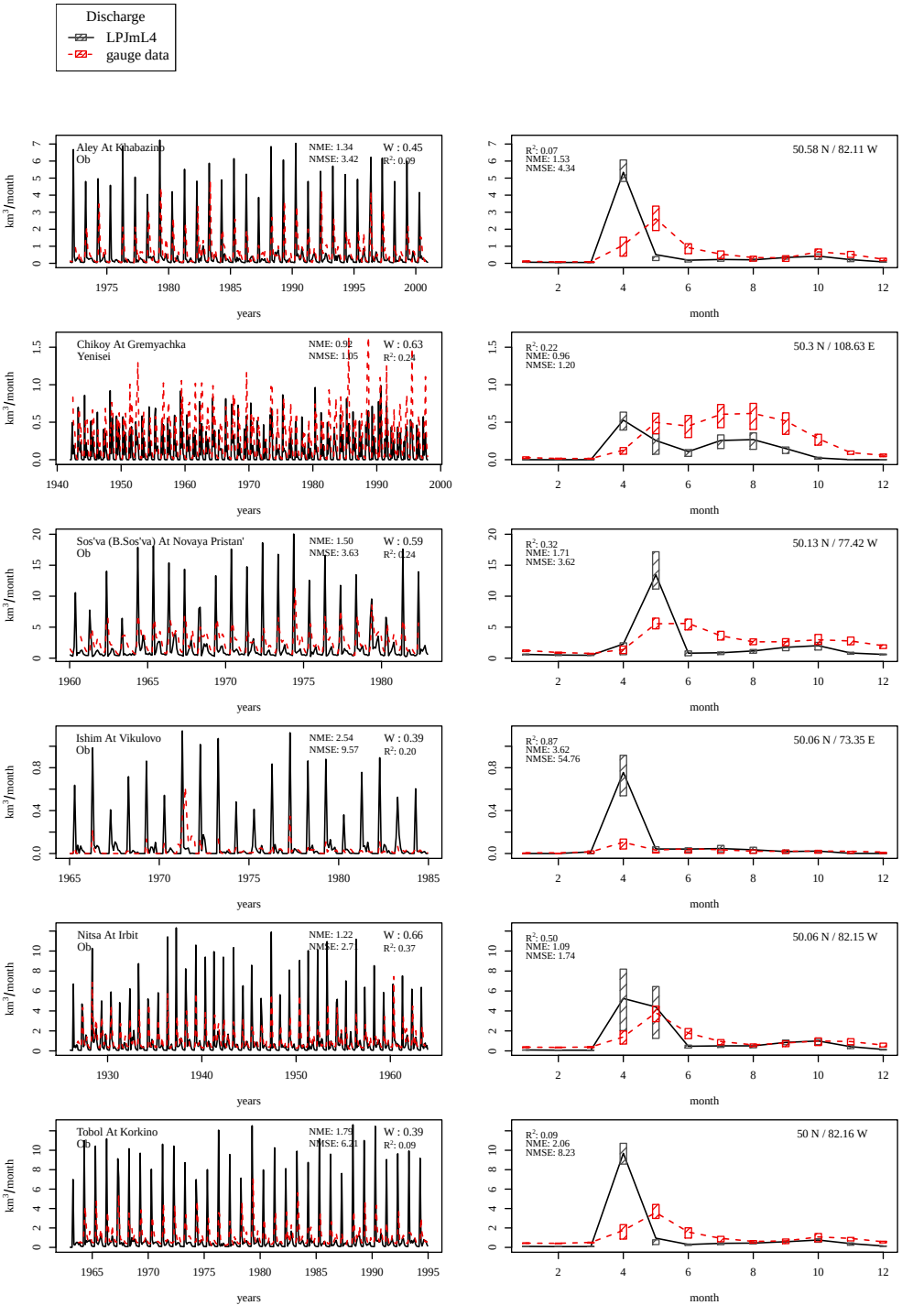

Figure S61. Evaluation of river discharge at gauging stations [43].

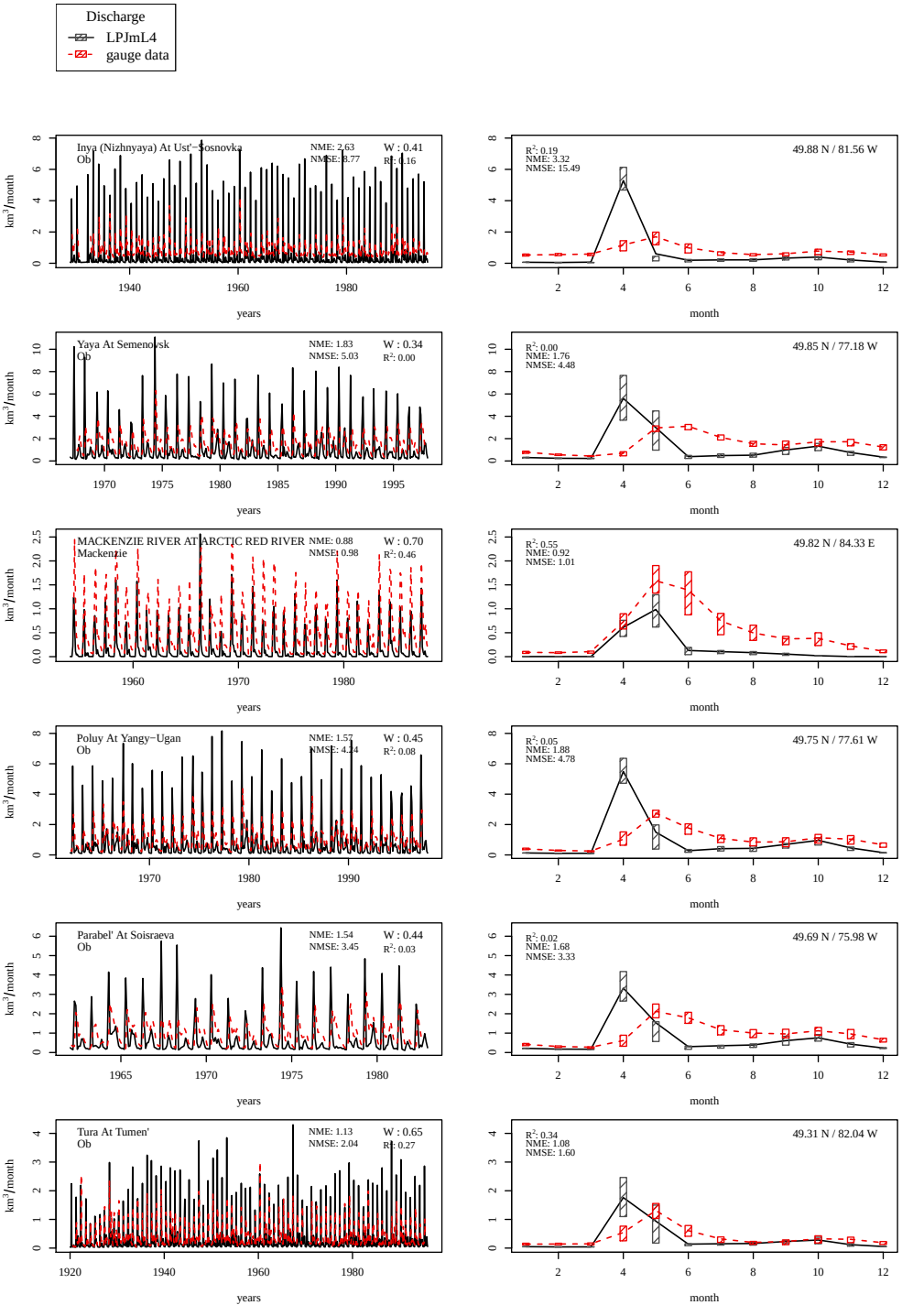

Figure S62. Evaluation of river discharge at gauging stations [44].

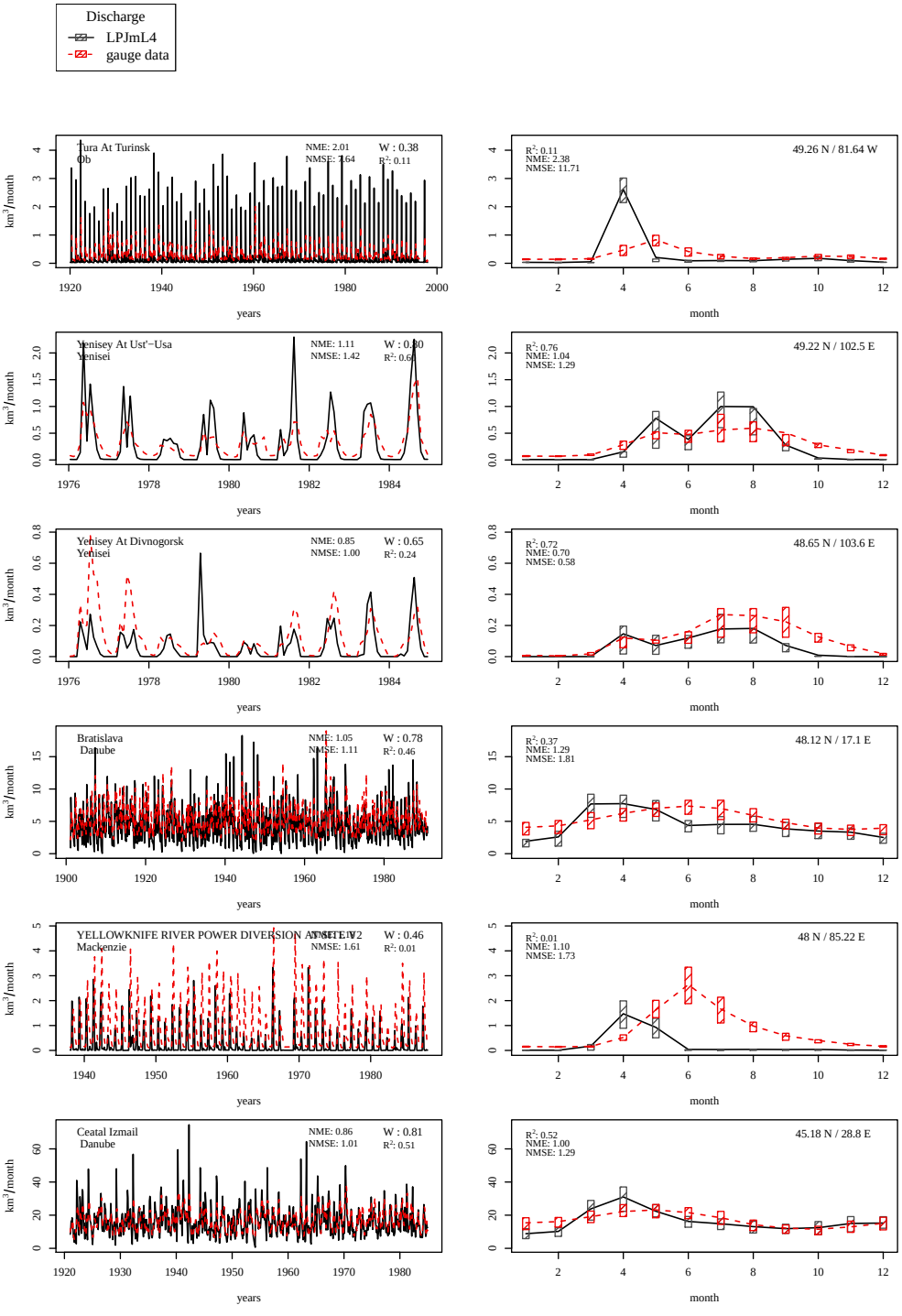

Figure S63. Evaluation of river discharge at gauging stations [45].

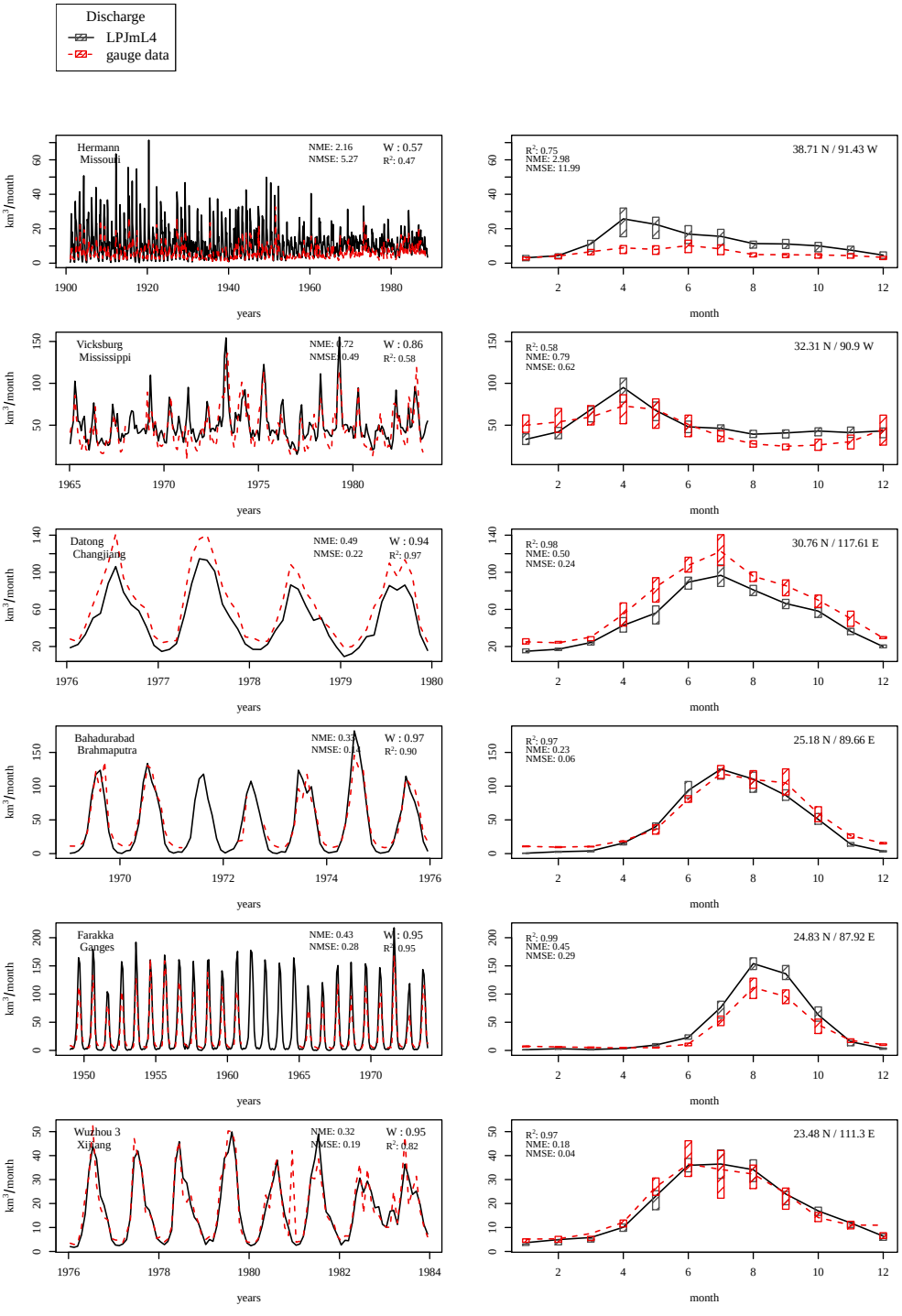

Figure S64. Evaluation of river discharge at gauging stations [46].

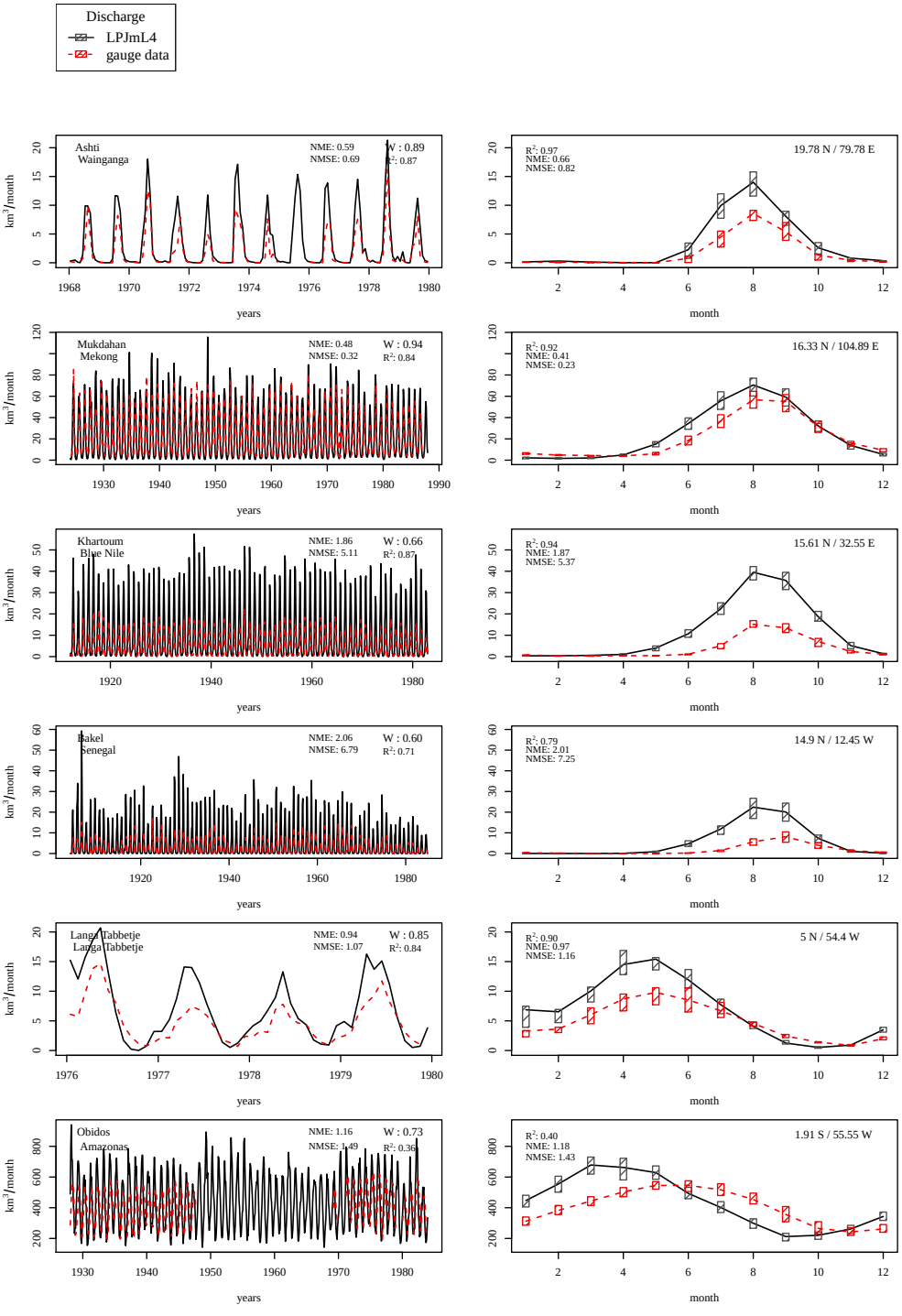

Figure S65. Evaluation of river discharge at gauging stations [47].

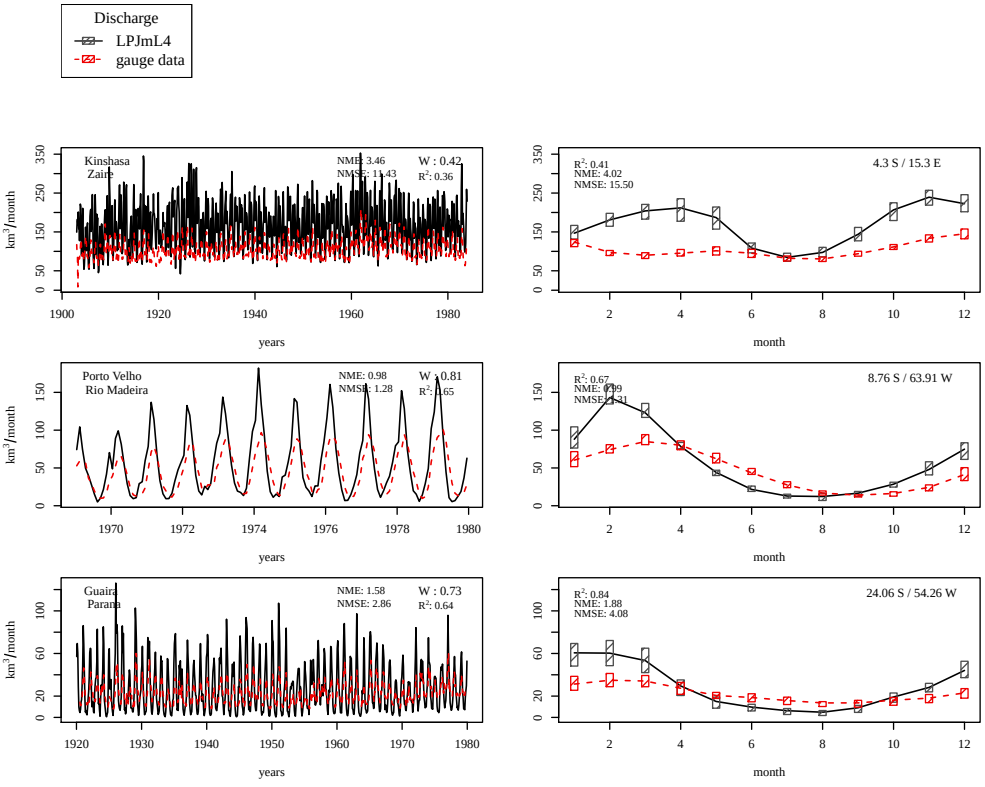

Figure S66. Evaluation of river discharge at gauging stations [48].

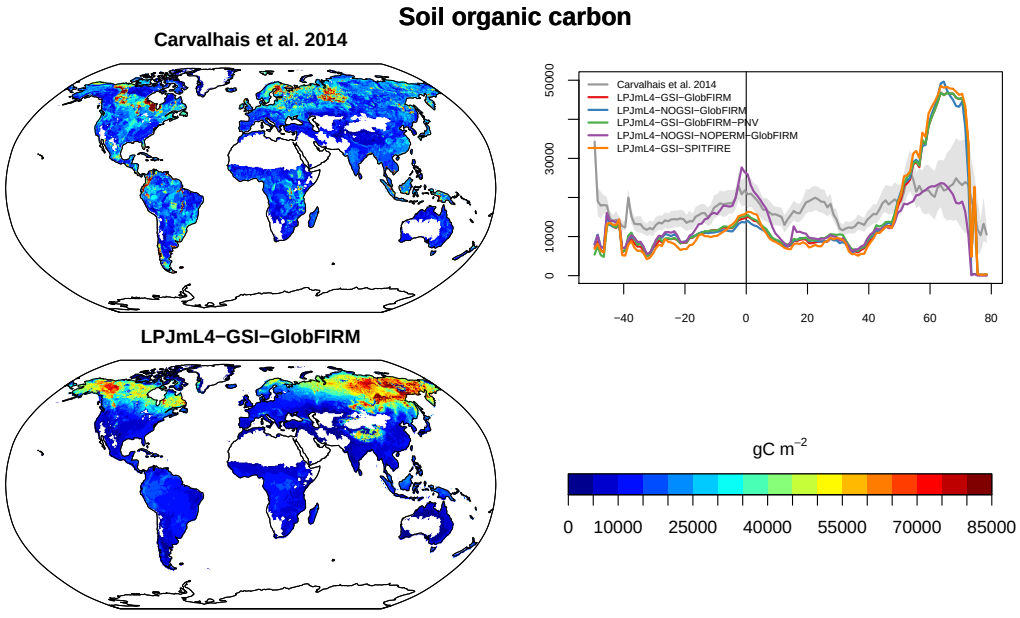

Figure S67. The maps (left side) show the spatial pattern of soil organic carbon [$\mathrm{gC\,m^{-2}}$] distribution from the standard LPJmL4 simulation against data from Carvalhais et al. (2014). The graph on the right side shows the latitudinal pattern of vegetation biomass distribution simulated by the different versions of LPJmL4 against data from Carvalhais et al. (2014).

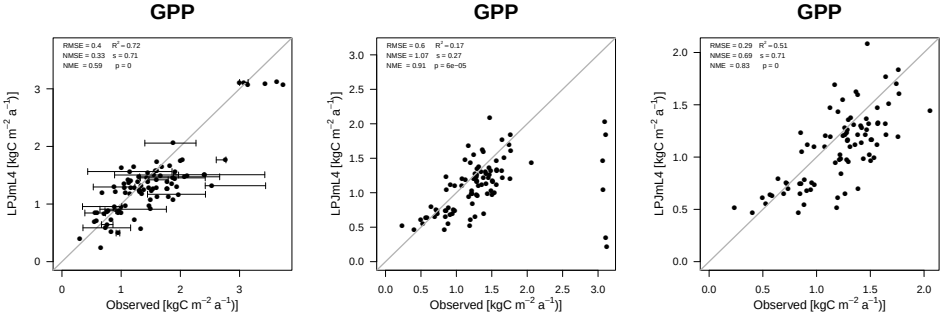

(a) (b) (c)

Figure S68. Comparison of GPP from different sources; MTE data (Jung et al., 2011) against plot data (Luyssaert et al., 2007) (a), LPJmL4 against MTE data (Jung et al., 2011) (b), and LPJmL4 against MTE data (Jung et al., 2011) but without the outliers of very high GPP in the MTE data (c).

(a)

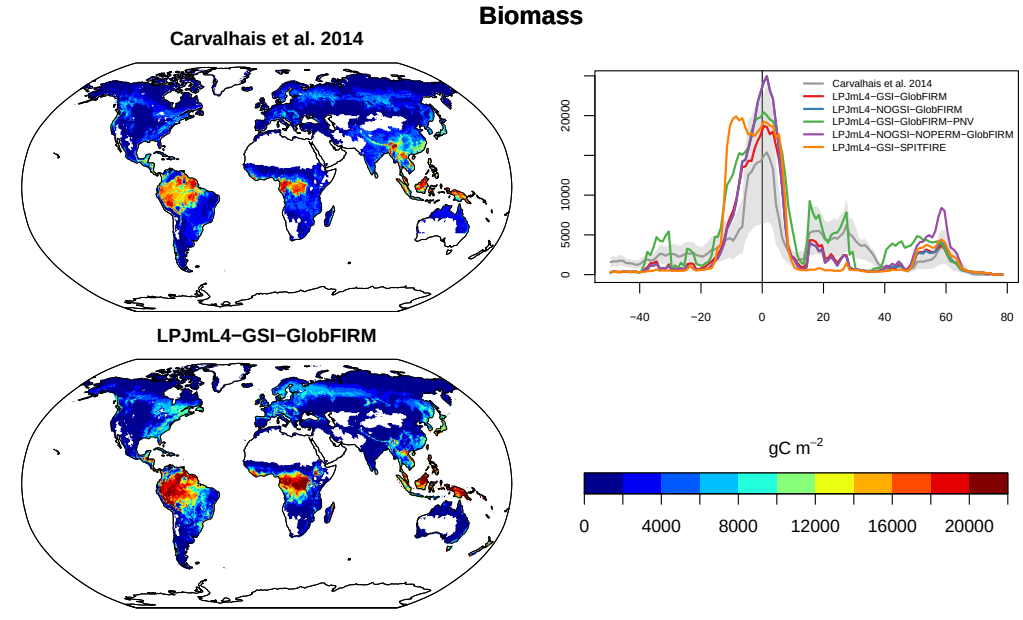

(b)

(b)

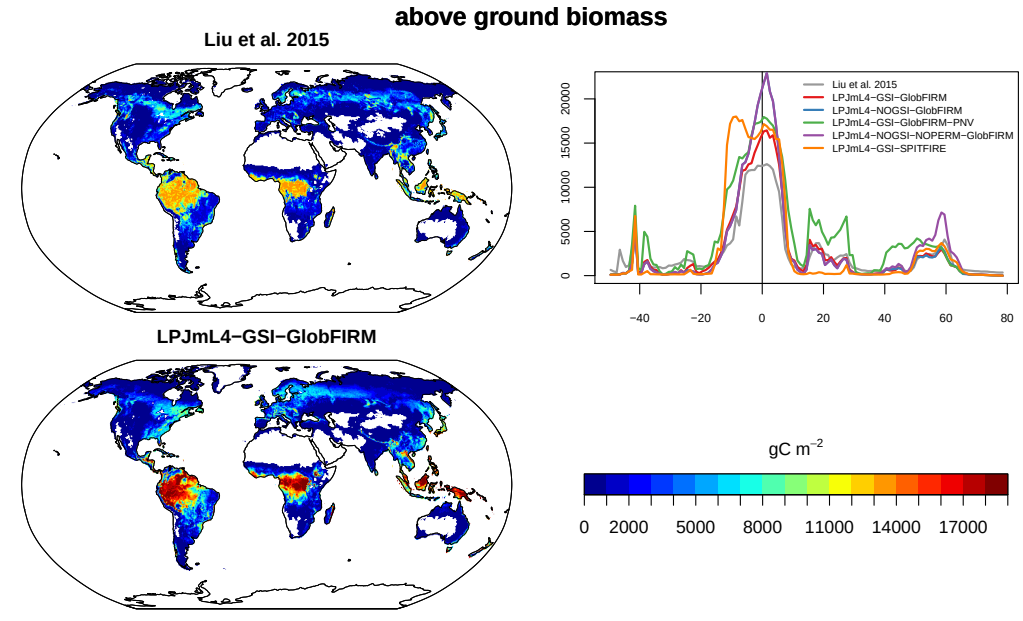

Figure S69. (a) The maps (left side) show the spatial pattern of vegetation biomass [gC m^{-2}] distribution from the standard LPJmL4 simulation against data from Jung et al. (2011); Carvalhais et al. (2014). The graph on the right side shows the latitudinal pattern of vegetation biomass distribution simulated by the different versions of LPJmL4 against data from Jung et al. (2011); Carvalhais et al. (2014). (b) Similar as above but for aboveground biomass [gC m^{-2}] from Liu et al. (2015).

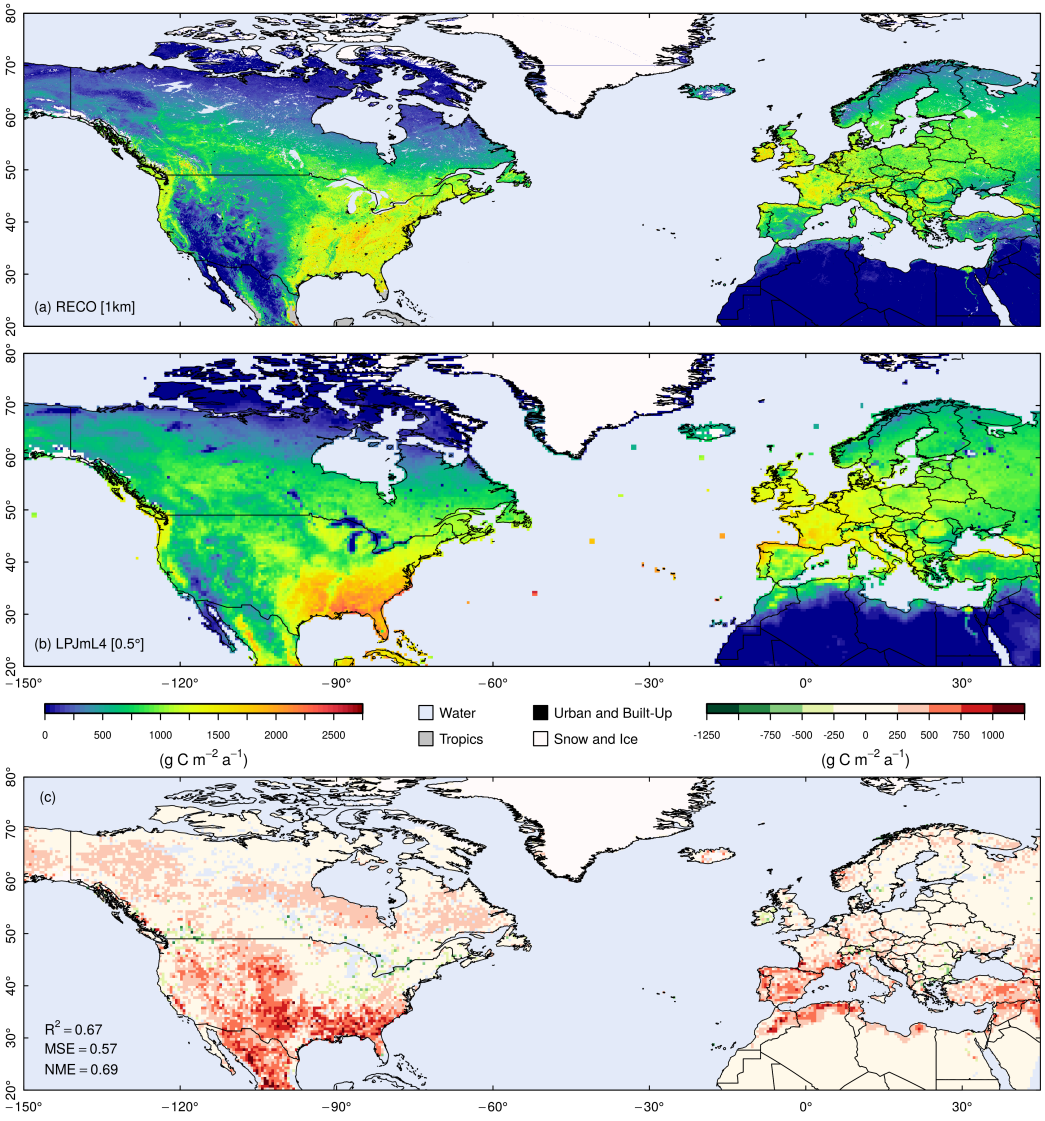

Figure S70. Evaluation of ecosystem respiration [gC m^{-2} a^{-1}] comparing LPJml4 with satellite-derived ecosystem respiration (Jägermeyr et al., 2014).

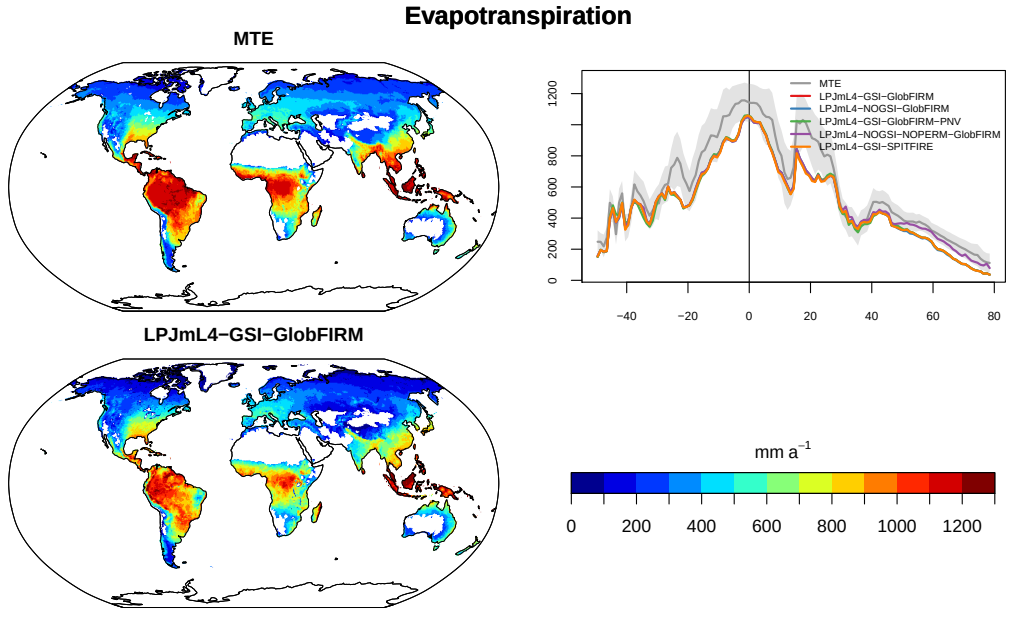

Figure S71. The maps (left side) show the spatial pattern of evapotranspiration [mm a^{-1}] distribution from the standard LPJmL4 simulation against the MTE data (Jung et al., 2011). The graph on the right side shows the latitudinal pattern of evapotranspiration distribution simulated by the different versions of LPJmL4 against data from Jung et al. (2011).

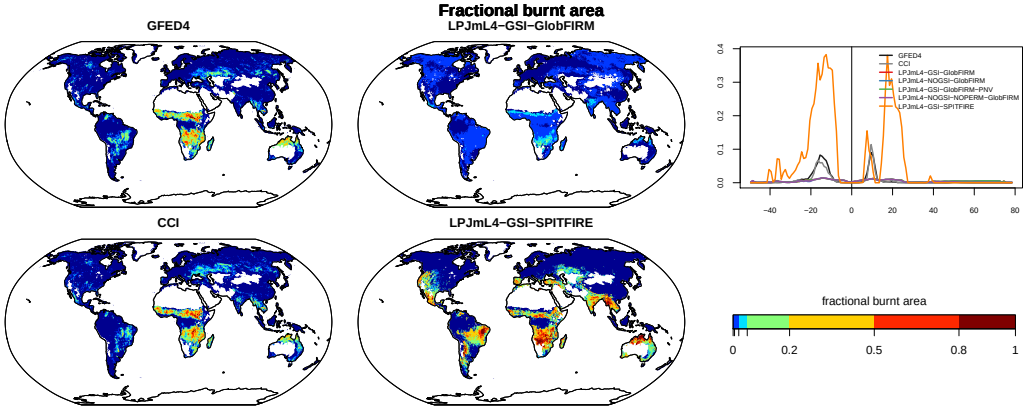

Figure S72. Observed and simulated estimations of fractional area burnt. Observed estimation both are based on remote sensing data (GFED4: http://www.globalfiredata.org/ and CCI Fire Version 4.1: http://cci.esa.int/data).

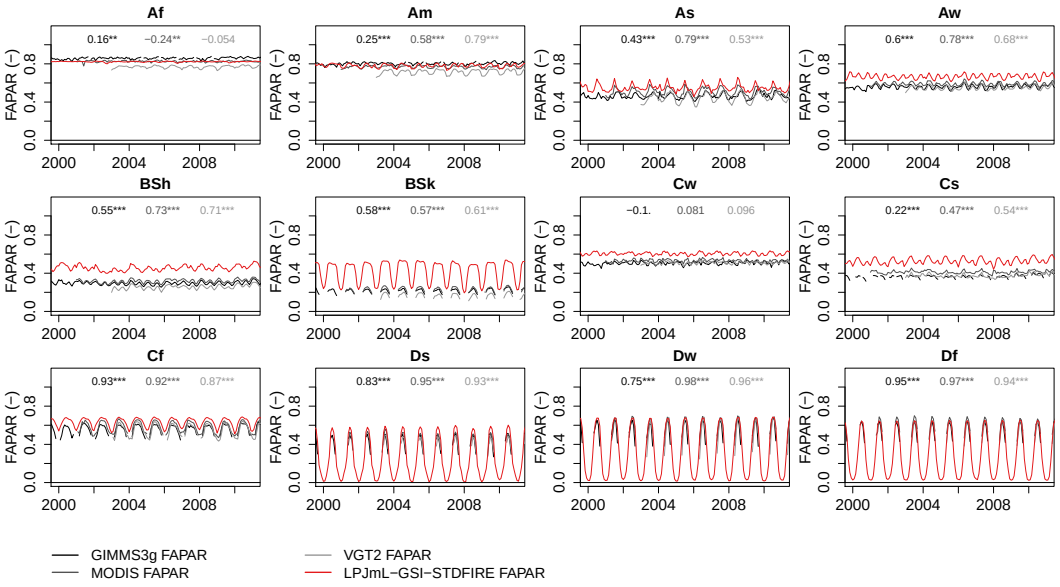

Figure S73. FAPAR comparison of seasonal dynamic for Koeppen-Geiger classification against 3 different remote sensing products: MODIS FAPAR, GIMMS3g FAPAR, and VGT2 FAPAR.
A map of the Köppen classification can be found here [http://koeppen-geiger.vu-wien.ac.at].

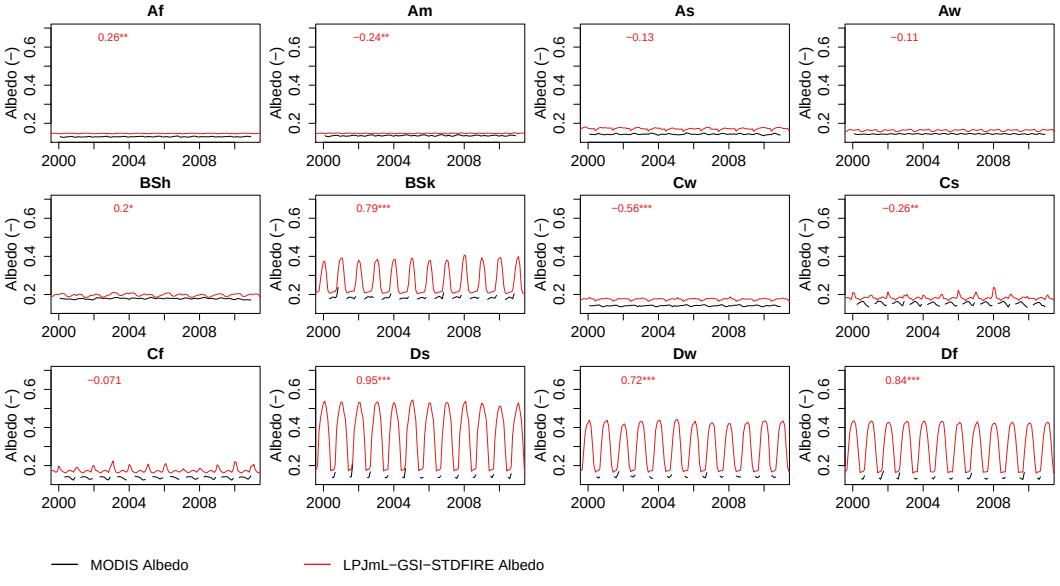

Figure S74. Albedo comparison for Koeppen-Geiger classification with MODIS remote sensing data.
A map of the Köppen classification can be found here [http://koeppen-geiger.vu-wien.ac.at].

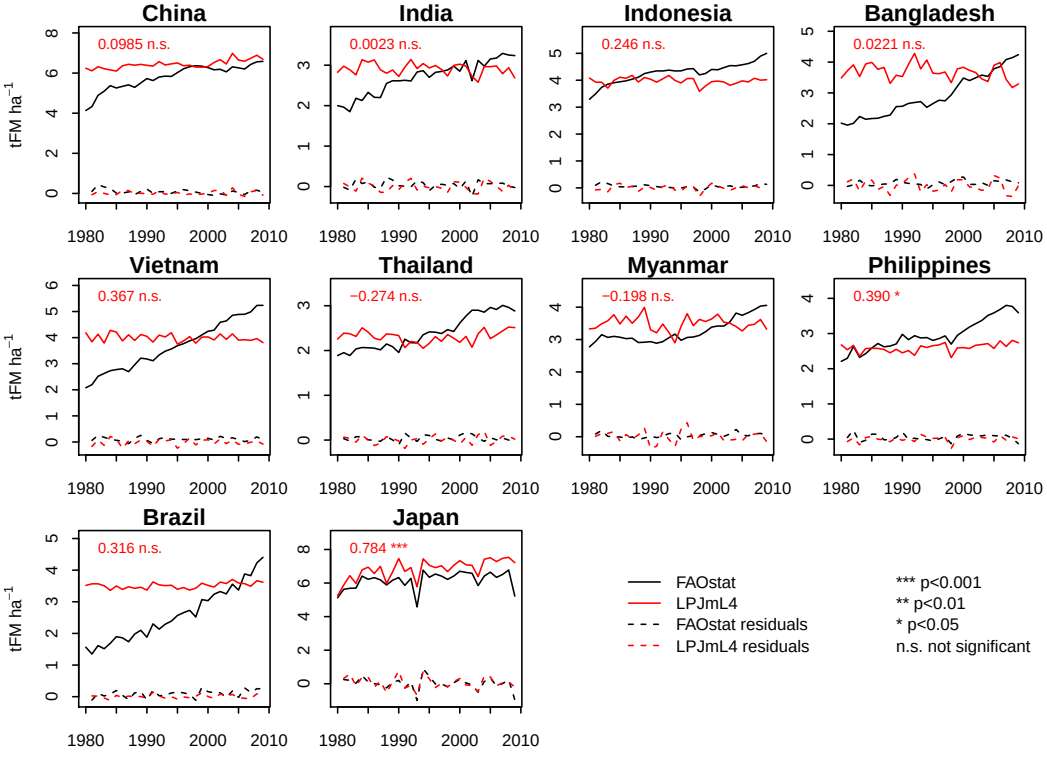

Figure S75. Evaluation of crop variability comparing rice yields computed by LPJml4 with FAO yield data.

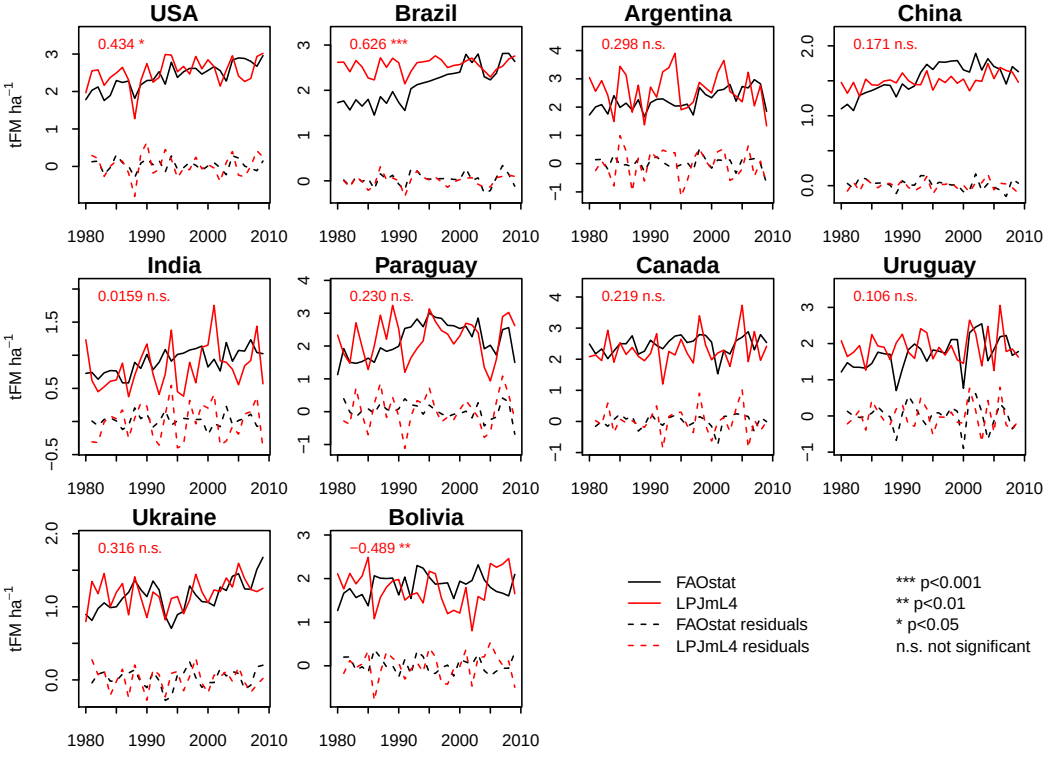

Figure S76. As Fig. S75 for soy.

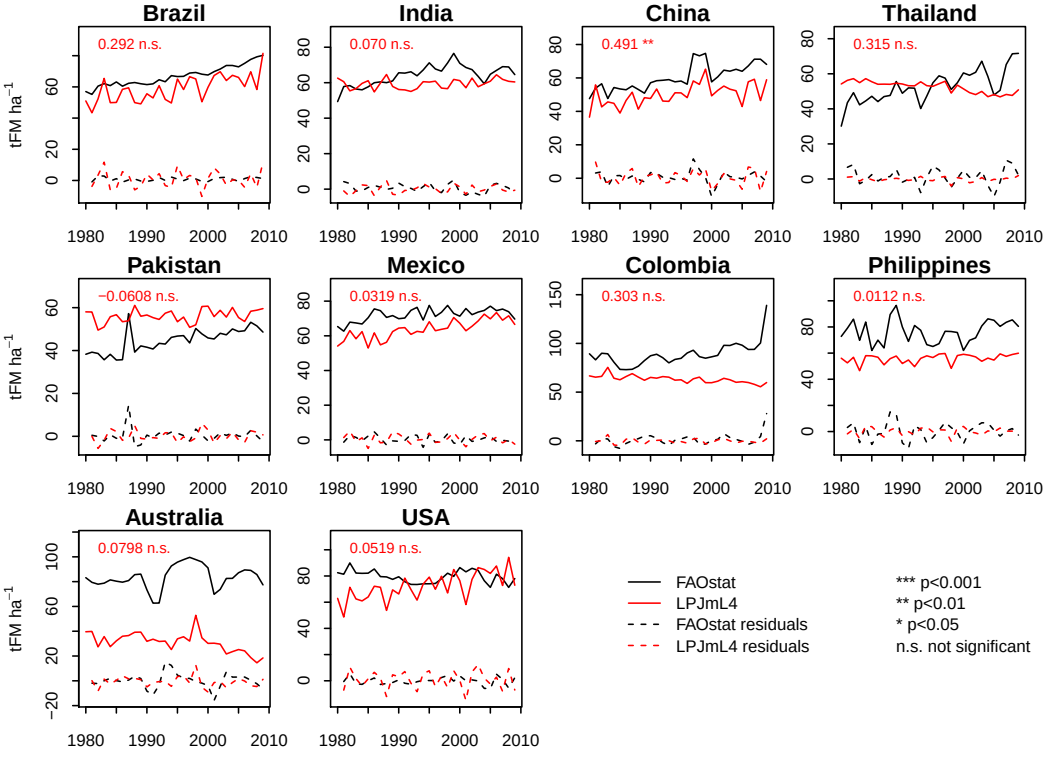

Figure S77. As Fig. S75 for sugarcane.

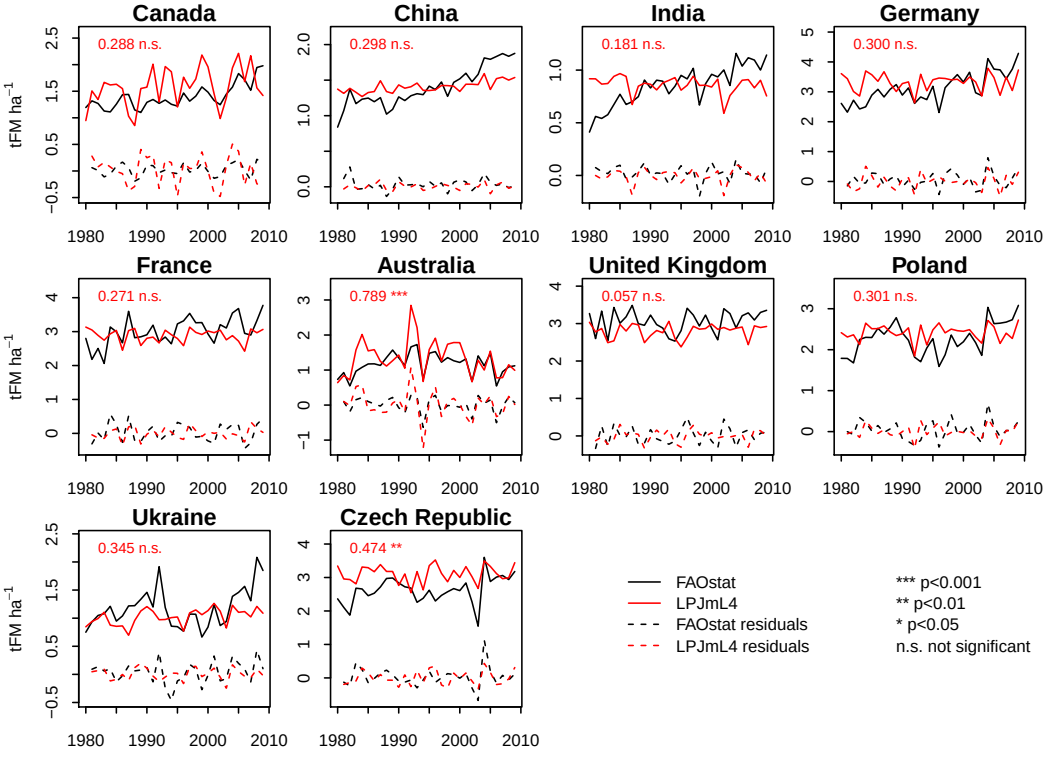

Figure S78. As Fig. S75 for rapeseed.

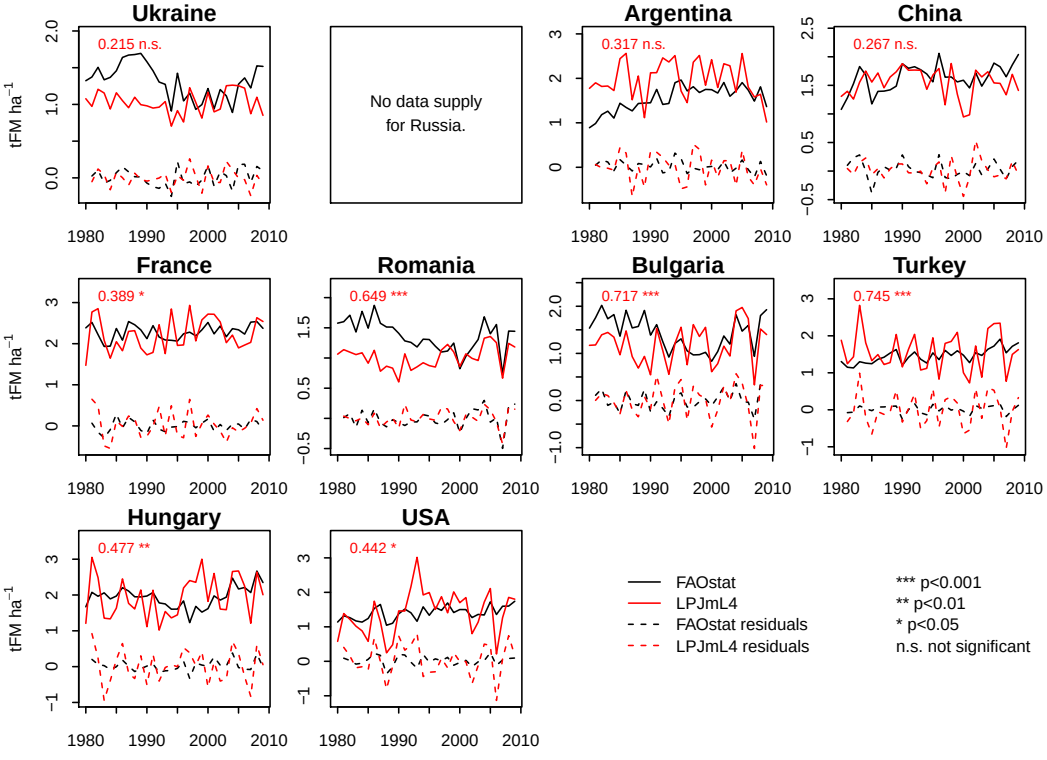

Figure S79. As Fig. S75 for sunflower.

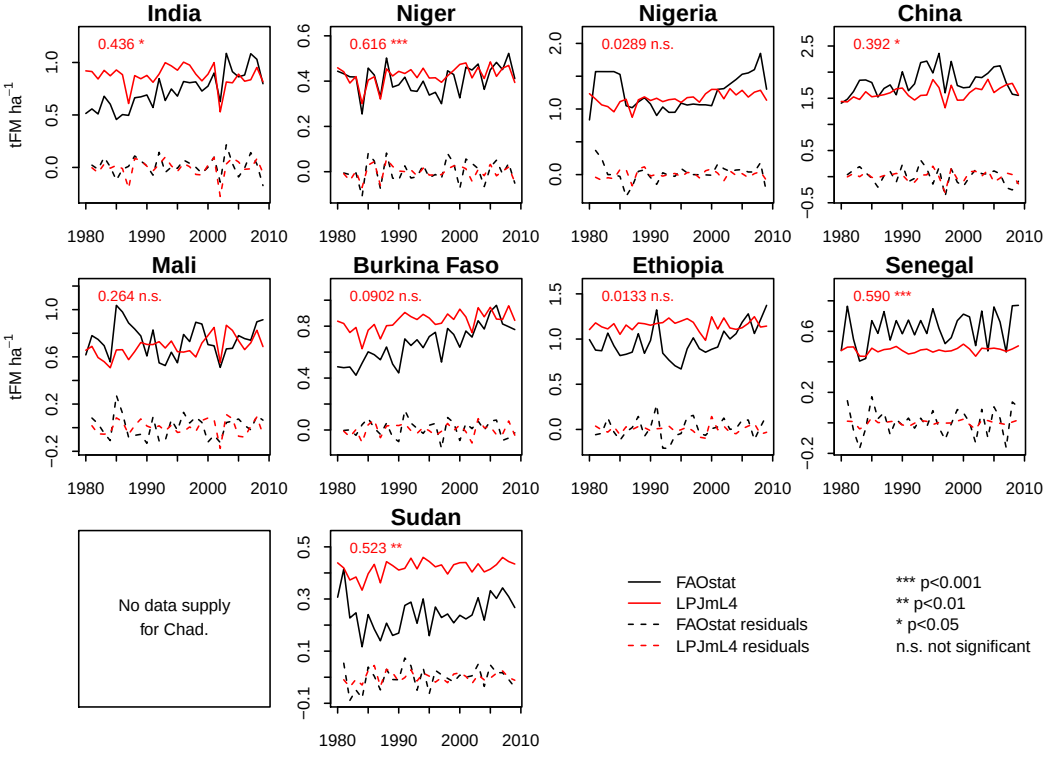

Figure S80. As Fig. S75 for millet.

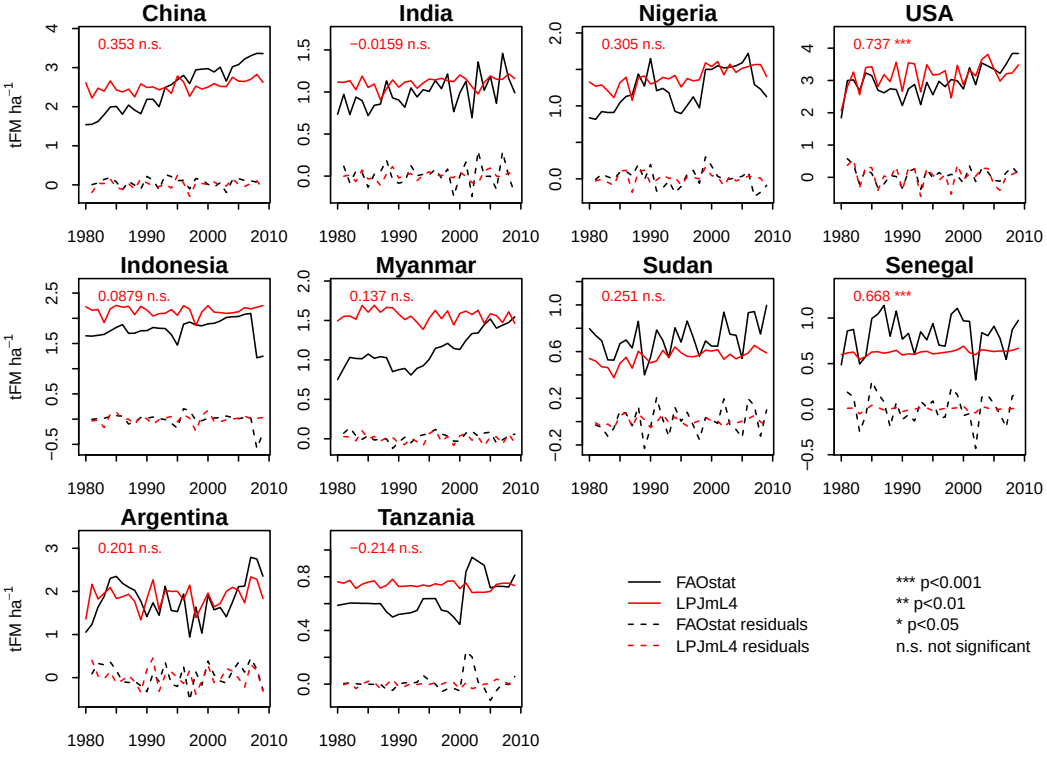

Figure S81. As Fig. S75 for peanut.

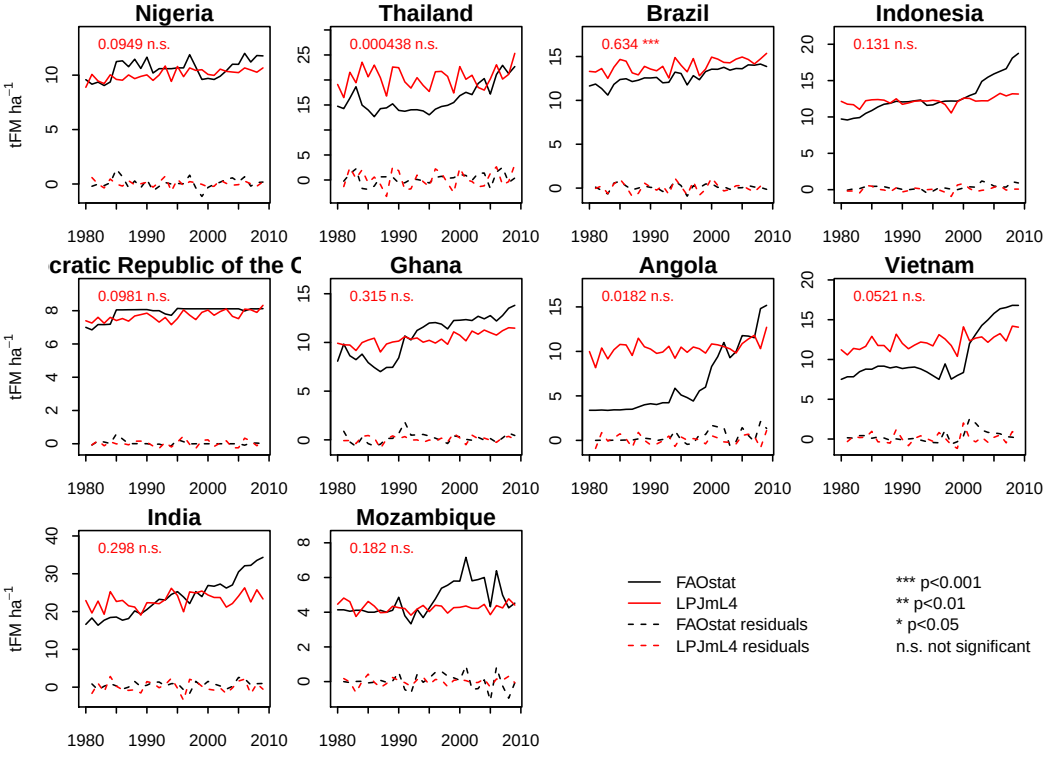

Figure S82. As Fig. S75 for cassava.

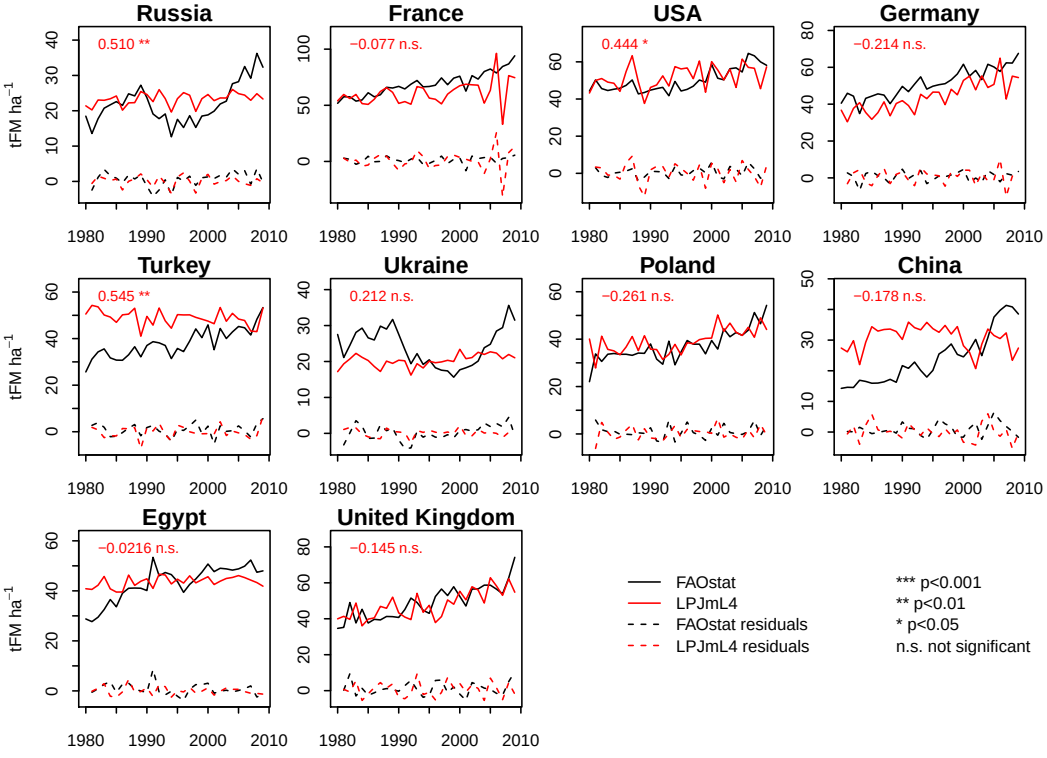

Figure S83. As Fig. S75 for sugar beet.

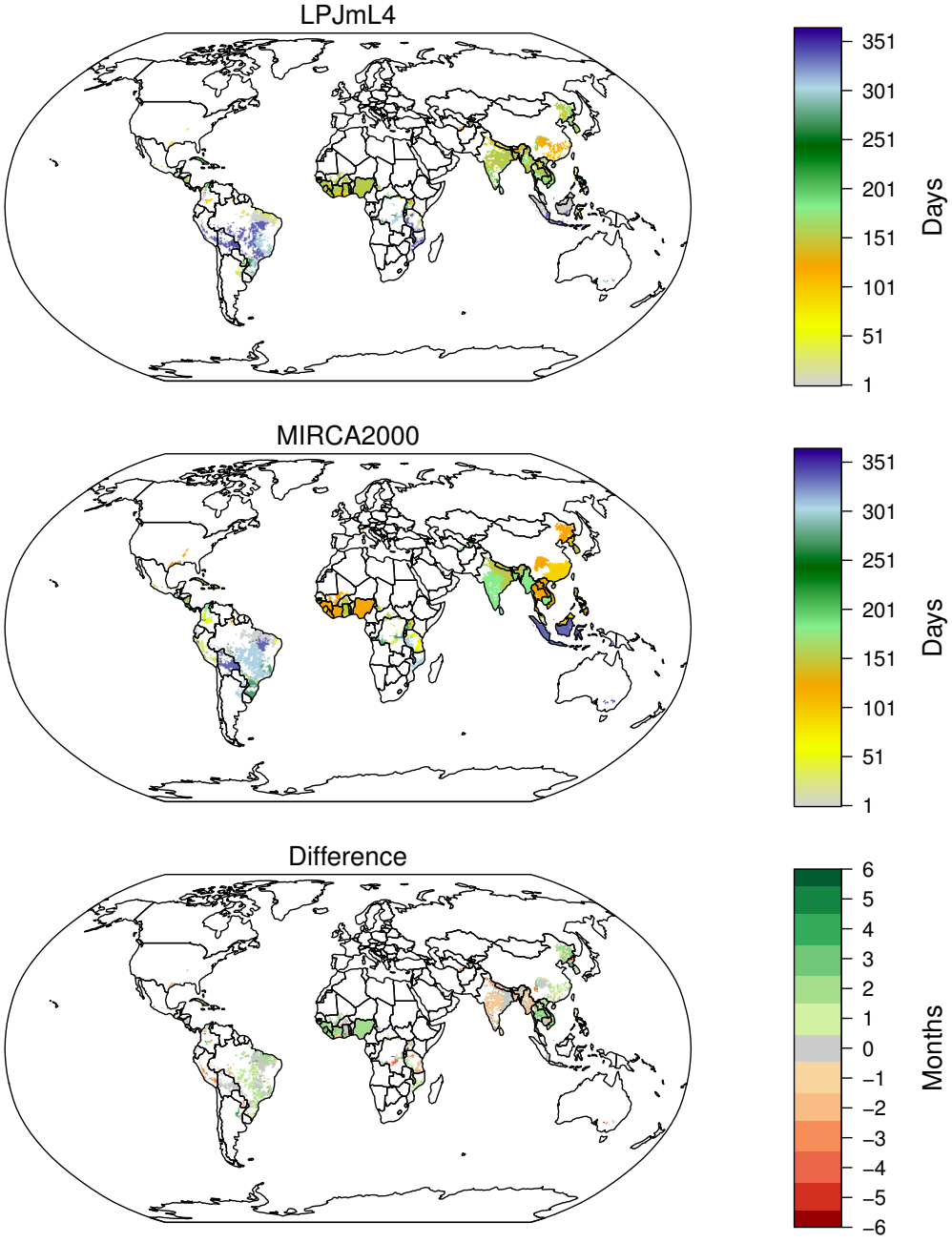

Figure S84. Evaluation of sowing dates of rice: (from top to bottom panel) simulated (LPJmL4) sowing date, observed (MIRCA2000) sowing date and difference between simulated and observed sowing date. Green colours (red colours) in the difference map indicate that simulated sowing dates are too late (too early) compared to observations. White colours indicate crop area smaller than 0.001% of grid cell area. Sowing dates in regions without seasonality are not shown.

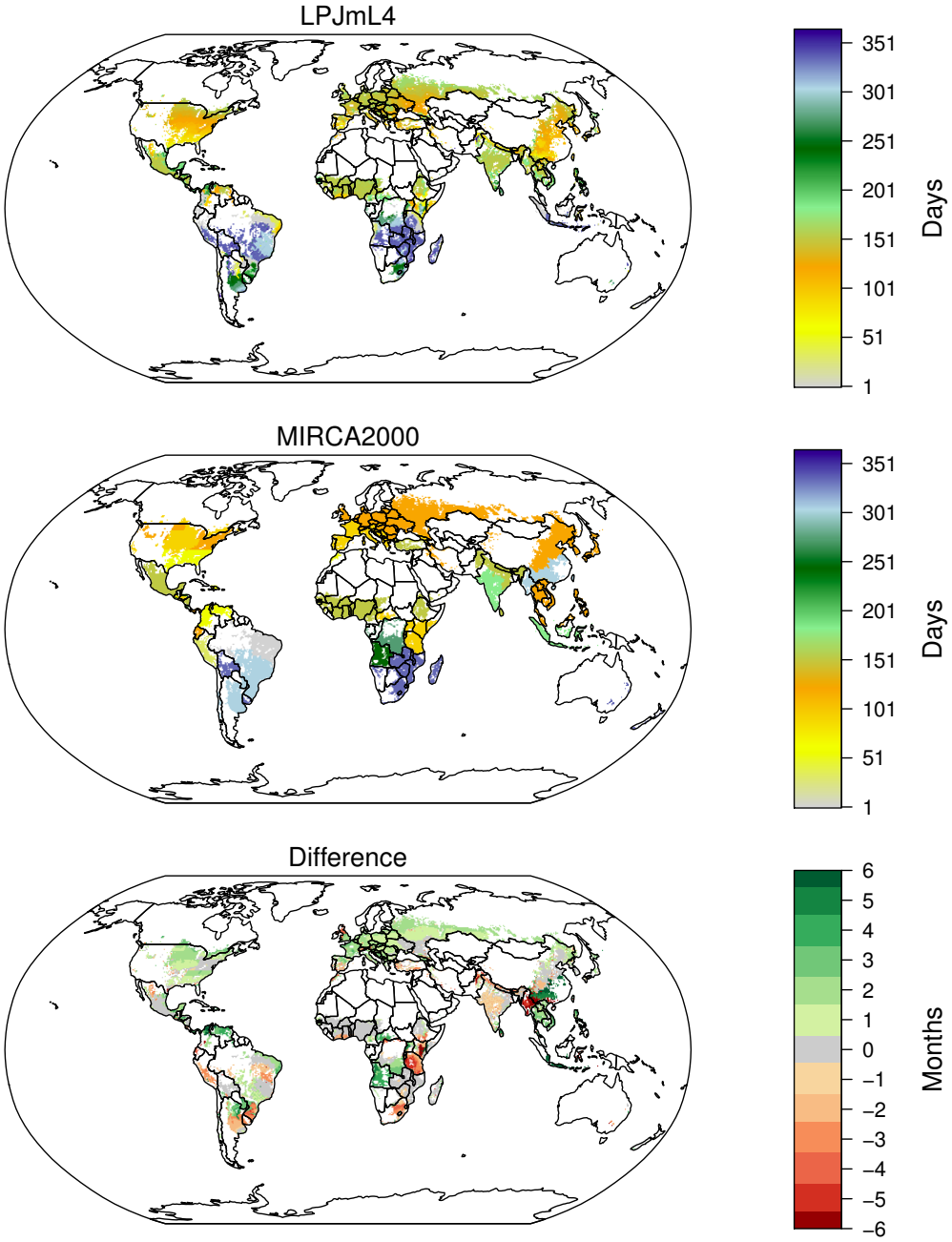

Figure S85. Evaluation of sowing dates of maize: Caption as for Fig.S84.

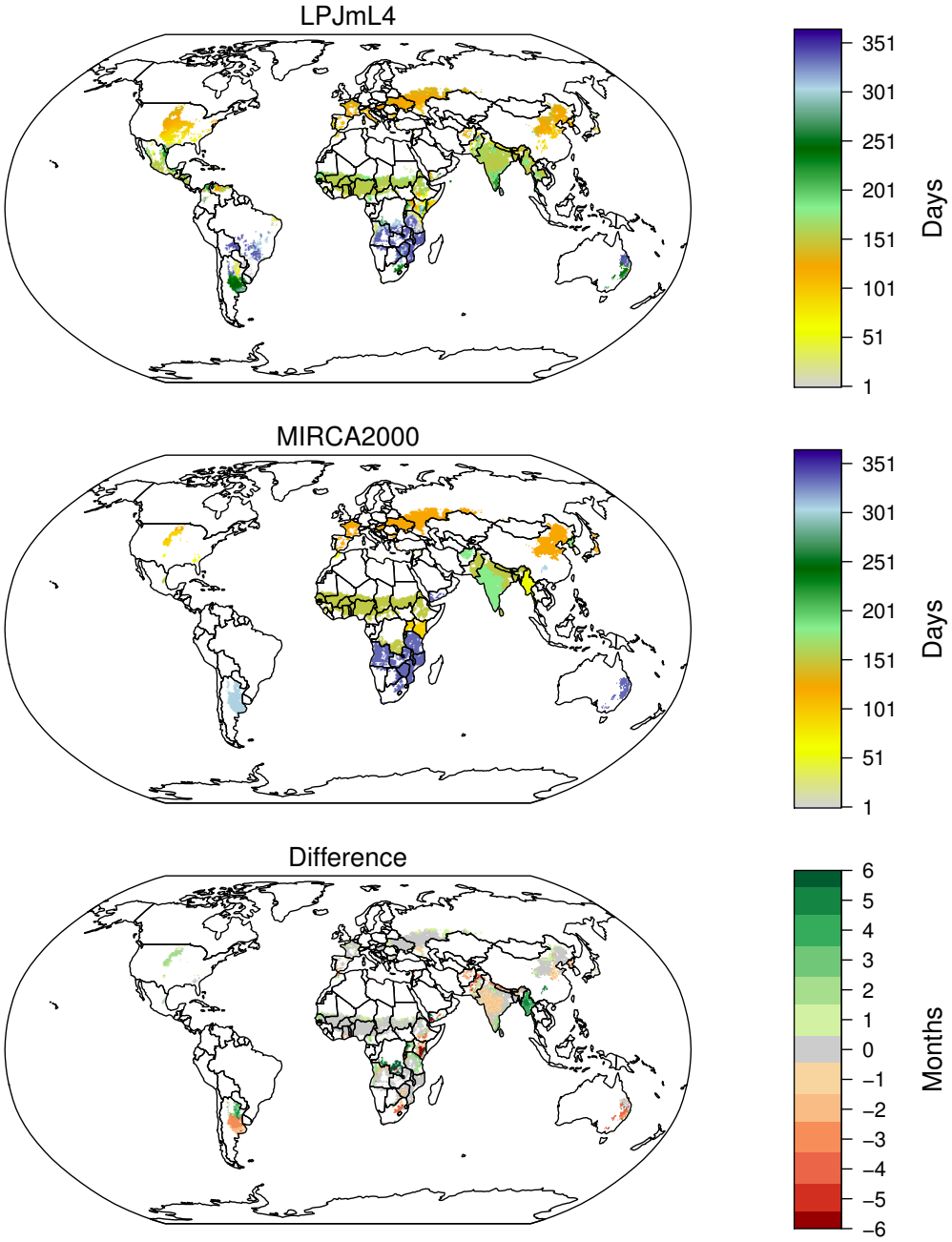

Figure S86. Evaluation of sowing dates of millet: Caption as for Fig.S84.

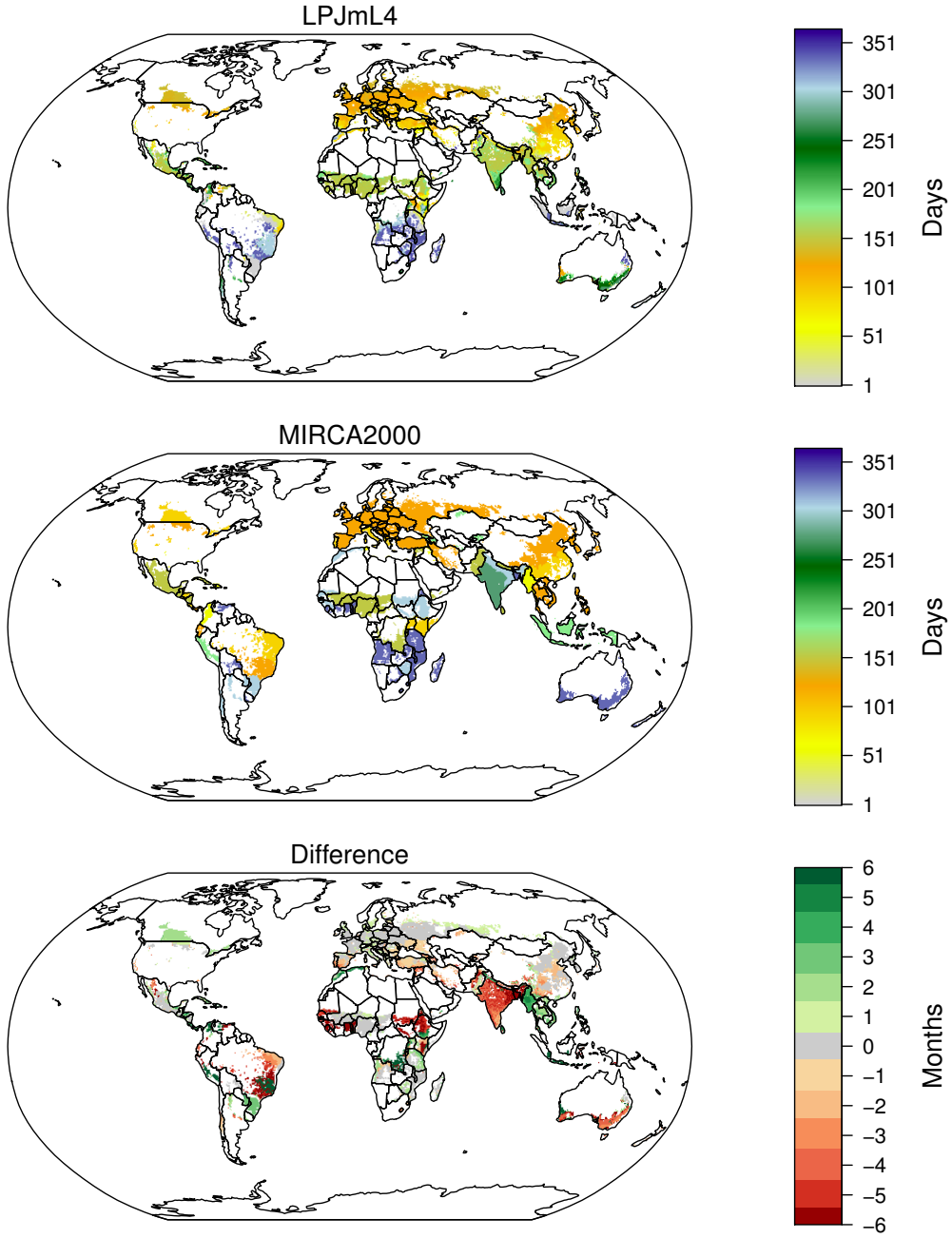

Figure S87. Evaluation of sowing dates of pulses: Caption as for Fig.S84.

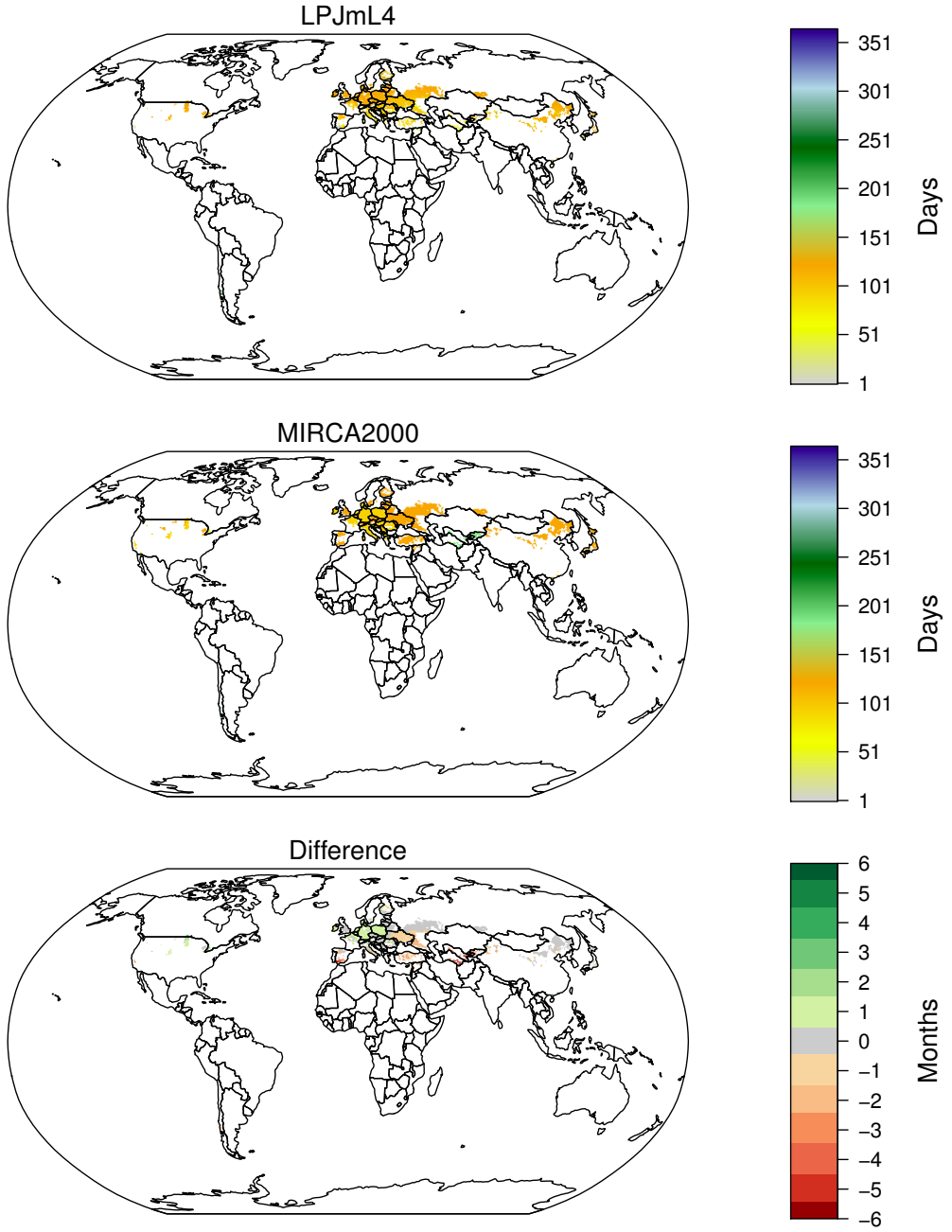

Figure S88. Evaluation of sowing dates of sugarbeet: Caption as for Fig.S84.

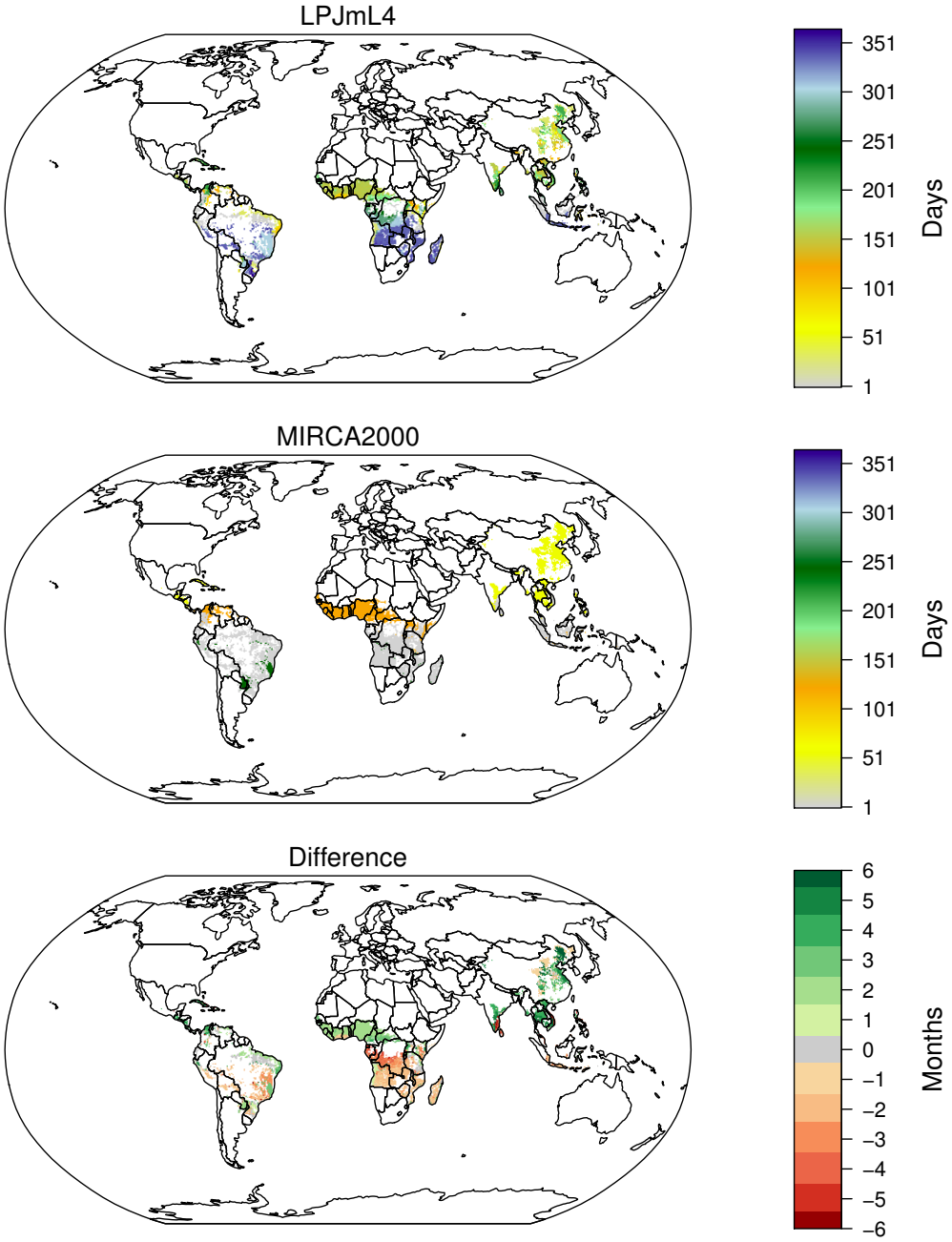

Figure S89. Evaluation of sowing dates of cassava: Caption as for Fig.S84.

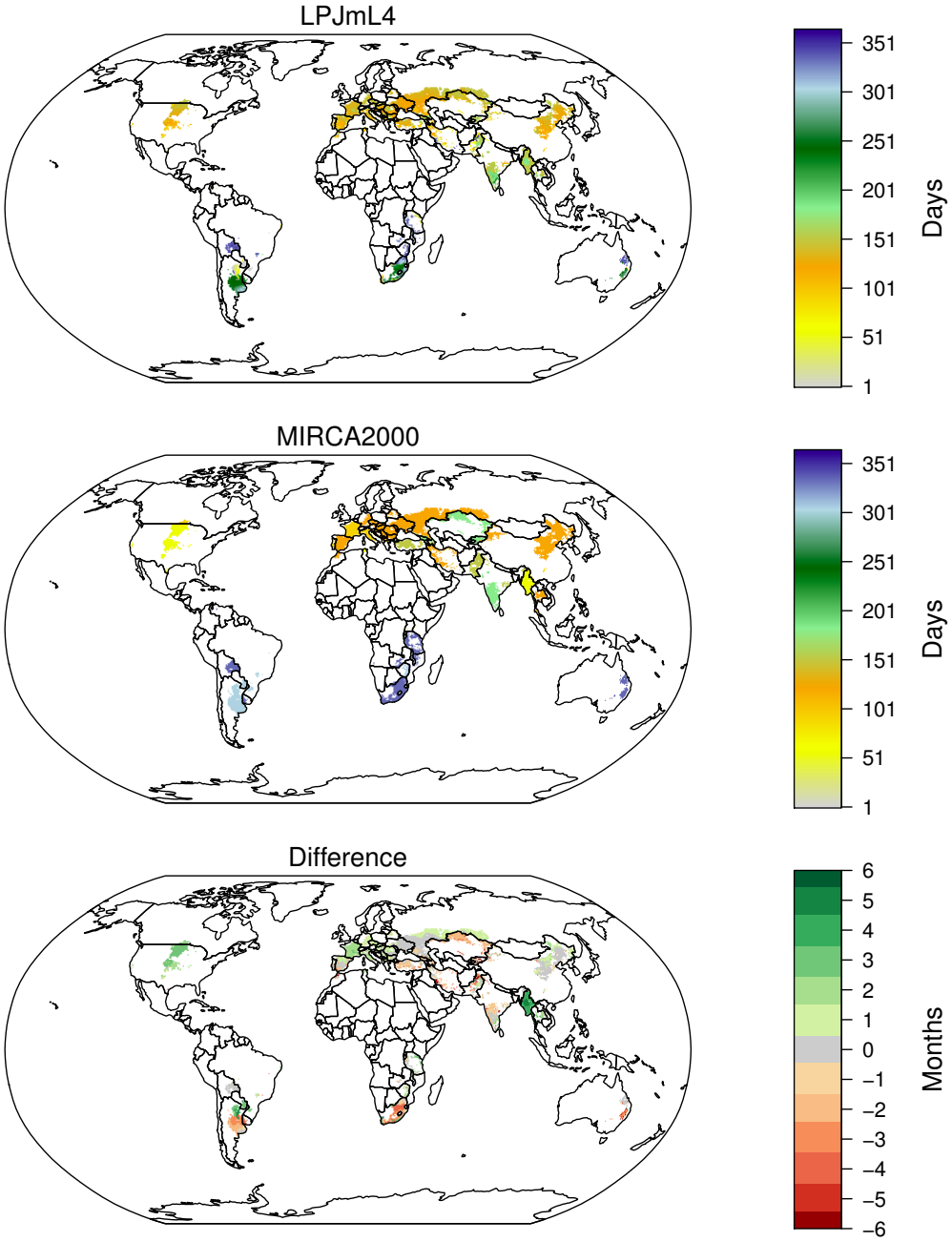

Figure S90. Evaluation of sowing dates of sunflower: Caption as for Fig.S84.

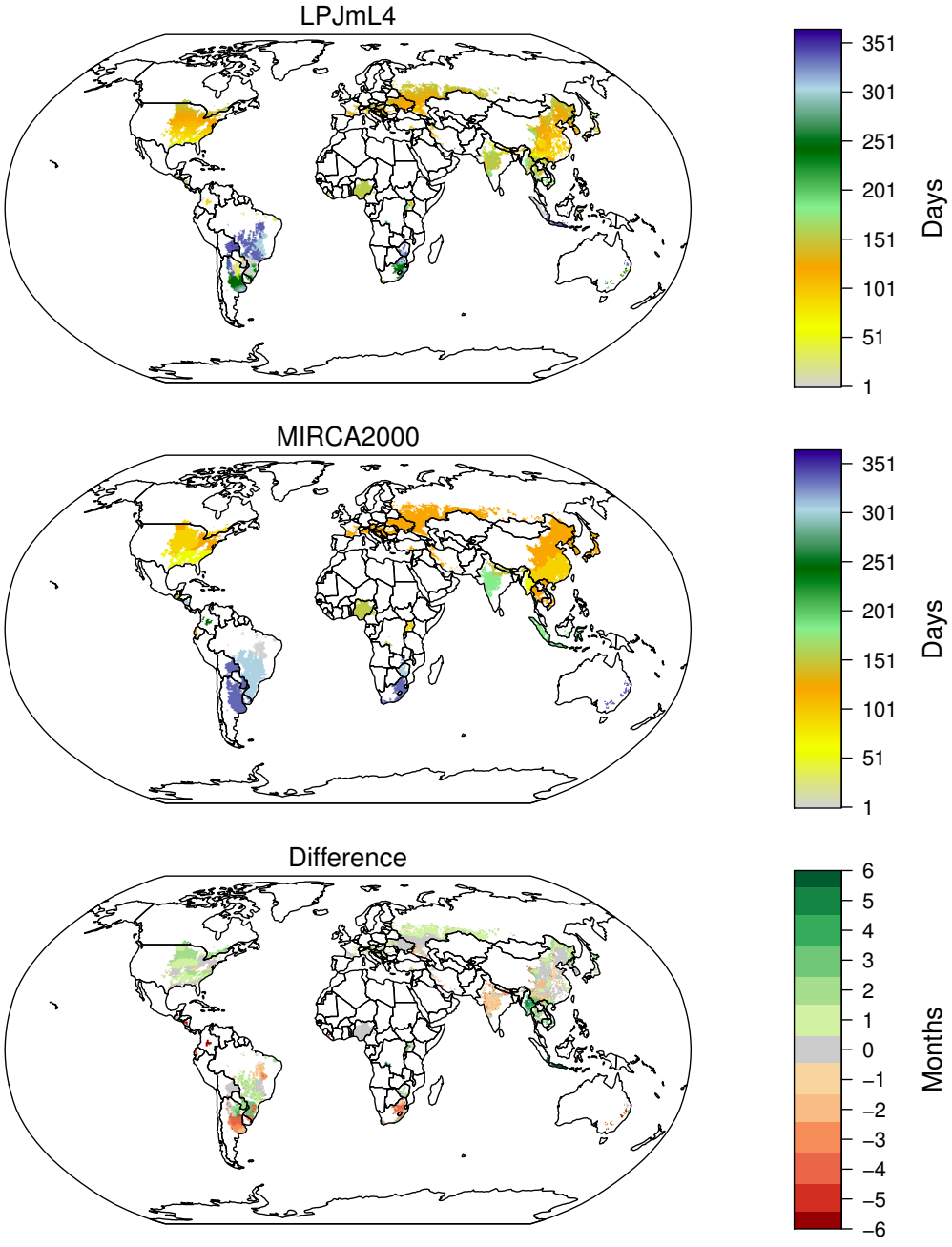

Figure S91. Evaluation of sowing dates of soybean: Caption as for Fig.S84.

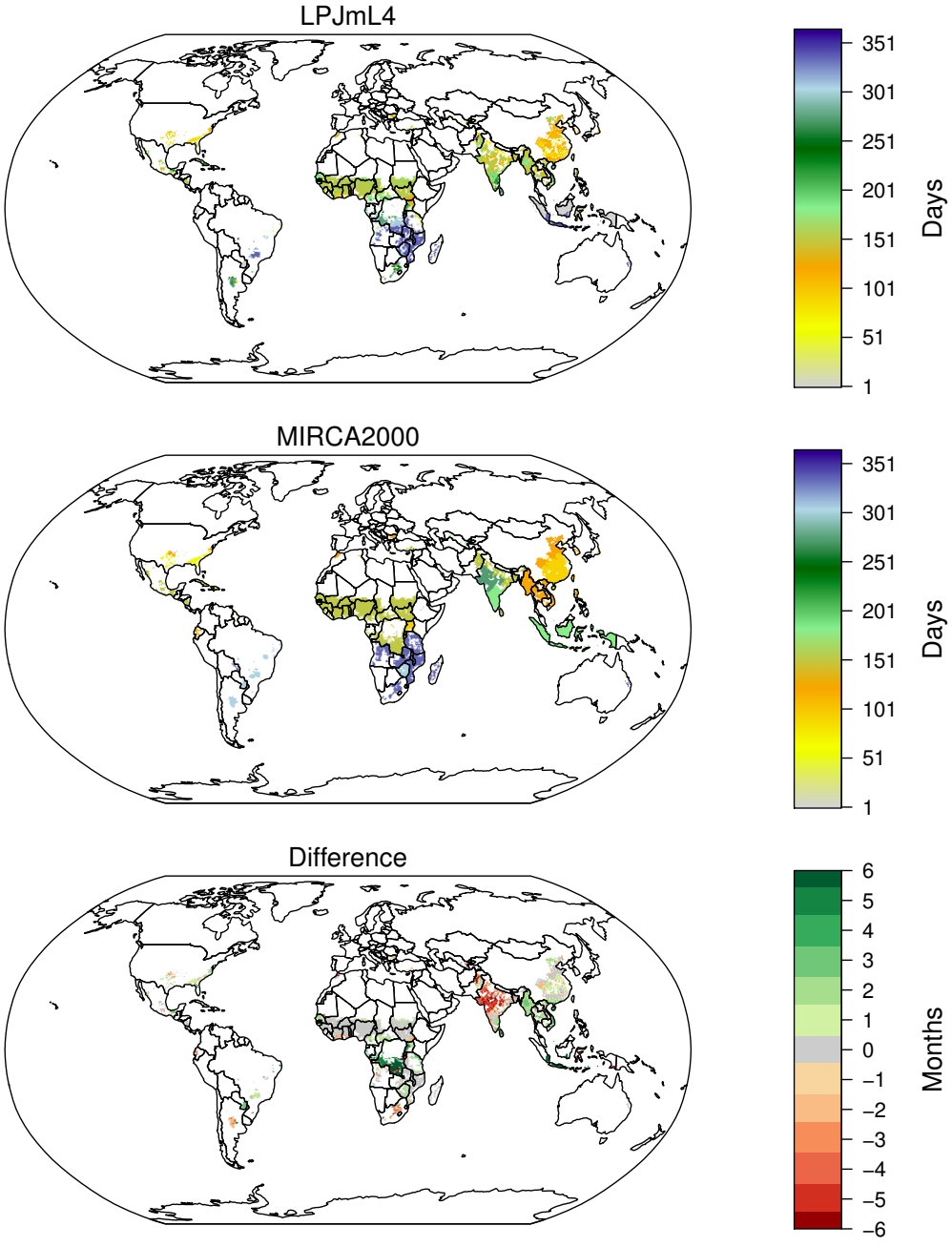

Figure S92. Evaluation of sowing dates of groundnut: Caption as for Fig.S84.

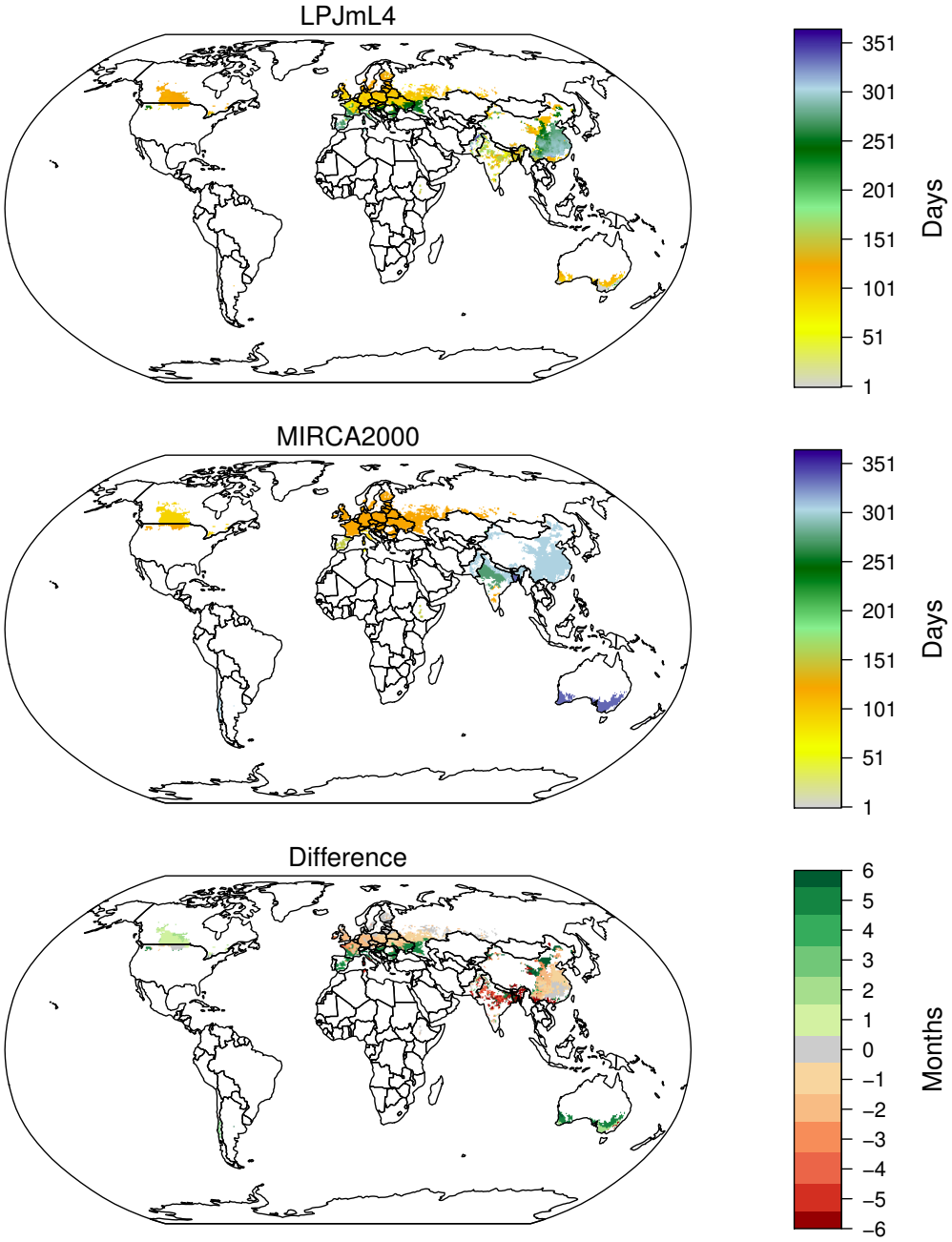

Figure S93. Evaluation of sowing dates of rapeseed: Caption as for Fig.S84.

]

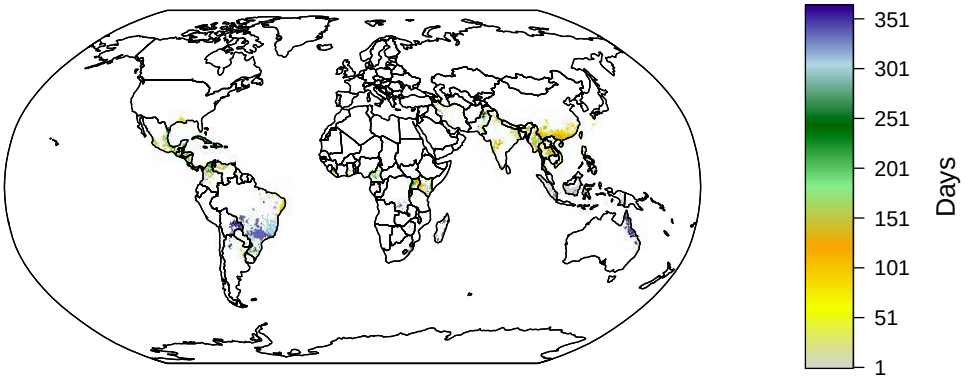

Figure S94. Simulated sowing dates of rainfed sugar cane.

Table S1. Comparison of field application efficiencies

World region	Surface	Sprinkler	Drip	Surface	Sprinkler	Drip	Surface	Sprinkler	Drip
	(this study)			(Rohwer et al., 2007)			(Sauer et al., 2010)		
North America	52	78	88	48	68	90	50	85	93
South America	50	77	87	51	68	90	38	75	88
Europe and Russia	52	80	90	53	73	90	52	86	93
Mena	62	89	95	49	69	90	22	60	80
SSA	51	70	90	54	75	90	28	64	82
Central and East Asia	50	79	82	48	68	90	42	79	89
South Asia	47	85	92	48	68	90	32	68	84
SE Asia and Oceania	48	67	85	48	71	90	38	75	88
World	50	79	89	49	70	90	42	78	89

For reasons of comparison, we employ here the traditional definition: consumed per applied irrigation water for major world regions compared with literature values in %. This study's results are area-weighted averages, based on current distribution of irrigation systems (source: Jägermeyr et al. (2015)). MENA – Middle East and North Africa; SSA – sub-Saharan Africa.

References

Carvalhais, N., Forkel, M., Khomik, M., Bellarby, J., Jung, M., Migliavacca, M., Mu, M., Saatchi, S., Santoro, M., Thurner, M., Weber, U., Ahrens, B., Beer, C., Cescatti, A., Randerson, J. T., and Reichstein, M.: Global covariation of carbon turnover times with climate in terrestrial ecosystems, Nature, 514, 213–217, 10.1038/nature13731, 2014.

Jägermeyr, J., Gerten, D., Lucht, W., Hostert, P., Migliavacca, M., and Nemani, R.: A high-resolution approach to estimating ecosystem respiration at continental scales using operational satellite data, Global change biology, 20, 1191–1210, doi:10.1111/gcb.12443, 2014.

Jägermeyr, J., Gerten, D., Heinke, J., Schaphoff, S., Kummu, M., and Lucht, W.: Water savings potentials of irrigation systems: global simulation of processes and linkages, Hydrology and Earth System Sciences, 19, 3073–3091, doi:10.5194/hess-19-3073-2015, 2015.

Jung, M., Reichstein, M., Margolis, H. A., Cescatti, A., Richardson, A. D., Arain, M. A., Arneth, A., Bernhofer, C., Bonal, D., Chen, J., Gianelle, D., Gobron, N., Kiely, G., Kutsch, W., Lasslop, G., Law, B. E., Lindroth, A., Merbold, L., Montagnani, L., Moors, E. J., Papale, D., Sottocornola, M., Vaccari, F., and Williams, C.: Global patterns of land-atmosphere fluxes of carbon dioxide, latent heat, and sensible heat derived from eddy covariance, satellite, and meteorological observations, Journal of Geophysical Research: Biogeosciences, 116, doi:10.1029/2010JG001566, 2011.

Liu, Y. Y., van Dijk, A. I. J. M., de Jeu, R. A. M., Canadell, J. G., McCabe, M. F., Evans, J. P., and Wang, G.: Recent reversal in loss of global terrestrial biomass, Nature Clim. Change, 5, 470–474, doi:10.1038/nclimate2581, 2015.

Luyssaert, S., Inglima, I., Jung, M., Richardson, A. D., Reichstein, M., Papale, D., Piao, S. L., Schulze, E. D., Wingate, L., Matteucci, G., Aragao, L., Aubinet, M., Beer, C., Bernhofer, C., Black, K. G., Bonal, D., Bonnefond, J. M., Chambers, J., Ciais, P., Cook, B., Davis, K. J., Dolman, A. J., Gielen, B., Goulden, M., Grace, J., Granier, A., Grelle, A., Griffis, T., Grünwald, T., Guidolotti, G., Hanson, P. J., Harding, R., Hollinger, D. Y., Hutyra, L. R., Kolari, P., Kruijt, B., Kutsch, W., Lagergren, F., Laurila, T., Law, B. E., Le Maire, G., Lindroth, A., Loustau, D., Malhi, Y., Mateus, J., Migliavacca, M., Misson, L., Montagnani, L., Moncrieff, J., Moors, E., Munger, J. W., Nikinmaa, E., Ollinger, S. V., Pita, G., Rebmann, C., Roupsard, O., Saigusa, N., Sanz, M. J., Seufert, G., Sierra, C., Smith, M. L., Tang, J., Valentini, R., Vesala, T., and Janssens, I. A.: CO_2 balance of boreal, temperate, and tropical forests derived from a global database, Global Change Biology, 13, 2509–2537, doi:10.1111/j.1365-2486.2007.01439.x, 2007.

ORNL DAAC, Oak Ridge, T. U.: Oak Ridge National Laboratory Distributed Active Archive Center (ORNL DAAC), http://fluxnet.ornl.gov/, 2011.

Rohwer, J., Gerten, D., and Lucht, W.: Development of functional irrigation types for improved global crop modelling - PIK report No. 104, Tech. Rep. 104, Potsdam Institute for Climate Impact Research, Potsdam, Germany, https://www.pik-potsdam.de/research/publications/pikreports, 2007.

Sauer, T., Havlík, P., Schneider, U. a., Schmid, E., Kindermann, G., and Obersteiner, M.: Agriculture and resource availability in a changing world: The role of irrigation, Water Resources Research, 46, doi:10.1029/2009WR007729, 2010.

Schaphoff, S., Forkel, M., Müller, C., Knauer, J., von Bloh, W., Biemans, H., Gerten, D., Heinke, J., Jaġermyer, J., Lucht, W., Rammig, A., Thonicke, K., and Waha, K.: The LPJmL4 Dynamic Global Vegetation Model with managed Land: PART II - Evaluation of a global consistent vegetation, hydrology and agricultural model, Geoscientific Model Development, under Revision.